Preprint typeset using LaTeX style emulateapj v. 12/16/11

275 CANDIDATES AND 149 VALIDATED PLANETS ORBITING BRIGHT STARS IN K2 CAMPAIGNS 0-10

Andrew W. Mayo[1,2,3,†,‡,⋆], Andrew Vanderburg[4,3,‡,□], David W. Latham[3], Allyson Bieryla[3], Timothy D. Morton[5], Lars A. Buchhave[1,2], Courtney D. Dressing[6,7,□], Charles Beichman[8], Perry Berlind[3], Michael L. Calkins[3], David R. Ciardi[8], Ian J. M. Crossfield[9], Gilbert A. Esquerdo[3], Mark E. Everett[10], Erica J. Gonzales[11,‡], Lea A. Hirsch[6], Elliott P. Horch[12], Andrew W. Howard[13], Steve B. Howell[14], John Livingston[15], Rahul Patel[16], Erik A. Petigura[13,††], Joshua E. Schlieder[17], Nicholas J. Scott[14], Clea F. Schumer[3], Evan Sinukoff[13,18], Johanna Teske[19,‡‡], Jennifer G. Winters[3]

ABSTRACT

Since 2014, NASA's K2 mission has observed large portions of the ecliptic plane in search of transiting planets and has detected hundreds of planet candidates. With observations planned until at least early 2018, K2 will continue to identify more planet candidates. We present here 275 planet candidates observed during Campaigns 0-10 of the K2 mission that are orbiting stars brighter than 13th magnitude (in Kepler band) and for which we have obtained high-resolution spectra (R = 44,000). These candidates are analyzed using the `vespa` package (Morton 2012, 2015b) in order to calculate their false positive probabilities (FPP). We find that 149 candidates are validated with a FPP less than 0.1%, 39 of which were previously only candidates and 56 of which were previously undetected. The processes of data reduction, candidate identification, and statistical validation are described, and the demographics of the candidates and newly validated planets are explored. We show tentative evidence of a gap in the planet radius distribution of our candidate sample. Comparing our sample to the *Kepler* candidate sample investigated by Fulton et al. (2017), we conclude that more planets are required to quantitatively confirm the gap with K2 candidates or validated planets. This work, in addition to increasing the population of validated K2 planets by nearly 50% and providing new targets for follow-up observations, will also serve as a framework for validating candidates from upcoming K2 campaigns and the Transiting Exoplanet Survey Satellite (TESS), expected to launch in 2018.

Keywords: methods: data analysis, planets and satellites: detection, techniques: photometric

1. INTRODUCTION

The field of exoplanets is relatively young compared to most other disciplines of astronomy: the announcement of the first exoplanet orbiting a star similar to our own was only in 1995[26] (Mayor & Queloz 1995). Since then, the field has expanded rapidly, with several thousand exoplanets having now been discovered. With many upcoming extremely large telescopes, the number of known exoplanets and our understanding of them will only increase.

One of the most important moments in the history of exoplanet science was the beginning of the *Kepler* mission (Borucki et al. 2008). Launched in 2009, the *Kepler* space telescope observed over 100,000 stars in a single patch of sky for four years in order to look for transits. *Kepler* has been an overwhelming success. According to the NASA Exoplanet Archive[27] (accessed 2018 February 14), it is currently responsible for 2341 verified exoplanets, more

† awm@space.dtu.dk
‡ National Science Foundation Graduate Research Fellow
⋆ Fulbright Fellow
□ NASA Sagan Fellow
†† NASA Hubble Fellow
‡‡ Carnegie Origins Fellow, jointly appointed by Carnegie DTM & Carnegie Observatories
[1] DTU Space, National Space Institute, Technical University of Denmark, Elektrovej 327, DK-2800 Lyngby, Denmark
[2] Centre for Star and Planet Formation, Natural History Museum of Denmark & Niels Bohr Institute, University of Copenhagen, Øster Voldgade 5-7, DK-1350 Copenhagen K., Denmark
[3] Harvard–Smithsonian Center for Astrophysics, 60 Garden St., Cambridge, MA 02138
[4] Department of Astronomy, University of Texas at Austin, Austin, TX 76712
[5] Department of Astrophysical Sciences, 4 Ivy Lane, Peyton Hall, Princeton University, Princeton, NJ 08544
[6] Astronomy Department, University of California, Berkeley, CA 94720
[7] Division of Geological & Planetary Sciences, California Institute of Technology, 1200 E California Blvd MC 150-21, Pasadena, CA 91125 USA
[8] NASA Exoplanet Science Institute, California Institute of Technology, Pasadena, CA 91125
[9] Department of Physics and Kavli Institute for Astrophysics and Space Research, Massachusetts Institute of Technology, Cambridge, MA 02139
[10] National Optical Astronomy Observatory, 950 North Cherry Avenue, Tucson, AZ 85719
[11] Department of Astronomy and Astrophysics, University of California, Santa Cruz, CA 95064
[12] Department of Physics, Southern Connecticut State University, 501 Crescent Street, New Haven, CT 06515
[13] Cahill Center for Astrophysics, California Institute of Technology, Pasadena, CA 91125
[14] Space Science and Astrobiology Division, NASA Ames Research Center, Moffett Field, CA 94035
[15] Department of Astronomy, The University of Tokyo, 7-3-1 Hongo, Bunkyo-ku, Tokyo 113-0033, Japan
[16] Infrared Processing and Analysis Center, California Institute of Technology, Pasadena, CA 91125
[17] NASA Goddard Space Flight Center, Greenbelt, MD 20771
[18] Institute for Astronomy, University of Hawai'i at Mānoa, Honolulu, HI 96822
[19] Carnegie Observatories, 813 Santa Barbara Street, Pasadena, CA 91101

[26] The exoplanet, 51 Peg b, was not fully confirmed to be a planet until the absolute mass was measured by Martins et al. (2015). Also, a reported brown dwarf discovered in 1989 (Latham et al. 1989) may in fact be an exoplanet, depending on its inclination.

[27] https://exoplanetarchive.ipac.caltech.edu/

than every other exoplanet survey combined.

Unfortunately, in 2013 the second of four reaction wheels on the *Kepler* spacecraft failed, preventing the spacecraft from looking at its designated field and bringing an end to the original mission. Fortunately, a follow up mission, called K2, was developed that used the spacecraft's thrusters as a makeshift third reaction wheel (Howell et al. 2014). Unlike the original *Kepler* mission, the K2 mission must observe new fields roughly every 83 days[28]. As a result, K2 observations are divided into "campaigns" each corresponding to a field.

With every new campaign, K2 observes more bright stars and finds more planets orbiting these stars, so there are new bright targets available for follow-up (such as RV measurements or transmission spectroscopy). K2 has led to the discovery of numerous candidate and confirmed planets (Vanderburg et al. 2015b; Crossfield et al. 2015; Foreman-Mackey et al. 2015; Montet et al. 2015; Vanderburg et al. 2016a; Schlieder et al. 2016; Sinukoff et al. 2016; Crossfield et al. 2016; Barros et al. 2016; Pope et al. 2016; Adams et al. 2016; Dressing et al. 2017b; Martinez et al. 2017; Hirano et al. 2017), as well as the identification of planets orbiting rare types of stars, including particularly bright nearby dwarf stars (Petigura et al. 2015; Vanderburg et al. 2016b; Rodriguez et al. 2017b; Crossfield et al. 2017; Christiansen et al. 2017; Rodriguez et al. 2017a; Niraula et al. 2017), young, pre-main-sequence stars (Mann et al. 2016; David et al. 2016), and disintegrating planetary material transiting a white dwarf (Vanderburg et al. 2015a).

Here, we take advantage of the large number of bright stars observed by K2 and present the identification and follow-up of a sample of 275 exoplanet candidates orbiting stars (brighter than 13th magnitude) in the *Kepler* bandpass identified from K2 Campaigns 0 through 10. Since the beginning of the K2 mission, we have also obtained spectra for all of our candidates as well as many high-resolution imaging observations, in order to measure the candidate host stars' parameters and identify nearby stars (both types of follow-up aid in identification and ruling out of false positive scenarios). We also attempt to validate[29] our candidates with `vespa`, a statistical validation tool developed by Morton (2012, 2015b), finding 149 to be validated with a false positive probability less than 0.1%. Of these newly validated exoplanets, 39 were previously only exoplanet candidates and 56 have not been previously detected (see Table 2). This work will increase the validated K2 planet sample from 212 (according to the Mikulski Archive for Space Telescopes[30]; accessed 2018 February 14) to 307, a nearly 50% increase. Similarly, this work increases the K2 candidate sample by ∼20%.

In this paper we describe the identification and analysis of our candidate sample, as well as our validation process and the resulting validated planet sample. Section 2 discusses the process by which we use K2 data to identify exoplanet candidates. Section 3 describes our ground-based observations of the planet candidate host stars detected by K2. Section 4 explains the analysis of the K2 light curves and the follow-up spectroscopy and high-contrast imaging. Section 5 details how we use `vespa` to calculate false positive probabilities for our planet candidates. Section 6 presents the results of the our candidate identification, vetting, follow-up observations, and analysis in detail for a single, instructive planet. Then the results for the entire planet candidate sample are similarly presented. In Section 7, we discuss the results of our work, including confirmation of features in the exoplanet population previously identified using data from the original *Kepler* mission. Finally, we summarize and conclude in Section 8.

2. PIXELS TO PLANETS

In this section, we first explain how K2 observations are collected, then we describe the process by which systematic errors are removed from K2 data, and finally we discuss analysis of the systematics-corrected K2 data in order to identify planet candidates.

2.1. *K2 Observations*

Since 2014, the K2 mission has served as the successor to the original *Kepler* mission. By observing fields along the ecliptic plane and firing its thrusters approximately once every six hours, the probe can maintain an unstable equilibrium against solar radiation. However, the spacecraft can only point toward a given field for roughly 83 days before re-pointing (in order to keep sunlight on the spacecraft's panels and out of its telescope).

Due to on-board data storage constraints, not all data collected by the CCD array can be retained and transmitted to the ground. As a result, targets must be identified within each campaign field prior to observation so that non-target data can be discarded and a postage stamp (a small group of pixels) around each target can be saved and transmitted to the ground.

In the original *Kepler* mission, the primary objective was to determine the frequency of Earth-like planets orbiting Sun-like stars (Batalha et al. 2010b). Although some planet search targets were selected during mission adjustments and others were selected through a Guest Observer program for secondary science objectives, most targets were selected pre-launch for the primary objective. However, K2 operates in a very different manner. For each K2 campaign, targets are exclusively selected

[28] Roughly 75 of those days are devoted to science.

[29] The difference between an exoplanet candidate and a validated exoplanet is very important. During the original *Kepler* mission, an exoplanet candidate was a transit signal that had passed a battery of astrophysical false positive and instrumental false alarm tests. In K2, however, the usage is looser; the term is commonly used to refer to any exoplanet signal that a particular team has identified as a possible planet. So long as the reasoning is sound and the results are published, the signal is effectively a candidate. A validated planet is a candidate that has been vetted with follow-up observations and determined quantitatively to be far more likely an exoplanet than a false positive (according to some likelihood threshold). Validated planets, because confidence in their planethood is higher than for a regular candidate, are far more promising targets than planet candidates for follow-up observations, characterization, and eventual confirmation. We note that validation is not the same thing as confirmation, which is ideally attained through a reliable mass determination. In this work, we are in general not attempting to "confirm" planets. Confirmation is more rigorous than validation, in the same way that validation is more rigorous than candidacy. Confirmation is usually accomplished via the RV method, the TTV method, or, less commonly, methods such as a full photo-dynamical modeling solution (e.g. Carter et al. 2011) or Doppler tomography (e.g. Zhou et al. 2016).

[30] https://archive.stsci.edu/k2/published_planets/search.php

through the Guest Observer (GO) program, which evaluates observing proposals submitted by the astronomical community for any scientific objective, not just exoplanet related objectives. Ideally, GO proposals have scientifically compelling goals that can be achieved through K2 observations and cannot easily be achieved with other instruments or facilities.

In a typical K2 campaign, the number of targets ranges between 10,000 and 40,000 with long cadence observations (≈30 minute integration), and about 50 to 200 with short cadence observations (≈1 minute integration). Exceptions include C0, which served primarily as a proof-of-concept campaign to show that the K2 mission was viable, and C9, which focused on microlensing targets in the Galactic Bulge. Both C0 and C9 had fewer targets than normal in both long cadence and short cadence. It should also be noted that there are occasional overlaps between campaign fields. Despite fewer new targets, overlaps provide a longer baseline of observations for targets of interest in the overlapping region.

This paper focuses on Campaigns 0 through 10 (excluding Campaign 9). However, the process implemented in this research can easily be extended and applied to additional K2 campaigns.

2.2. *K2 Data Reduction*

Because of the loss of two reaction wheels, the *Kepler* telescope is perpetually drifting off target and must be regularly corrected by thruster fires, causing shifts in the pixels that targets fall on. These shifts, coupled with variable sensitivity between pixels on the telescope CCDs and variable amounts of starlight falling inside photometric apertures, lead to systematic variations in the signal from K2 targets, introducing noise into the photometric measurements. Howell et al. (2014) estimated that raw K2 precision is roughly a factor of 3-4 times worse than *Kepler*'s original precision (depending on stellar magnitude). Fortunately, an understanding of the motion of the *Kepler* spacecraft allows for modeling and correction of the induced systematic noise. In particular, we rely on the method of systematic correction described by Vanderburg & Johnson (2014, hereafter referred to as VJ14), as well as the updates to the method described in Vanderburg et al. (2016a, hereafter referred to as V16). We briefly describe here the method developed by VJ14.

First, 20 different aperture masks were chosen for each target star, 10 circular masks of varying size and 10 masks shaped liked the *Kepler* pixel response function for the target with varying sensitivity cutoffs. These masks were used to perform simple aperture photometry to produce 20 different "raw" light curves. Then the motion of the target star across the CCD was estimated by calculating centroid position for each cadence[31]. Next, the recurrent path of the centroid across the CCD between thruster fires was identified. Data collected during thruster fires were identified and removed. Then, for each of the 20 raw light curves produced, low-frequency variations (> 1.5 days) were removed with a basis spline and the relationship between centroid position and flux was fit with a piecewise function. Because the centroid path would shift on timescales longer than 5-10 days, the flux-centroid piecewise function was applied separately to each 5-10 day light curve segment. This function was then used to correct the raw data so that low-frequency variations could be recalculated. This process was then repeated iteratively until convergence. Finally, after all 20 raw light curves per star were processed in this way, a "best" aperture was chosen to maximize photometric precision. An example of a light curve before and after the full data reduction procedure can be seen in Fig. 1 for the planet host EPIC 212521166. We note that light from any nearby companion stars could potentially enter the best aperture mask, which may lead to a diluted transit and an underestimated planet radius (Ciardi et al. 2015; Hirsch et al. 2017). However, we expected this effect to be small even when present and therefore do not correct for it.

[31] Although it is possible to produce light curves by decorrelating with centroid positions measured from each star, we used the centroids measured from one hand-selected isolated, bright K2 target per campaign, which we found gives better results.

2.3. *Identifying Threshold Crossing Events*

Once the roll systematics were removed from the photometry according to the method described by VJ14, we conducted a transit search of each K2 target using the method of Vanderburg et al. (2016a). We give a short description of the transit search process here.

First, low-frequency variations were removed via a basis spline and outliers were removed. Then a box-least-squares (BLS) periodogram (Kovács et al. 2002) was calculated over periods between 2.4 hours and half the length of the campaign. All periodic decreases in brightness with SNR > 9 were investigated. If putative transits lasted longer than 20% of their period, or were composed of a single data point, or changed depth by over 50% when the lowest point was removed, the signal was removed and the BLS periodogram recalculated. Any detection passing these tests was deemed a "Threshold Crossing Event" (TCE). We identified $\sim 30,000$ TCEs across C0-C10 in this manner.

Each TCE was fit with the Mandel & Agol (2002) transit model to estimate transit parameters, then the TCE was removed from the light curve, and the BLS periodogram was recalculated. Once all TCEs had been identified, they subsequently underwent "triage", in which each candidate was inspected by eye in order to remove obvious astrophysical false positives and instrumental false alarms from subsequent analysis. TCEs identified as neither type of false signal passed the triage phase and moved on to a "vetting" phase.

2.4. *Identifying K2 Candidates*

During vetting, we subjected the surviving TCEs to a battery of additional tests to identify astrophysical false positives and instrumental false alarms. Some of these tests were identical or similar to the tests conducted for the *Kepler* mission, while others are specific to K2 data. For each test we produced a diagnostic plot, examples of which are shown in Figs. 2, 3, and 4. Here we describe the tests we conducted in more detail:

1. The times of a TCE's "in transit" points were compared against the position of the *Kepler* spacecraft at those times, as many instrumental false alarms were composed of data points near the edges of *Kepler*'s rolls where the K2 flat field is less well

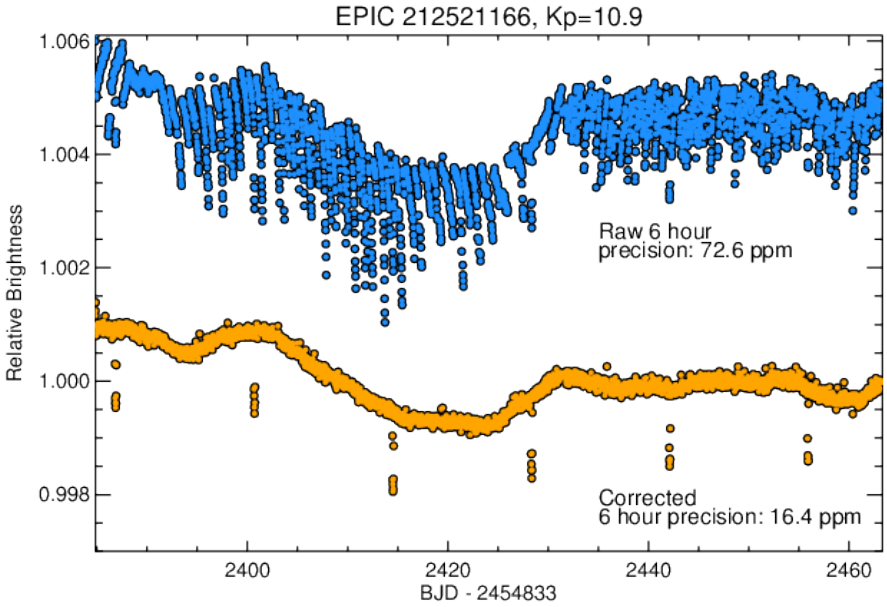

Figure 1. Example of the K2 systematics reduction process on the light curve of the planet host EPIC 212521166. The blue points show the light curve before correcting for the systematics induced by the roll motion of the *Kepler* spacecraft, while the yellow points show the same light curve after those systematics have been removed via the data reduction process summarized in Section 2.2 and documented in Vanderburg & Johnson (2014) and Vanderburg et al. (2016a). The remaining downward dips in the corrected (yellow) light curve are transits of a mini-Neptune sized exoplanet, validated in this work and already confirmed in Osborn et al. (2017).

constrained, and our analysis method can leave in systematics. The plots we use to identify these false alarms are shown in Figs. 2 and 3.

2. We compared the signal of a TCE in light curves produced using multiple different photometric apertures. This test is a powerful way to identify signals caused by instrumental systematics (as these systematics present differently in different photometric apertures), as well as identifying astrophysical false positives, such as when a candidate transit signal was due to contamination from a nearby star. An example of these tests are shown in Fig. 3. We note that although this test rules out transits or eclipses originating from a nearby companion, it does not rule out the possibility of light contamination from a nearby companion, which could dilute the observed transit and lead to an underestimation of the planetary radius (Ciardi et al. 2015; Hirsch et al. 2017).

3. Individual transits of a TCE were visually inspected, since instrumental false alarms were less likely to have consistent, planet-like transit depths or shapes (see Fig. 2). This metric is qualitatively similar to the "transit patrol" metrics introduced in the DR25 *Kepler* planet candidate catalog (in particular the Rubble, Marshall, Chases, and Zuma tests, Thompson et al. 2017).

4. Flux centroid motion, phase variations (possibly caused by relativistic beaming, reflected light, or ellipsoidal effects), differences in depth between odd and even numbered transits, and secondary eclipses were all searched for as evidence of astrophysical false positives. Similar tests have been used since the beginning of the *Kepler* mission (Batalha et al. 2010a). Example diagnostic plots for identifying phase variations, the difference between even and odd numbered transits, and secondary eclipses near phase 0.5 are shown in Fig. 2; flux-centroid shift tests are shown in Fig. 3. We searched for secondary eclipses at arbitrary phases (not necessarily near phase = 0.5) using the "model-shift uniqueness" test designed by Coughlin et al. (2016). We show diagnostic plots for the model-shift uniqueness test in Fig. 4.

5. We searched for astrophysical false positive scenarios by "ephemeris matching". Sometimes the pixels surrounding a target star can be contaminated with a small amount of light from other nearby stars. When those nearby stars are variable themselves (like eclipsing binaries), the variability from the nearby stars can be introduced into the target's light curve (Coughlin et al. 2014). We identified cases where this happened by searching for planet candidates that have the same period (or integer multiples of the same period) and time of transit as eclipsing binaries observed by K2 using the same criteria as Coughlin et al. (2014). We found no examples of matched ephemerides due to direct Pixel Response Function (PRF) overlap that we had not also identified in our tests with multiple photometric apertures, but we did find two instances where candidate transit signals were caused by charge transfer inefficiency along one of the columns of the *Kepler* detector. We excluded a candidate around EPIC 212435047 caused by contamination from the eclipsing binary EPIC 212409377 located along the same CCD column about 2000 arcseconds away, and we excluded a candidate around EPIC 202710713 contaminated by the eclipsing bi-

nary EPIC 202685801 located along the same CCD column at a distance of about 300 arcseconds.

6. We estimated the SNR of a TCE by taking the difference between the mean baseline flux and the in-transit flux and dividing by the quadrature sum of the standard deviation of the flux in those two regions. We defined the boundaries of the in-transit region in two ways and calculated the SNR for both choices. In one case we used every data point collected between the second and third contact (minus a single long-cadence Kepler exposure on either side). This estimate of SNR could sometimes not be calculated if the transit was grazing. In the other case we used the central 20% of data collected from the first to fourth contact (which could be calculated even if the transit was grazing). Following standard practice from the Kepler mission, if both of these values (or just the latter in the grazing case) were below 7.1σ the candidate was excluded (7.1σ is the minimum significance level for a signal to qualify as a TCE in the *Kepler* Science Pipeline; Jenkins et al. 2010). We only encountered two such candidates: EPIC 220474074 and EPIC 201289302.

Although it is possible to automate diagnostic tests of this type (see, for example, the Robovetter that was designed for the main *Kepler* mission, Coughlin et al. 2016), we performed vetting tests 1-4 by eye.

Any TCE surviving all of these vetting stages was promoted to "planet candidate" ($\sim$1,000 were promoted in this way). All candidates orbiting sufficiently bright host stars (see Section 3.1) were then subjected to our validation process. Parameters for the 275 candidates that satisfied these requirements and were subjected to validation are listed in Table 4. Their associated stellar parameters are listed in Table 5.

3. SUPPORTING OBSERVATIONS

In this section, we describe follow-up observations we conducted to better characterize the candidate host stars. These observations are crucial for improving stellar parameters (e.g. Dressing et al. 2017a; Martinez et al. 2017; Mann et al. 2017), which in turn can help differentiate between a transiting planet and various false positive scenarios (i.e. stellar binary configurations) that might prefer different regions of stellar parameter space. We first discuss high-resolution optical spectroscopy of the planet candidate host stars from the Tillinghast Reflector Echelle Spectrograph (TRES), followed by speckle imaging from the Differential Speckle Survey Instrument (DSSI) and the NASA Exoplanet Star and Speckle Imager (NESSI) at the WIYN telescope[32], the Gemini South telescope, and the Gemini North telescope, then lastly adaptive optics imaging from Keck Observatory, Palomar Observatory, Gemini South Observatory, Gemini North Observatory, and the Large Binocular Telescope Observatory.

3.1. *The Tillinghast Reflector Echelle Spectrograph*

All of the spectra used in this work were obtained with TRES, a spectrograph with a resolving power of R = 44,000 and one of two spectrographs for the 1.5 meter Tillinghast telescope at the Whipple Observatory on Mt. Hopkins in Arizona. We obtained at least one usable TRES spectrum of each of the planet candidate host stars that we consider in this work and that we subject to our validation process (see Section 4.2 for our definition of "usable"). With a few exceptions, we only observed candidates brighter than 13th magnitude in the *Kepler* band with TRES because of the lengthy integration time required to collect spectra of stars fainter than this and the difficulty of subsequent follow-up observations (for example, with precise radial velocities) at other facilities. This limitation reduced the number of candidates we considered for validation significantly, from $\sim$1,000 to 275. In the future, observing these fainter candidates, either with TRES or other spectrographs on larger telescopes, could potentially more than double the number of K2 planets for our analysis.

3.2. *Speckle Observations*

We observed many of our planet candidates with speckle imaging from either the 3.5-m WIYN telescope, the Gemini-South 8.1-m telescope, or the Gemini-North 8.1-m telescope. Together, the three telescopes collected 162 speckle images of 73 stars with DSSI (Horch et al. 2009). DSSI is a speckle imaging instrument that travels between different telescopes. For each of the 73 targets, we collected DSSI speckle images at narrow band filters centered at 6920 Å and 8800 Å (at least one of each for every target). These observations were made in September and October of 2015, as well as January, April, and June of 2016.

Further, 160 speckle images were collected for a distinct sample of 70 stars at the WIYN telescope using NESSI, which is essentially a newer version of the DSSI instrument. For each of the 70 targets, we collected NESSI speckle images at narrow band filters centered at 5620 Å and 8320 Å (at least one of each). These observations were made in October through November of 2016 and March through May of 2017. A list of the observed stars can be found in Table 7.

3.3. *Adaptive Optics Observations*

In addition to speckle imaging, we also observed many of our planet candidate host stars with adaptive optics (AO) imaging.

We collected 47 AO images for 45 stars on the Keck II 10-m telescope in K filter with the Near Infra Red Camera 2 (NIRC2); 5 of those stars were also imaged using NIRC2 in J band. All of these observations were made during April, July, August, and October of 2015 as well as January and February of 2016.

We collected 27 AO images for 27 stars on the Palomar 5.1-m Hale telescope in K filter with the Palomar High Angular Resolution Observer (PHARO, Hayward et al. 2001); 6 of those stars were also imaged using PHARO in J band. All of these observations were made during February, May, and August of 2015 as well as June, September, and October of 2016.

We collected 19 AO images for 18 stars on the Gemini-North 8.1-m telescope in K band with the Near InfraRed Imager and spectrograph (NIRI, Hodapp et al.

[32] The WIYN Observatory is a joint facility of the University of Wisconsin-Madison, Indiana University, the National Optical Astronomy Observatory, and the University of Missouri.

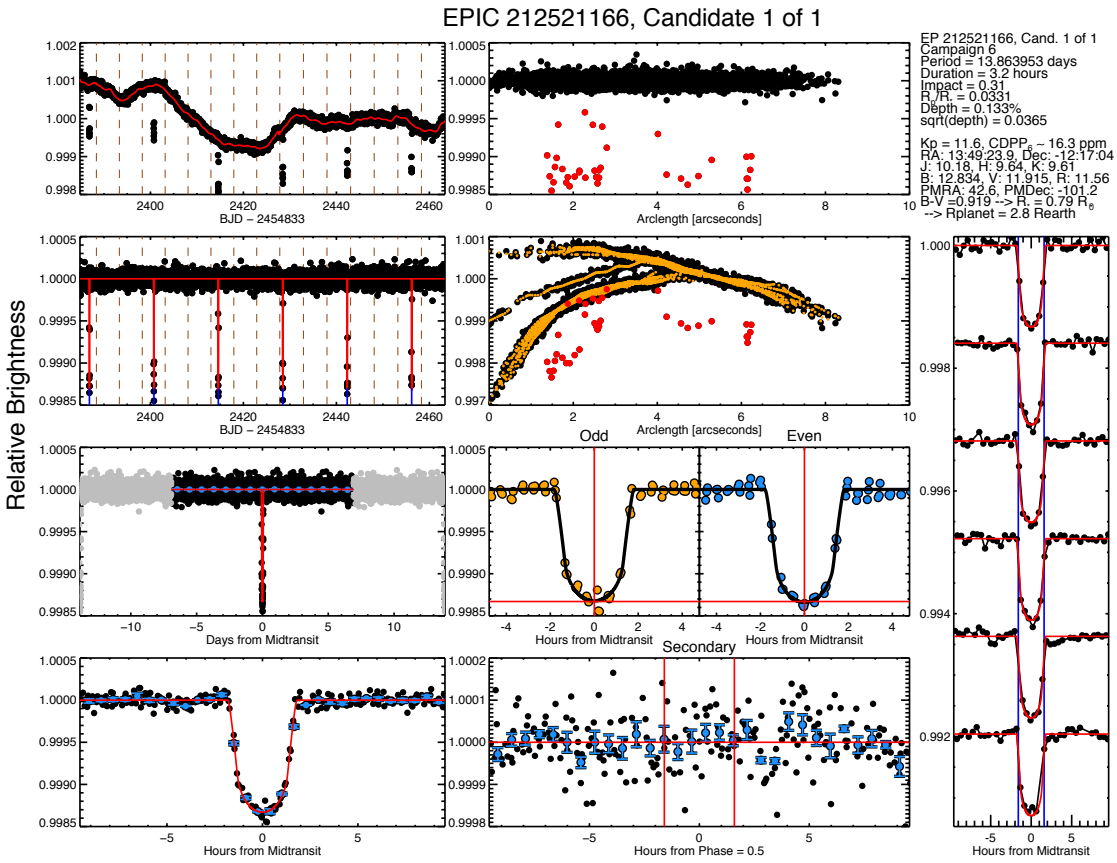

Figure 2. Diagnostic plots for EPIC 212521166.01. Left column, first (top) and second rows: K2 light curves without and with low frequency variations removed, respectively. The low frequency variations alone are modeled in red in the first row, whereas the best-fit transit model is in red in the second row. Vertical, brown, dotted lines denote the regions into which the light curve was separated to correct roll systematics. Left column, third and fourth rows: phase-folded, low frequency corrected K2 light curves. In the third row, the full light curve is shown (points more than one half period from the transit are gray), whereas in the fourth row, only the light curve near transit is shown. The red line is the best-fit model and the blue points are binned data points. Middle column, first and second rows: arclength of centroid position of star versus brightness, after and before roll systematics correction respectively. Red points denote in-transit data. In the second row, small orange points denote the roll systematics correction made to the data. Middle column, third row: separate plotting and modeling of odd (left panel) and even (right panel) transits, with orange and blue data points respectively. The black line is the best-fit model, the horizontal red line denotes the modeled transit depth, and the vertical red line denotes the mid-transit time (this is useful for detecting binary stars with primary and secondary eclipses). Middle column, fourth row: light curve data in and around the expected secondary eclipse time (for zero eccentricity). Blue data points are binned data, the horizontal red line denotes a relative flux = 1, and the two vertical red lines denote the expected beginning and end of the secondary eclipse. Right column: individual transits (vertically shifted from one another) with the best-fit model in red and the vertical blue lines denoting the beginning and end of transit.

2003). These observations were made during October and November of 2015 as well as June and October of 2016.

We collected a single AO image on the Large Binocular Telescope in K filter with the L/M-band mid-InfraRed Camera (LMIRCam, Leisenring et al. 2012). This observation was made in January of 2015.

There was some overlap between instruments; overall, AO images were collected for a total of 80 systems. A list of the observed stars can be found in Table 7.

4. DATA ANALYSIS

Once all of the photometry had been reduced and all of the necessary follow-up observations had been collected, the next step was to analyze the data, calculate relevant parameters, and prepare the results for the validation process. In this section, we explain the process of fitting a model to our reduced light curves (to determine transit parameters and create folded light curves), analyzing our spectra (to calculate stellar parameters), and extracting and reducing data from our high-contrast images (to create contrast curves).

4.1. *K2 light curves*

4.1.1. *Simultaneous Fitting of K2 Systematics and Transit Parameters*

In Sections 2.2, 2.3, and 2.4 we described the process of correcting K2 photometry for instrumental systematics and exploring the reduced light curves for candidates. Once those steps were complete, the planet candidates needed to be more thoroughly characterized. In order to assess transit and orbital parameters, we re-produced the K2 light curves for these planet candidates, re-deriving the systematics correction while simultaneously modeling the transits in the light curve. As in our original systematics correction, the light curve was divided into multiple sections and the systematics correction was applied to each section separately. A piecewise linear func-

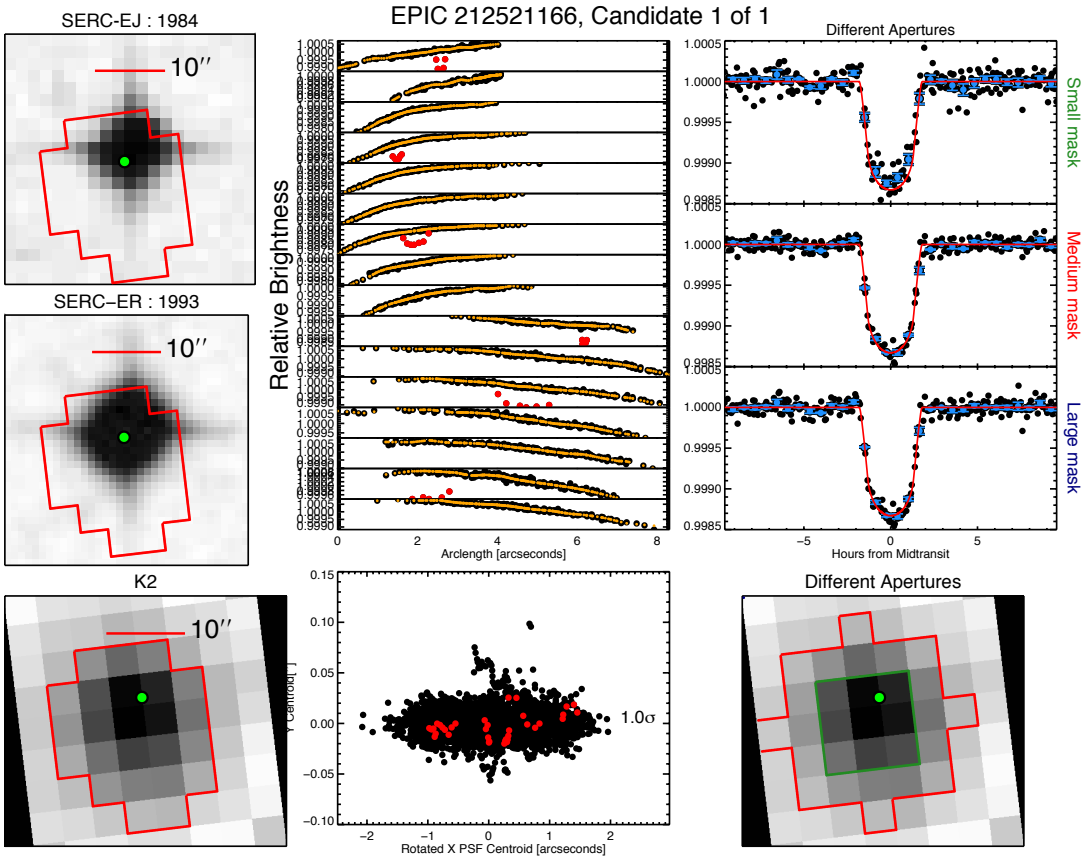

Figure 3. Diagnostic plots for EPIC 212521166.01. Left column, first (top), second, and third rows: images from the first Digital Sky Survey, the second Digital Sky Survey, and K2 respectively, each with a scale bar near the top and an identical red polygon to show the shape of the photometric aperture chosen for reduction. The K2 image is rotated into the same orientation as the two archival images (north up). Middle column, top row: multiple panels of uncorrected brightness versus arclength, chronologically ordered and separated into the divisions in which the roll systematics correction was calculated. In-transit data points are red, orange points denote the brightness correction applied to remove systematics. Middle column, bottom row: variations in the centroid position of the K2 image. In-transit points are red. The discrepancy (in standard deviations) between the mean centroid position in-transit and out-of-transit is shown on the right side of the plot. Right column, first row: the K2 light curve near transit as calculated using three differently sized apertures: "Small mask" (top panel), "Medium mask" (middle panel), and "Large mask" (bottom panel), each with the identical best-fit model in red. Aperture-size dependent discrepancies in depth could suggest background contamination from another star. Right column, third row: the K2 image overlaid with the three masks from the previous plot shown (in this figure, the large mask is fully outside the postage stamp and is therefore not visible).

tion was fit with breaks roughly every 0.25 arcseconds (varying slightly by target) to the arclength v. brightness relationship described in section 2.2 (arclength is a one-dimensional measure of position along the path an image centroid traces out on the *Kepler* CCD camera). The low-frequency variations in the light curve were modeled with a cubic spline (with breakpoints every 0.75 days), and the transits themselves were modeled with the Mandel & Agol (2002) transit model. The fit was performed using a Levenberg-Marquardt optimization (Markwardt 2009), and all of the parameters from the optimization (besides the transit parameters) were used in order to correct the systematics of the light curve (once again) and remove the low-frequency variations (once again). Since these parameters were determined in a *simultaneous* fit with the transits, the quality of the resulting light curves reduction tended to be better than the original light curves.

4.1.2. *Final Estimation of Transit Parameters and Uncertainties*

After we produced the systematics-corrected, low-frequency-extracted light curves, we analyzed them further in order to estimate final transit parameter values and their uncertainties. We based our model on the `BATMAN` Python package (Kreidberg 2015), which we used to calculate our synthetic transit light curves. We fit the transit light curves of all planet candidates around a given star simultaneously so that overlapping transits could be modeled, assuming that each of the planets were non-interacting and on circular orbits. For each planet candidate, five parameters were included: the epoch (i.e. time of first transit), the period, the inclination, the planetary to stellar radius ratio (R_p/R_*), and the semi-major axis normalized to the stellar radius (a/R_*). Additionally, two parameters for a quadratic limb-darkening law were included (Kipping 2013), as well as a parameter to allow the baseline to vary (in case there was an erroneous systematic offset from flux = 1 outside of transit), and a noise parameter that assigned the same uncertainties to each flux measurement (since flux error bars were

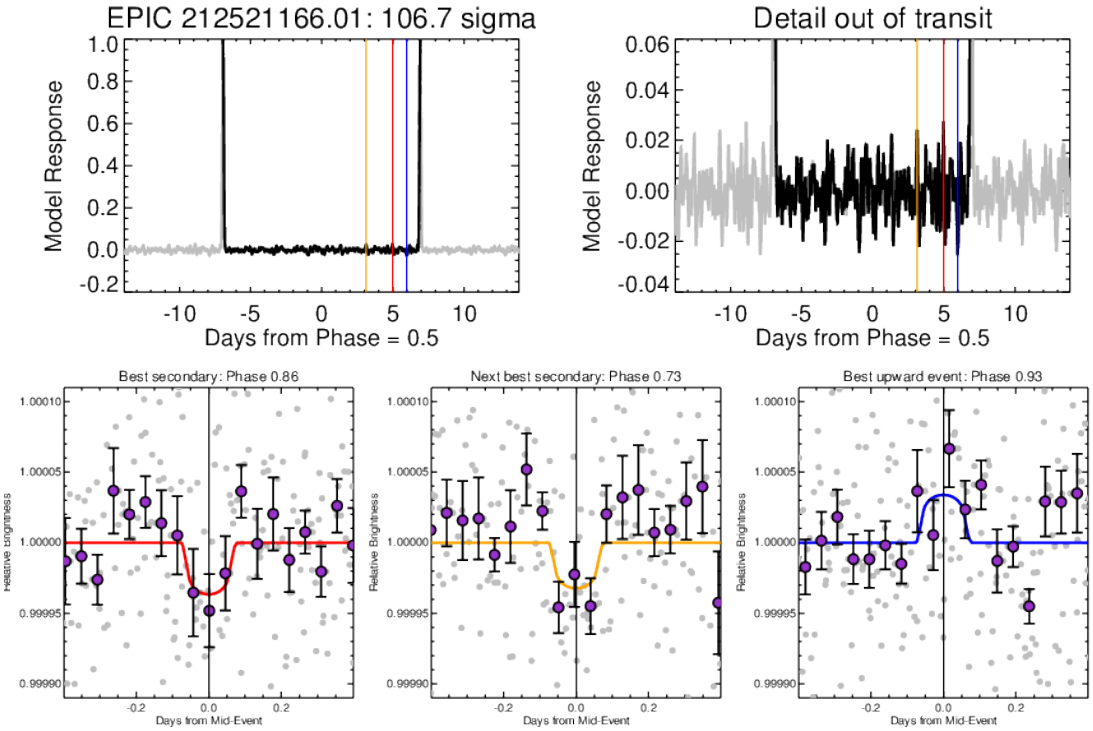

Figure 4. Model-shift uniqueness diagnostic plots for EPIC 212521166.01. We cross-correlated the phase-folded light curve of each planet candidate with the candidate's best-fitting transit model. The two plots in the top row show the cross-correlation function as a function of orbital phase with different scaling on the Y-axis. The tallest peak in the response is the primary transit, and the three vertical lines show the phase of the highest significance putative secondary event (red) , the second highest significance putative secondary event (orange), and the highest significance "upside-down" secondary event (blue). The bottom row of plots show the three segments of the light curve surrounding the highest and second highest significance putative secondary eclipses, and the highest significance "upside-down" event. Grey and purple data points are unbinned and binned observations respectively. Comparing the amplitudes of these three events gives an indication of their significance. Here, the two most significant putative secondary eclipses have a similar amplitude to the most significant upside-down event, indicating that they are all likely spurious. We find no significant secondary eclipse in the light curve of EPIC 212521166.01.

not calculated in the K2 data reduction process). For all of these planet and system parameters we assumed a uniform prior, except for the R_p/R_* parameter for each planet, which we gave a log-uniform prior.

For each candidate system, the transit parameters in this model were estimated using `emcee` (Foreman-Mackey et al. 2013), a Python package that runs simulations using a Markov chain Monte Carlo (MCMC) algorithm with an affine invariant ensemble sampler (Goodman & Weare 2010). In each simulation, the parameter space for a system with n candidates was sampled with $8 + 10n$ chains (equal to twice the number of model parameters). The MCMC process was ran for either 10,000 steps or until convergence, whichever came last. Convergence was defined according to the scale-reduction factor (Gelman & Rubin 1992), a diagnostic that compares variance for individual chains against variance of the whole ensemble. A simulation was considered converged when the scale reduction factor was less than 1.1 for each parameter. The Gelman-Rubin scale-reduction factor is properly defined for chains from distinct, non-communicating MCMC processes; however, we found that our simulations visually converged many times more quickly than the Gelman-Rubin diagnostic, so we decided the diagnostic would be sufficient for our purposes. An example of a converged model fit against transit data can be seen in Fig. 5.

Additionally, each simulation was checked after the minimum number of steps (10,000) and at the end of the simulation for any chains in the ensemble that could be easily categorized as "bad", i.e. trapped in a mini-

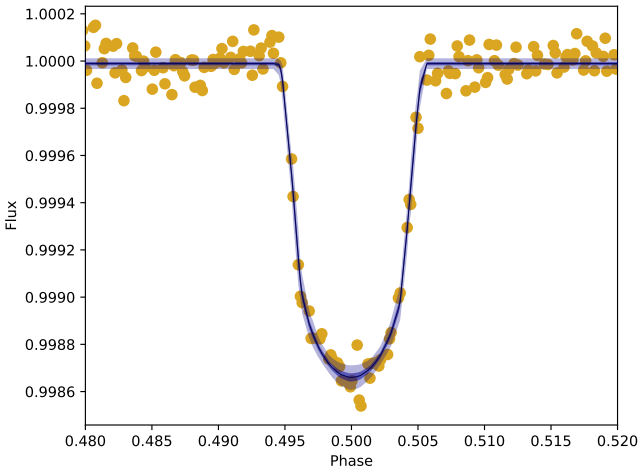

Figure 5. Fit of our transit model to corrected and normalized light curve data for EPIC 212521166.01. The yellow points are the observed data, normalized and phase-folded to the orbital period of the planet. The black line is our transit model with the median parameter values determined from an MCMC process. The dark blue and light blue regions are 1σ and 3σ confidence intervals, respectively.

mum of parameter space with a poorer best fit than the minimum of the ensemble majority. In detail, a chain was classified as "bad" if both of the following applied:

1. The Kolmogorov-Smirnov statistic between the chain with the highest likelihood step and the chain in question was greater than 0.5.

2. $\theta_{\rm l}/\theta_{\rm g} < 1/(100n)$, where $\theta_{\rm l}$ is the local maximum likelihood (the maximum likelihood within the chain in question), $\theta_{\rm g}$ is the global maximum likelihood throughout the ensemble, and n is the total number of steps. This test is our own invention, which is more likely to classify a chain as bad when its maximum likelihood is further from the global maximum likelihood. This test also accounts for the length of the simulation, since the maximum likelihood within each chain should be closer to the global maximum likelihood for longer simulations. We include a factor of 100 in the denominator to make the test sufficiently conservative, such that it only finds bad chains very rarely and only those extremely unlikely to rejoin the ensemble in the lifetime of the simulation.

If a chain was deemed bad after 10,000 steps, its position in parameter space was updated to that of a good chain from the previous step of the simulation. If a chain was deemed bad at the end of the simulation, it was simply removed and not replaced. Both after 10,000 steps and at the end of the simulation, bad chains only occurred about 15% of the time, typically for only one or two chains in the ensemble.

A representative sample of the converged posteriors for each exoplanet system transit fit has been archived at `https://zenodo.org/record/1164791`.

4.2. *TRES Spectroscopy*

We first visually inspected each of the spectra collected with TRES for our candidate host stars. Our main goal in visually inspecting the spectra was to identify cases in which the spectra were composite or otherwise indicative of multiple stars in the system. We looked at diagnostic plots produced by the TRES pipeline, which showed various echelle orders and a cross-correlation between a synthetic template spectrum and a single spectral order around 5280 Å.

After identifying composite spectra and confirming that the others were apparently single-lined, we prepared the spectra before determining the host stars' parameters. In particular, we manually removed cosmic rays from the spectra that might bias or otherwise affect the spectroscopic parameters we measured. We focused on three echelle orders in particular, orders 22, 23, and 24 (covering 5059-5158, 5135-5236, and 5214-5317 Å respectively), which are within the range we used to measure spectroscopic parameters.

Once we finished visually inspecting each spectrum and removing cosmic rays, we analyzed each TRES spectrum using the Stellar Parameter Classification (SPC) tool, developed by Buchhave et al. (2012). SPC determines key stellar parameters through a comparison of the input spectrum (between 5050 and 5360 Å) to a library grid of synthetic model spectra, developed by Kurucz (1992). The library is 4-dimensional, varying in effective temperature $T_{\rm eff}$, surface gravity $\log g$, metallicity [m/H], and line broadening (a good proxy for projected rotational velocity, or $v \sin i$). [m/H] is estimated rather than [Fe/H] because *all* metallic absorption features are used to determine metallicity rather than just iron lines. (SPC assumes all relative metal abundances are the same as in the Sun, and [m/H] simply scales all solar abundances by the same factor.) This library grid spans $T_{\rm eff}$ from 3500 K to 9750 K in 250 K increments, $\log g$ from 0.0 to 5.0 (cgs) in 0.5 increments, [m/H] from -2.5 to +0.5 in 0.5 dex increments, and line broadening from 0 km s^{-1} to 200 km s^{-1} in progressively spaced increments (from 1 km s^{-1} up to 20 km s^{-1}). In total, the library contains 51,359 synthetic spectra. The stellar parameters derived using SPC can be found in Table 5.

We also calibrated TRES against Duncan et al. (1991) for the S_{HK} stellar activity index, a measure of the strength of emission in the cores of the H and K Ca II spectral absorption features. Our calibration was only performed over a range of $0.244 <$ B-V < 1.629, $0.055 < S_{HK} < 2.070$, and $v \sin i < 20$ km s^{-1}. Additionally, we required a photon count of more than 250,000 in the R and V continuum regions (3901.07±10 Åand 4001.07±10 Årespectively). Within those ranges, we were able to calculate S_{HK} for 28 of our spectra collected for 4 stars. Although there are relatively few K2 planet candidates bright enough for this measurement on a 1 meter telescope, it will be much more common with TESS. A note has been made for the relevant stars in Table 5 and the full results are listed in Table 3. There is also a detailed description of the S_{HK} calibration process for TRES in the Appendix.

In cases where we observed a candidate host star more than once with TRES, we attempted to identify or rule out large velocity variations indicating a stellar companion to the host star. (For this purpose we collected one new TRES spectrum each for EPIC 220250254 and EPIC 210965800, but otherwise exclusively used the spectra from which we derived stellar parameters.) We phased the radial velocities to the photometric ephemeris and fit a sinusoid to the velocities at the period and ephemeris of each candidate (and assuming a circular orbit) in order to estimate the companion mass and mass uncertainty. If the companion mass was more than 3σ lower than 13 Jupiter masses, we ruled out the eclipsing binary scenario (see Section 5.1 and Table 6). If the semi-amplitude of the companion mass was more than 1 km s^{-1} we labeled the system as a binary. Five systems were labeled binaries in this manner (see Table 4). If neither of the above cases was true, no action was taken.

Out of the 233 candidate host stars, 43 had more than one TRES spectrum available. The stellar parameters calculated for the spectra of such candidates were combined via a weighted average based on the peak height of the cross-correlation function. The scatter between multiple spectra for the same candidate was not large relative to the assumed systematic errors. For example, Buchhave et al. (2012) set an internal error floor of 50 K for effective temperature; we found an average standard deviation of 40 K between spectra of the same candidate, and the scatter was less 100 K for ∼90% of candidates with multiple spectra.

There were some instances in which a TRES spectrum was not considered good enough for stellar parameter estimation with SPC. In particular, we did not use any spectrum for which the SNR per resolution element was < 20 or the cross-correlation function peak height of the spectrum was < 0.8. Further, we also did not use any spectra that yielded SPC results outside of certain trustworthy ranges. Specifically, we only used spectra that yielded $4250 < T_{\rm eff} < 6500$ and line broadening < 50 km s^{-1}. It should also be noted that all spectra used to determine stellar parameters were collected with TRES on or before 2017 June 10 (although some usable spectra have since been collected, they were not retroactively included in our stellar parameter analysis). No planet candidate underwent the validation process unless their host star had at least one spectrum (collected with TRES) that satisfied these criteria.

4.3. *Contrast Curves*

We quantified the constraints placed on the presence of additional companions in our high-resolution (speckle and adaptive optics) imaging by calculating "contrast curves". A contrast curve specifies at a given distance from the target star how bright a companion star would have to be in order to be detected.

Once speckle observations were collected, the data were reduced according to method described in Furlan et al. (2017), yielding a high-contrast image of a candidate. Then local minima and maxima were analyzed relative to the star's peak brightness to determine Δm (average sensitivity) and its uncertainties within bins of radial distance from the target star. The contrast curves used in this research were the 5σ upper limit on Δm as a function of radial distance. A more detailed description of the data reduction process can be found in Howell et al. (2011). An example of a contrast curve can be seen in Fig. 6.

As for AO observations, the creation of corresponding contrast curves was performed by injecting fake sources into the images and varying their brightness in order to determine the brightness threshold for the detection algorithm being used. This process is described in greater detail in Crossfield et al. (2016); Ziegler et al. (2017)

Note that these processes of creating a contrast curve were the same regardless of wavelength. So in the instances that multiple speckle or adaptive optics images at different wavelengths were available, multiple contrast curves were created that were all used in the validation process for a given candidate.

5. FALSE POSITIVE PROBABILITY ANALYSIS

5.1. *The Application of* `vespa` *to Planet Candidates*

Our validation work relied primarily on a method called Validation of Exoplanet Signals using a Probabilistic Algorithm, or `vespa`, a public package (Morton 2015b) based on the work of Morton (2012). It operates within a Bayesian framework and calculates the False Positive Probability (FPP), the probability that a candidate is an astrophysical false positive rather than a true positive (i.e. a planet).

Once photometry, spectroscopy, and any available high-contrast imaging had been collected and reduced for a candidate system, that system underwent our validation procedure using `vespa`. For each candidate, the following information was supplied:

1. A folded light curve containing the planetary transit and roughly one transit duration of baseline on either side. Identical error bars were assigned to all data points based on the noise parameter determined by our transit fitting procedure. This light curve had the presence of other planets in the system removed using the best-fit parameters determined by the fitting procedure.

2. A secondary threshold limit. We calculate this limit by first cutting out all transits from all candidates in a system. Then, for a given candidate, we phase-fold the data to the candidate's period, bin the baseline flux according to the transit duration of the candidate, calculate the standard deviation between the bin averages, and multiply by three. Effectively, we are asserting that a secondary eclipse has not been detected at a 3σ level or higher.

3. A contrast curve. When available, this lowered the FPP by eliminating the possibility of bound or background stars above a certain brightness at a given projected distance, thus reducing the parameter space in which a false positive scenario could exist. Note that `vespa` doesn't *require* a contrast curve to operate, and in many cases a candidate host star had no contrast curve data available. However, contrast curves were collected from AO or speckle data and provided to `vespa` for 186 of our 233 candidate host stars (see Table 7).

4. RA and Dec. The likelihood of a false positive scenario is calculated by `vespa` based on the target star's location on the celestial sphere. For example, near the Galactic plane a target star's FPP will increase significantly due to the crowded field.

5. $T_{\rm eff}$, $\log g$, and [m/H] (collected from SPC). These constraints help rule out false positive scenarios that would otherwise be allowed given only stellar magnitude information. Although `vespa` *could* operate without these values, we did not apply `vespa` to any candidate system for which stellar parameters could not be estimated from a TRES spectrum.

6. Stellar magnitudes. The K2 Ecliptic Plane Input Catalog (Huber et al. 2016) was queried to find magnitude information on each target star in the Kepler, J, H, and K band passes. The J, H, and K band passes originated from the 2MASS catalog (Cutri et al. 2003; Skrutskie et al. 2006). Magnitude uncertainties were not required or provided for the Kepler band pass, while uncertainties for the J, H, and K band passes were added in quadrature with 0.02 magnitudes of systematic uncertainty to be conservative.

7. Parallaxes. Whenever parallaxes were available from HIPPARCOS (Perryman et al. 1997) or GAIA (Gaia Collaboration et al. 2016a,b) those were also included.

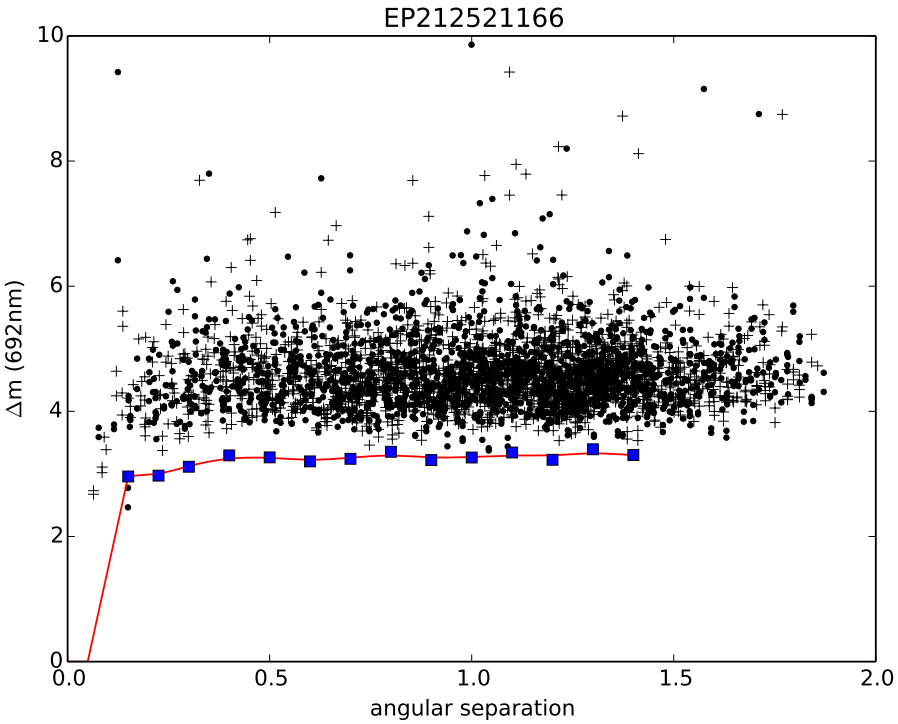

Figure 6. Contrast curve developed from a speckle image at 692 nm (6920 Å) for candidate system EPIC 212521166. The contrast curve is plotted as Δm (average sensitivity to a companion in magnitude difference between the primary and secondary) versus angular separation (in arcseconds). Plus signs and circles are maxima and minima respectively of the background sensitivity in the image. The blue squares are the 5σ sensitivity limit within adjacent angular separation annuli. The red line is the contrast curve itself, a spline fit to the sensitivity limit (the blue squares).

Given all this input, `vespa` makes a representative population for each false positive scenario (and the transiting planet scenario). False positive scenarios considered by `vespa` include a background (or foreground) eclipsing binary blended with the target star, a hierarchical eclipsing binary system, or a single eclipsing binary system (as well as each of those scenarios with twice the period). Then `vespa` calculates a prior for each scenario by multiplying together the probability that the scenario exists within the photometric aperture, the geometric probability that the scenario leads to an eclipse, and the fraction of instances in which the eclipse is appropriate. Here "appropriate" means an instance's eclipse takes place within the photometric aperture, the secondary eclipse (if it exists) is not deep enough to cross the detection threshold, the instance's primary star has wavelength-dependent magnitudes within 0.1 magnitudes of those provided as input, and the instance's primary star has $T_{\rm eff}$ and $\log g$ that agree with the input values to within 3σ.

Then the likelihood for each scenario is calculated using the folded light curve by fitting against a distribution of transit durations, depths, and ingress/egress slopes calculated from each scenario. Once priors and likelihoods have been determined for each scenario, the last step is simply to combine them for each scenario in order to determine an overall posterior likelihood for every scenario. If the posterior likelihood for the planet scenario is exceedingly larger than all of the other scenarios combined, then the candidate can be classified as a validated planet. In our case, we required the sum of all false positive scenario probabilities to be < 0.001.

The output from `vespa` includes simulation information from the underlying light curve fitting process, as well as figures and text files conveying likelihood information of various false positive scenarios and the transiting planet scenario. Section 6.1 provides a concrete validation example with characteristic input and output. Additionally, the full `vespa` input and output for each exoplanet candidate has been archived at `https://zenodo.org/record/1164791`.

As we noted in Section 4.2, for systems where we had collected more than one good TRES spectrum, we phased the RVs to search for or eliminate the possibility of an eclipsing binary scenario. (Small RVs would not rule out hierarchical or background eclipsing binary scenarios since large RVs would be reduced by the third star in the aperture.) In cases where the eclipsing binary scenario could be eliminated, we reduced the probability of the scenario (and the similar scenario analyzed by `vespa` with double the period) to zero. We then divided the probability of all the remaining scenarios investigated by `vespa` by their sum so that the total probability was still one. The values reported in Table 6 already have this adjustment applied.

Systems with multiple planet candidates are more likely to be hosting multiple planets than multiple false positive signals. In fact, the likelihood of the planet scenario for each individual candidate is consequently boosted relative to false positive scenarios in multiplanet candidate systems (Latham et al. 2011). To account for this effect, we apply a "multiplicity boost" to the planet scenario prior in such systems, deflating the FPP by the multiplicity boost factor to account for the nature of these systems. We choose a boost factor of 25 for double candidate systems and a boost factor of 50 for systems with 3+ candidates based on the values used by Lissauer et al. (2012), Vanderburg et al. (2016b), and Sinukoff et al. (2016). The FPP values reported in Table 4 already have the appropriate multiplicity boost factor applied.

5.2. *Criteria for Planet Validation*

Following standard practice, we only validated planets for which the following were true, since `vespa` assumes we have checked for and ruled out each of them:

1. There is not a composite spectrum.
2. There is not a companion in the aperture. (This was determined from archival imaging.)
3. There is not a companion in AO and/or speckle images. (This was determined from our AO and speckle images as well as any images for our candidates uploaded to https://exofop.ipac.caltech.edu/k2/ before 2017 August 9.)
4. There is no evidence of a secondary eclipse (at any arbitrary phase).
5. There is not an ephemeris match (see Section 2.4).

If any of the above were false, the FPP was not reported in Table 4 and the candidate was not validated regardless of the FPP value `vespa` provided.

It is worth noting that recently there have been six validated planets shown to be false positives by follow-up observations and analysis (Cabrera et al. 2017; Shporer et al. 2017). We briefly examine whether these instances are a cause for concern in our own results.

In the case of Cabrera et al. (2017), they found that two false positives exhibited increased transit depths for larger aperture masks (suggesting a nearby star was responsible for the eclipses) while the third showed a secondary eclipse at phase = 0.62 when they used a different data reduction process. The first two false positives would have failed the variable-sized mask test we apply via our diagnostic plots, while the secondary eclipse from the third false positive would have been caught through a combination of our data reduction process and the "model-shift uniqueness" test we apply (Coughlin et al. 2016).

As for Shporer et al. (2017), the `vespa` fit to the available photometry for each false positive was very poor and all three of the false positives were reported to be very large "planets". We addressed these concerns in two ways. First, we decided to only use 2MASS photometry in order to avoid systematic errors between photometric bands. Second, we chose not to validate any planet candidates larger than 8 $R_\oplus$, since a candidate of that size or larger could actually be a small M dwarf. The only exception to this rule is if there are RV measurements that can rule out the eclipsing binary scenario, in which case we do report the FPP (and validate for FPP < 0.001) regardless of planet size.

6. RESULTS

The results section is divided into two parts. In the first part, the process of validation is described in detail

Table 1
System and planetary parameters of EPIC 212521166

Parameter	Unit	This Paper	Osborn et al. (2017)
Orbital parameters			
Period P	days	$13.86391^{+0.00022}_{-0.00023}$	$13.86375 \pm 2.6\times10^{-4}$
Time of first transit[a]	BJD-2454833	$2386.87440^{+0.00072}_{-0.00068}$	$2442.32992 \pm 6.1\times10^{4}$
Orbital eccentricity e	-	0 (fixed)	0.079 ± 0.07
Inclination	degrees	$89.36^{+0.43}_{-0.75}$	$89.35^{+0.41}_{-0.24}$
Transit parameters			
System scale a/R_*	-	$32.3^{+2.0}_{-5.7}$	30.8 ± 1.0
Impact parameter b	-	$0.36^{+0.28}_{-0.23}$	$0.34^{+0.14}_{-0.22}$
Transit duration T_{14}	hours	$3.181^{+0.072}_{-0.047}$	3.22 ± 0.03
Radius ratio $R_{\rm p}/R_*$	-	$0.0334^{+0.0018}_{-0.0007}$	$0.0333 \pm 6.6\times10^{-4}$
Planet parameters			
Planet radius R_p	$R_\oplus$	$2.52^{+0.16}_{-0.10}$	2.592 ± 0.098
Stellar parameters			
Stellar mass M_*	$M_\odot$	0.724 ± 0.025	0.738 ± 0.018
Stellar radius R_*	$R_\odot$	$0.692^{+0.025}_{-0.023}$	0.713 ± 0.020
Effective temperature $T_{\rm eff}$	K	4877 ± 50	5010 ± 50
Surface gravity $\log g$	g cm^{-2}	4.51 ± 0.10	4.60 ± 0.03
Metallicity [m/H][a]	dex	-0.30 ± 0.08	-0.34 ± 0.03
Validation parameters			
FPP	-	8.44×10^{-7}	-

[a]Our reported transit time and that reported by Osborn et al. (2017) differ by 4 orbital periods.
[b]Our reported metallicity is [m/H] (derived from many metal absorption features) while the metallicity reported in Osborn et al. (2017) is [Fe/H] (derived from iron absorption lines only).

for a single planet candidate, in order to explain precisely how the photometry and follow-up observations are used. In the second part, our validation process is more widely applied to every selected candidate and the results for each candidate are reported.

6.1. *Validating a single planet: EPIC 212521166.01*

In order to understand the process that was applied to each of our candidates, it is instructive to look at validation for a single, concrete example. Here, we describe in detail the validation process for a typical planet candidate system, EPIC 212521166 (K2-110). We chose this system because 1) it was detected in our pipeline, and 2) Osborn et al. (2017) has already confirmed and characterized the planet, which allows us to compare some of the system parameters we calculated against their results.

EPIC 212521166 was observed by K2 during Campaign 6. After we produced a light curve from calibrated K2 pixel data and removed systematics (as described in Section 2.2), we searched for transits in our processed light curve (as described in Section 2.3). Our transit search pipeline detected a single, high signal-to-noise threshold crossing event with a period of 13.87 days and a depth of about 0.1%. The signal passed triage (see Section 2.3) and moved on to vetting (see Section 2.4). We confirmed the signal was transit-like, and observed no significant secondary eclipse, phase variations, differences in depth between odd and even transits, aperture-size dependent transit depths, or other indications of a false positive or instrumental false alarm (see Figs. 2, 3, and 4). As a result, we promoted the EPIC 212521166 threshold crossing event to a planet candidate.

Upon its identification as a planet candidate, we observed EPIC 212521166 with the TRES spectrograph on the Mt. Hopkins 1.5m Tillinghast reflector and with the DSSI speckle imaging camera on the 3.5m WIYN telescope at Kitt Peak National Observatory. Using the orbital and transit parameters determined with our transit model, the stellar parameters derived from SPC, a folded light curve of the planetary transit, and two contrast curves in r-band and z-band collected via high-contrast speckle imaging from DSSI on the WIYN telescope (see Fig. 6), `vespa` was employed to determine the FPP for EPIC 212521166.01. The FPP was found to be 8.44×10^{-7}, which was well below the cutoff threshold, so the planet candidate was classified as validated. The key output figure of `vespa` can be seen in Fig. 7.

Like us, Osborn et al. (2017) found EPIC 212521166 to be a metal-poor K-dwarf star hosting planet candidate with $P = 13.9$d and $R_p = 2.6\ R_\oplus$. A comparison of planetary and system parameters can be see in Table 1. Our analyses and theirs are in good agreement for all parameters. Additionally, Osborn et al. (2017) took the further step of obtaining precise radial velocity observations to *confirm* the existence of EPIC 212521166.01, so we can be confident that in this case, `vespa`'s assessment of a low false positive probability was well justified.

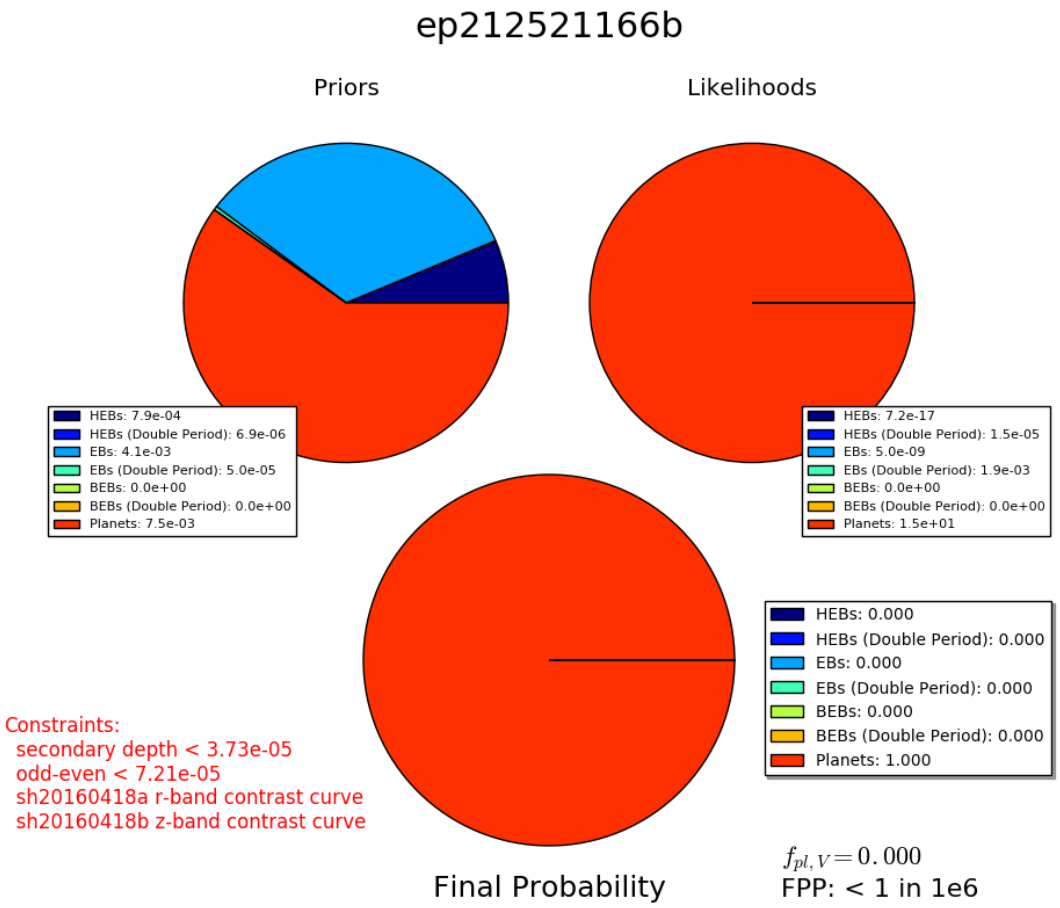

Figure 7. False Positive Probability analysis of EPIC 212521166.01. HEB, EB, and BEB refer to a hierarchical eclipsing binary, eclipsing binary, and background eclipsing binary scenario respectively. Combining the prior likelihood of a false positive scenario (given sky position, contrast curve data, and wavelength-dependent magnitudes), as well as the likelihood of the transit photometry under various scenarios, the posterior distribution highly favors the planet scenario, with FPP = 8.44×10^{-7}. (Note: the true FPP value is always reported in a supplementary file, but for FPP < 1 in 1e6 the figure produced by `vespa` simply reports the FPP as < 1 in 1e6.)

6.2. *Full Validation Results*

The process of validation described for EPIC 212521166.01 in the previous section was similarly applied to the remaining candidates suitable for validation. We identified 275 candidates in 233 systems that had at least one usable TRES spectrum, and the FPP was calculated for each of these candidates (see Table 4).

Occasionally `vespa` failed to return a FPP; in such cases, the lowest data point in the light curve was removed (to aid the initialization process for `vespa`'s trapezoidal transit fit) and `vespa` was reran. This approach worked in most cases, but if it failed again the lowest two data points were removed and `vespa` was reran. If that too was unsuccessful then the FPP was not reported. (Most of the time `vespa` only failed after these steps because of a Roche lobe overflow error.) 149 candidates in 111 systems had a FPP < 0.001 and were thus promoted to validated planet status.

To date, the largest single release of K2 validation results has been Crossfield et al. (2016), with 197 candidates and 104 validated planets in C0-C4. In comparison, 108 of our candidates are from C0-C4, 69 of which are validated. The two samples share 53 candidates in common, 37 of which are validated and 9 of which remain candidates in both analyses. (Additionally, 2 candidates in common are only validated in this work while 5 are only validated in Crossfield et al. 2016). That leaves 55 candidates in our C0-C4 sample (30 of which are validated) that were undetected by Crossfield et al. (2016), as well as 146 candidates (62 of which are validated) in the Crossfield et al. (2016) sample undetected in our own C0-C4 sample. Only ∼21% of the total candidates were detected by both analyses, and only ∼26% of the total validated planets were validated by both analyses.

Table 2
Breakdown of Candidate Dispositions

Previous	Updated Disposition		
Disposition[1]	VP	PC	**All**
VP	53	15	**68**
PC	39	55	**94**
FP	1[2]	1[3]	**2**
UK	56	55	**111**
All	**149**	**126**	**275**

[1] VP = Validated Planet, PC = Planet Candidate, FP = False Positive, UK = Unknown
[2] EPIC 210894022.01. See Section 6.2
[3] EPIC 202900527.01. See Section 6.2

The sample overlap may seem surprisingly small, but it makes more sense when the candidate selection and validation processes are examined. For example, Crossfield et al. (2016) only considered candidates with 1d $<$ P $<$ 37d (19% of our C0-C4 sample was outside that range) and we only considered candidates with $K_{\rm p} < 13$ (48% of their sample was outside that range). If we only consider C0-C4 candidates within those ranges (137 total), both teams find over half of each other's samples, and the overlap between samples rises to 39% (53 candidates). Similarly, for validated planets within those ranges (77 total), both teams find more than two thirds of each other's samples, and the overlap between samples rises to 57% (44 validated planets).

There are many further examples of differences that created discrepancies between the two samples. We required that each planet candidate had at least one usable TRES spectrum (see Sections 3.1 and 4.2), even though in early campaigns TRES spectra weren't collected for all bright candidates. This led to the exclusion of many otherwise promising candidates that are included in Crossfield et al. (2016). Further discrepancies could have arisen from the temperature and planet radius cuts applied to our validated planet sample, the elimination of objects with companions closer than 4" in the Crossfield et al. (2016) candidate sample, and a difference in significance thresholds for TCEs (we used 9σ while they used 12σ).

Table 2 compares the candidate dispositions found in this work against their previous dispositions (according to the NASA Exoplanet Archive[33] and the Mikulski Archive for Space Telescopes[34] (both accessed 2018 February 14). We should note that 15 of our candidates were not validated in this work even though they have been previously validated elsewhere. However, all of these candidates were either restricted from being validated by our conservative criteria for validation (see Section 5.2), or had a FPP value close to our validation cutoff of FPP = 0.001, or were validated using different or additional observations as input to `vespa`. We also note that our work classifies two targets previously labeled as false positives: EPIC 202900527.01 (K2-51 b) and EPIC 210894022.01 (K2-111 b). Shporer et al. (2017) clearly showed EPIC 202900527.01 to be a stellar binary. We don't claim otherwise by labeling it a candidate (since we label all targets with FPP > 0.001 as candidates). On the other hand, Crossfield et al. (2016) previously identified EPIC 210894022.01 as a false positive, but a subsequent, improved `vespa` run showed the target to in fact be a planet (I. Crossfield, private communication). Therefore we do claim this target to be validated.

Another case worth mentioning is the multiplanet system EPIC 228725972, which hosts one validated planet and one candidate ruled out by a companion in the aperture and in a NESSI speckle image. The smallest aperture mask we tested excluded the companion (located approximately 12 arcseconds from the primary) but only exhibited transits for one of the candidates, hence the difference in flags for the two candidates.

In addition to the FPPs and other parameters derived through the validation process described in previous sections, we also calculated the radii and masses of the stars in our sample (having a stellar radius allowed us to calculate absolute planetary radius). We calculated these parameters by inputting stellar effective temperature, metallicity, and surface gravity into the `isochrones` Python package (Morton 2015a). We also found that inputting 2MASS photometry into `isochrones` along with the aforementioned stellar parameters had no noticeable effect on the resulting stellar radius and mass values (or their uncertainties). Although isochrones have been found to underestimate stellar radii before (Dressing et al. 2017a; Martinez et al. 2017; Dressing et al.

[33] https://exoplanetarchive.ipac.caltech.edu/
[34] https://archive.stsci.edu/k2/published_planets/search.php

2017b), this effect is confined to M dwarfs and late K dwarfs, which are largely excluded from our host star sample since we do not consider stars with effective temperatures below 4250 K (see Section 4.2). The derived stellar masses and radii are reported in Table 4. (Also note that all stellar parameters for each system are reported in Table 5).

7. DISCUSSION

7.1. *Lessons Learned*

There have been a few recent instances of false positive misclassification (Cabrera et al. 2017; Shporer et al. 2017), in which a target has been classified as a validated planet but later shown to be a false positive through subsequent analysis. Here, we discuss some of the pitfalls of statistical validation, and share some lessons we have learned and solutions we have implemented to prevent false positive misclassification.

First, spectroscopy is key. Stellar parameters are crucial to understanding the host star and correctly classifying the candidates. For example, identifying the star as highly evolved can prevent an orbiting brown dwarf or M dwarf from being incorrectly labeled as a smaller planet orbiting a main sequence star. One might attempt to avoid this issue by estimating stellar surface gravity via photometry alone, but that is notoriously difficult to do and can lead to incorrectly estimated stellar parameters. Collecting at least one spectrum from which to estimate spectroscopic parameters (including surface gravity) can avoid many issues like this. And collecting more spectra may exclude (or reveal) large RV variations from an eclipsing binary scenario.

Second, a search for secondary eclipses at *all* phases should be performed to exclude highly eccentric binary scenarios. The search method used here was the "model-shift uniqueness" test designed by Coughlin et al. (2016). This method compared off-transit portions of the light curve against the transit portion of the best-fit transit model (and the transit model inverted, to provide a visual comparison of detection significance). An even more rigorous method would consider secondary eclipses of duration and depth distinct from that of the transit.

Third, when validating exoplanets using `vespa` one should be very careful about what broadband photometry is used and what offsets and systematics there are. Statistical validation work on data from the original *Kepler* mission took advantage of high-quality and uniform broadband photometry from the *Kepler* Input Catalog (KIC, Brown et al. 2011). The analogous EPIC catalog for K2 is similarly vital to the analysis of the K2 star and planet sample. However, it is approximately four times larger and was produced by collecting archival photometric measurements; therefore, it is more heterogeneous and more prone to systematic errors and offsets than the KIC. We have found that in some cases, these systematic errors or offsets in photometry can result in untrustworthy FPP estimates, in particular, extremely low FPP measurements for known or likely false positives. For example, when we input to `vespa` all available broadband photometry from the EPIC catalog for the candidate EPIC 211418290.01, `vespa` yields a FPP less than 10^{-6} because it is unable to find an acceptable fit to a binary star model due to underestimated photometric uncertainties and therefore incorrectly rules that false positive scenario out. However, inputting only 2MASS photometry to `vespa` yields a better fit to the eclipsing binary scenario, and `vespa` therefore returns a much higher FPP of about 0.6. Situations like this were not uncommon, which is why we ultimately decided to use only photometry from the all sky 2MASS survey. We chose to use only the 2MASS survey because it provides broadband photometry for all of our candidates and operates in the infrared, reducing the effects of reddening. Including photometry from additional surveys that are calibrated differently and have distinct systematic uncertainties would introduce non-uniformity that would be difficult to quantify and could bias our results.

To be conservative, we also added 0.02 mags of systematic error in quadrature with the reported error for each 2MASS band we used. This will continue to be important after the launch of TESS, which will observe targets selected from the TESS Input Catalog (TIC, Stassun et al. 2017). The TIC will be very important for selecting candidates for observation and follow-up; however, it is being assembled in a manner similar to the EPIC and is approximately ten times larger, so it may have similar or even greater photometric offsets.

Fourth, it is very important to make and remake a candidate's light curve with multiple apertures of varying sizes, in order to determine whether the transit signal originates from the target star or a nearby background star (and thus exclude background false positive scenarios). This test caught many false positives in our own analysis, and has been used successfully before in other candidacy analyses (e.g. Dressing et al. 2017b).

Fifth, transiting giant planets are nearly indistinguishable from eclipsing brown dwarfs or small M-dwarf stars, since they have roughly equal radii. Great care should be taken when interpreting the output of `vespa` for giant planets, and unless there is a clear way to distinguish between the two scenarios (via RV measurements, secondary eclipse detection, composite spectra, etc.), attempts to validate large planets can be difficult and prone to error.

By considering each of the above lessons and incorporating them into future validation analyses, misclassifications of validated planets can be significantly reduced and hopefully eliminated in all but the most perverse scenarios.

We will now investigate some of the individual validated planets in our sample as well as the characteristics of our sample as a whole.

7.2. *A New Brightest Host Star in the K2 and Kepler Planet Samples*

One interesting target in our sample is EPIC 205904628 (HIP 110758, HD 212657), a F7 star observed in Campaign 3. We detected and validated a 2.8 $R_\oplus$ planet on a 10 day orbit. At a V magnitude of 8.24, EPIC 205904628 is now the brightest star at optical wavelengths in the entire *Kepler* and K2 samples to host a validated planet. EPIC 205904628 is just slightly brighter than *Kepler*-21 (V = 8.25), a star of similar spectral type found during the original *Kepler* mission to host a single short-period exoplanet (López-Morales et al. 2016; Howell et al. 2012). TESS is expected to discover planets around many stars this bright and brighter.

We note that due to its brightness, we applied some special care to this star. In particular, we re-reduced the K2 light curve by extracting light curves from larger photometric apertures than our standard pipeline uses. We also incorporated information from 2MASS J-band imaging to rule out additional stars in the photometric aperture by calculating a contrast curve and inputting it to `vespa` to provide deeper imaging constraints than our speckle image.

7.3. *Characteristics of the Sample*

In addition to individual planets in our sample, it is interesting to explore a few of the demographics of the newly validated exoplanet population. Figs. 8-15 reveal various aspects of the validated exoplanet sample and the exoplanet candidate sample.

7.3.1. *The Stellar Magnitude Distribution*

Fig. 8 is a histogram of the distribution of brightnesses for the host stars in our sample compared against brightness for stars hosting known Kepler planets (downloaded from https://exofop.ipac.caltech.edu/; accessed 2017 December 4). Most of the candidates in our population are clustered near stellar magnitudes of $K_{\rm p}$ = 12 to $K_{\rm p}$ = 13, and the cutoff we imposed at $K_{\rm p}$ = 13 is very evident. Also in Fig. 8 is the distribution of brightnesses for host stars to known Kepler planets. That distribution peaks near $K_{\rm p}$ = 15 and drops rapidly at brighter magnitudes. It is more difficult to find planet candidates around faint targets for K2 than for Kepler since the baseline is shorter. Therefore K2 candidates tend to orbit very bright host stars relative to Kepler candidates, making K2 candidates excellent targets for follow-up observations.

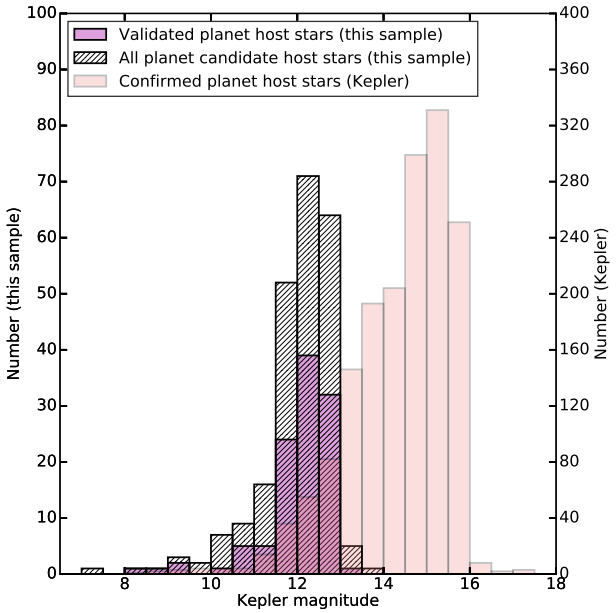

Figure 8. Histograms of Kepler magnitude for host stars to validated planets (purple) and candidate planets (diagonal lines) from C0-C10 of K2 that have been identified in this work, as well as a comparison against host stars to confirmed Kepler planets (pink). There is a fairly sharp cutoff in our sample near magnitude 13, since validation was only conducted on stars for which we had a spectrum and almost all of the spectra we used were for targets brighter than 13th magnitude. The typical Kepler host star is much fainter, with the peak of the distribution near 15th magnitude, which makes K2 target stars much more suitable for follow-up observations than Kepler stars. Also of note: the brightest star hosting a validated planet in our sample is EPIC 205904628, a V = 8.2 star with a 2.8 $R_\oplus$ planet on a 10 day orbit. Validated in this work, EPIC 205904628 is now the brightest host star for a validated planet in either the *Kepler* or K2 samples.

7.3.2. *The Effective Temperature Distribution*

Most of the validated planets and candidates we identified orbit host stars with effective temperatures in the 5000 − 6000 K range. However, out of 233 stars in our sample 41 are cooler than 5000 K and 25 are hotter than 6000 K. No stars in our sample are cooler than 4250 K or hotter than 6500 K. See Fig. 9 for a comparison against the Kepler sample (downloaded from https://exofop.ipac.caltech.edu/; accessed 2017 December 4).

7.3.3. *The Period Distribution*

We also explored the period distribution of our candidate population. As can be seen in Fig. 10, the typical validated planet or candidate has an orbital period of 20 days or less. This should come as no surprise, given the ∼75 day baseline of K2 observations per campaign field. Of 275 candidates in our sample, only 46 have periods over 20 days and only 10 have periods over 40 days.

7.3.4. *The Multiplicity Distribution*

Most of the candidates in our sample (validated or otherwise) are the only candidate in their system to have been detected. However, our sample does include 21 systems with two candidates (15 of those have only validated planets), 9 systems with three candidates (8 of those have only validated planets), and 1 system with four candidates (EPIC 212157262; all candidates in this system are validated). The full multiplicity distribution can be seen in Fig. 11.

7.3.5. *The Planet Radius Distribution*

One of the more interesting features of our sample was the radius distribution. Fig. 12 demonstrates the full planetary radius distribution of our sample for both validated planets and candidates. As expected, there is a sharp cutoff in planet radius for validated planets at $R_{\rm p}$ = 8 $R_\oplus$ (since we generally chose not to validate larger planets).

In order to investigate the radius distribution of the underlying planet population, we adopted and applied a rough completeness correction to our planet sample. We determined the completeness of our K2 planet detection pipeline by performing injection/recovery tests. We injected planet signals into K2 light curves over a range of expected signal-to-noise ratios (analogous to the injection/recovery tests performed by Christiansen et al. 2016, Petigura et al. 2013, and Dressing & Charbonneau 2015 on the *Kepler* pipeline). We then calculated for each of our planet candidates the number of stars observed by K2 around which we could have detected the planet, and weighted the planet's contribution to the histograms by that factor and the geometric transit probability.

The uncorrected and corrected distributions for validated planets and candidates can be seen in Fig. 13, while

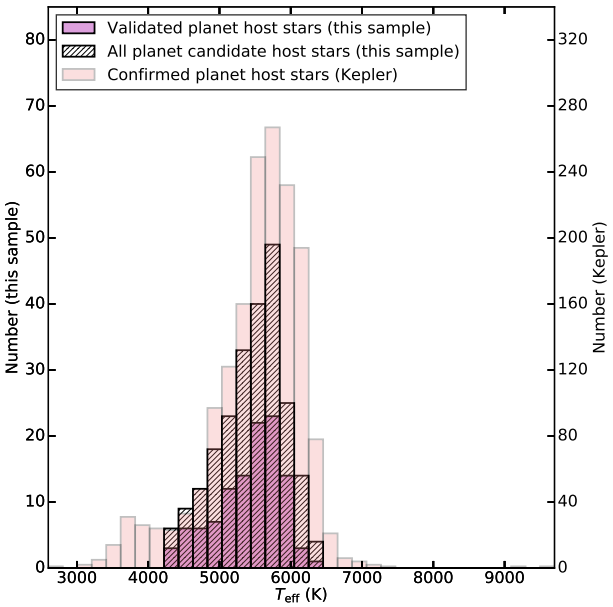

Figure 9. Histograms of effective temperature for host stars to validated planets (purple) and candidate planets (diagonal lines) from C0-C10 of K2 that have been identified in this work, as well as a comparison against host stars to confirmed Kepler planets (pink). Apart from the cutoffs we impose at $T_{\rm eff}$ = 4250 K and 6500 K, our sample follows a similar effective temperature distribution as the Kepler sample.

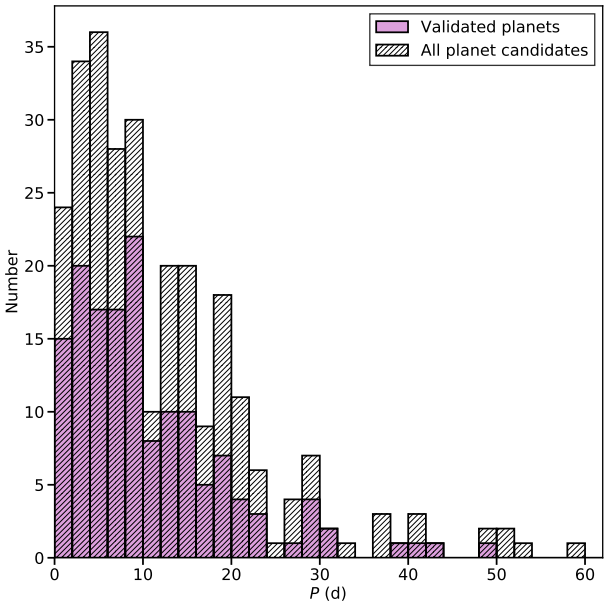

Figure 10. Histogram of orbital period for the validated planets (purple) and candidates (diagonal lines) in C0-C10 of K2 that have been identified in this work. The steep drop off in validated planets and candidates around 20 days is due to the K2 strategy of observing each field for only ∼75 days.

a comparison of our corrected candidate sample to the Fulton et al. (2017) sample and a log-uniform distribution can be seen in Fig. 14. Additionally, a completeness-corrected contour plot of stellar incident flux versus planetary radius for our candidate sample can be seen in Fig. 15 (constructed in the same way as Fig. 10 from Fulton et al. 2017).

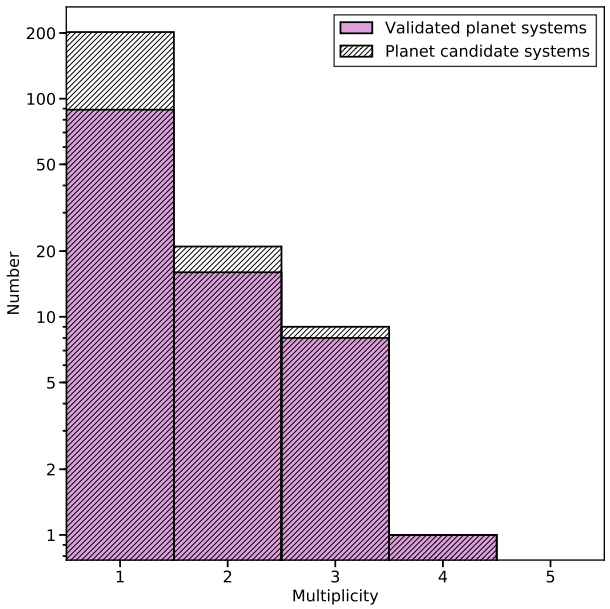

Figure 11. Histogram of multiplicity for the validated planet systems (purple) and planet candidate systems (diagonal lines) in C0-C10 of K2 that have been identified in this work. (A validated planet system is a system for which all candidates have been validated.) Most validated planets and candidates have no detected candidate companions in their system. The largest system in the sample is EPIC 212157262, which hosts four validated planets.

By visual inspection of these figures alone, our corrected candidate sample appears to exhibit a gap in the radius frequency around 1.8 to 2.0 $R_\oplus$, similar to the gap in the Kepler planet sample explored by Fulton et al. (2017). They argued that the underlying astrophysical effect could be photoevaporation, whereby stellar incident flux strips a planet's H/He atmosphere if the atmosphere is not thick enough, leaving a population of stripped, rocky planets and an untouched population of larger, gaseous mini-Neptunes (Owen & Wu 2013; Lopez & Rice 2016; Owen & Wu 2017; Van Eylen et al. 2017). As an alternative hypothesis, they also suggested that gas accretion could be delayed during planet formation until the protoplanetary disk is already gas poor, creating a population of small, rocky planets (Lee et al. 2014; Lee & Chiang 2016).

We wanted to analyze in a more quantitative fashion how the completeness-corrected radius distribution of our K2 candidates compared to the completeness-corrected Kepler candidates from Fulton et al. (2017); we also decided to compare against a log-uniform distribution to probe the significance of a possible bimodality Fulton et al. (as 2017, does). We binned all three normalized distributions in 0.1 $R_\oplus$ intervals from $1.2 - 2.5$ $R_\oplus$. We assigned error bars to our own sample and the Fulton et al. (2017) sample via Poisson statistics (for the number of candidates in each bin) and then scaled the uncertainty according to the completeness-correction scaling applied to each bin.

We then calculated $\chi^2_{\rm reduced}$ between our sample and that of Fulton et al. (2017) as well as our sample and

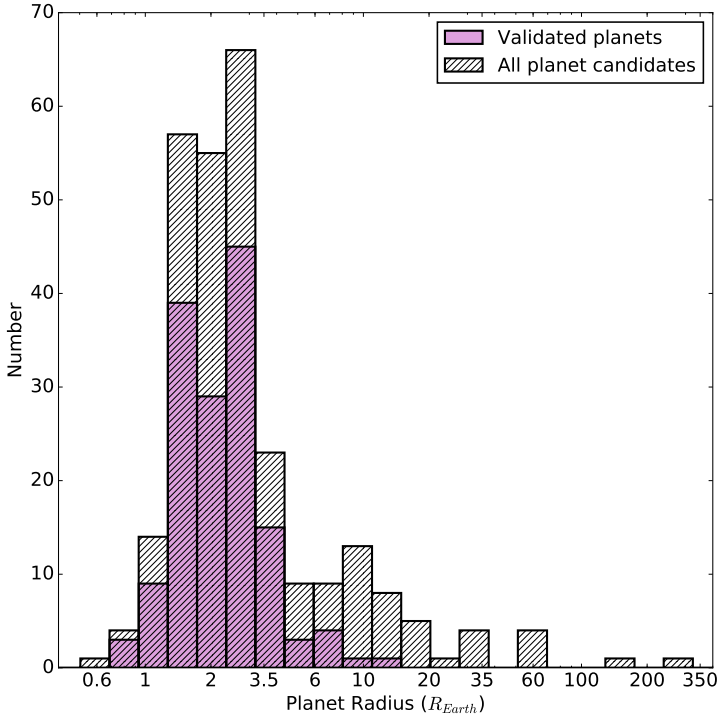

Figure 12. Histogram of planetary radius for the validated planets (purple) and candidates (diagonal lines) in C0-C10 of K2 that have been identified in this work. See Figs. 13 and 14 for narrower ranges, a completeness correction, and a comparison against the Fulton et al. (2017) planet candidate sample.

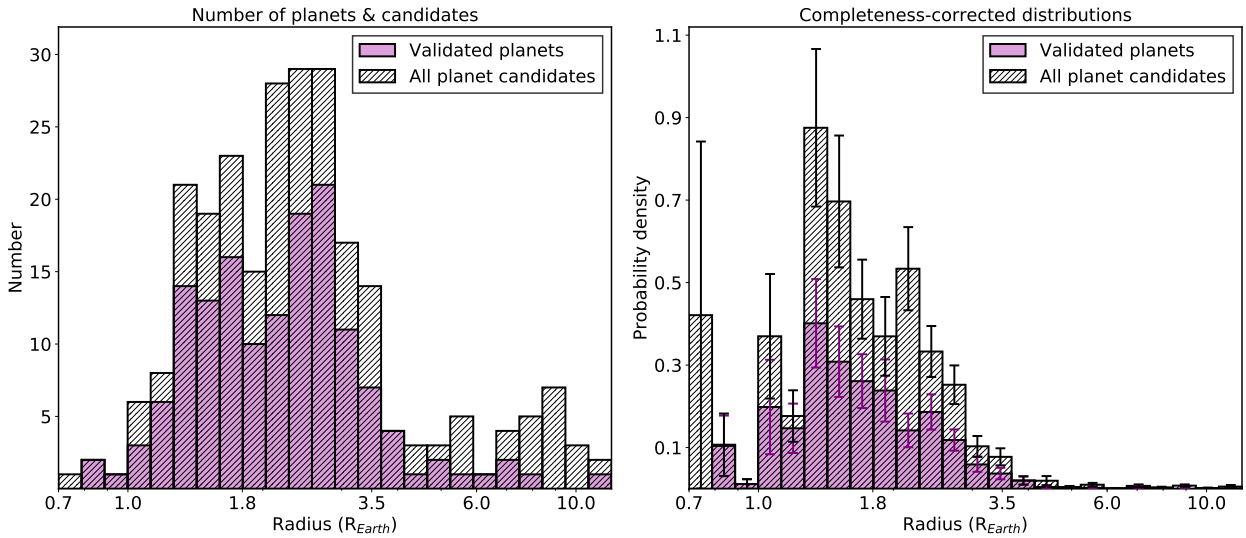

Figure 13. Left: Histogram of planetary radius for the validated planets (purple) and candidates (diagonal lines) in C0-C10 of K2 that have been identified in this work (between $0.7 - 12$ $R_{\oplus}$). Right: Same data as presented in the left panel, with a completeness-corrected applied to estimate the underlying planet population. Error bars for each bin correspond to $1/\sqrt{n}$ (where n is the number of objects in the bin) scaled according to the completeness correction subsequently performed. Through visual inspection, the full candidate sample appears to exhibit a frequency gap centered near 1.8 to 2.0 $R_{\oplus}$.

the log-uniform distribution, finding values of 2.21 and 2.34 respectively. Across all bin numbers from 5 to 20 for which there were more than two candidates in every (equally sized and spaced) bin for all samples, the average $\chi^2_{\rm reduced}$ was 2.21 between our sample and the Fulton et al. (2017) and 2.95 between our sample and the log-uniform distribution. However, we note that a large portion of the $\chi^2_{\rm reduced}$ between our sample and that of Fulton et al. (2017) is caused by only the smallest radius bin. Still, the Fulton et al. (2017) sample did not provide a significant improvement in goodness of fit than a simple log-uniform distribution. This suggests that the visual gap in our candidate sample cannot be quantitatively confirmed unless future observations and planet detections are made to increase the sample size.

7.3.6. *Future Applications*

The K2 mission has thus far conducted observations through more than 15 campaigns, and it will continue observations for future campaigns until it expends all of its fuel. Given that the validation infrastructure built for this research is directly applicable to future campaigns, we will be able to identify and validate exoplanet candidates from upcoming campaigns as quickly as the necessary follow-up observations can be collected.

This research will also be useful even after the end of the K2 mission. The upcoming TESS mission (Ricker et al. 2015) is expected to yield more than 1500 total exoplanet discoveries, but it is also estimated that TESS will detect over 1000 false positive signals (Sullivan et al. 2015). Even so, one (out of three) of the level one baseline science requirements for TESS is to measure the masses of 50 planets with $R_p < 4\ R_\oplus$. Therefore, there will need to be an extensive follow-up program to the primary photometric observations conducted by the spacecraft, including careful statistical validation to aid in the selection of follow-up targets. The work presented here will be extremely useful in that follow-up program, since only modest adjustments will allow for the validation of planet candidate systems identified by TESS rather than K2.

8. SUMMARY AND CONCLUSIONS

In this paper, we processed 208,423 targets from C0-C10, removed instrumental systematics from the K2 photomtry, and searched for threshold crossing events. We identified ∼30,000 TCEs, which were subjected to triage and vetting. Of those, ∼1,000 targets systems passed both and were upgraded to candidates. And of those, 275 candidates in 233 systems had at least one usable TRES spectrum. For each candidate, we also collected and analyzed follow-up observations including spectroscopy and high-contrast imaging. We derived transit/orbital parameters from the K2 photometry, stellar parameters from the spectra, and contrast curves from the high-contrast imaging. Then, using these results, we determined the false positive probability (FPP) of each planet candidate using the `vespa` validation procedure (Morton 2012, 2015b), which calculates the likelihood of various false positive scenarios as well as the true positive scenario. These FPP values were then adjusted appropriately for systems with radial velocity measurements and for multiplanet systems (see Section 5.1). We reported the resulting FPPs for our planet candidates (see Table 4) and classified candidates with FPP < 0.001 as validated planets.

149 of the 275 candidates had a FPP below the validation threshold of 0.001, while 126 remained candidates (FPP > 0.001). According to the NASA Exoplanet Archive[35] and the Mikulski Archive for Space Telescopes[36] (both accessed 2018 February 14), of the 149 newly validated exoplanets, 56 have not been previously detected, 39 have already been identified as candidates, 53 have already been validated, and 1 has previously been classified as a false positive (EPIC 210894022.01; see Section 6.2). As a result, this work will increase the validated K2 planet sample by nearly 50% (and increase the K2 candidate sample by ∼20%. The full disposition results can be found in Table 2.

Most of the newly validated exoplanets orbited host stars with $12 < K_{\rm p} < 13$ and 5000 K $< T_{\rm eff} <$ 6000 K. Additionally, the majority of validated planets had orbital periods < 20d and planetary radii between $1 - 4$ $R_\oplus$. Our complete candidate sample also shows signs of a frequency gap in the radius distribution (see Fig 14), similar to the gap found by Fulton et al. (2017). However, further analysis with a larger planet sample is required to confirm the radius gap for K2 planets.

This work has clear broader implications. The ability to validate planet candidates is vital to conducting a successful follow-up and confirmation program. The wide applicability of the validation infrastructure developed in this research is clear from the large number of candidates subjected to our validation process. By continuing to apply the validation process described here, future K2 campaigns and the upcoming TESS mission will benefit from a valuable source of validated planets and a useful validation pipeline able to process the large and constant supply of identified planet candidates.

Many thanks to Guillermo Torres and Dimitar Sasselov for their review and grading of this work during its phase as a thesis project. We thank Joey Rodriguez, George Zhou, Sam Quinn, Jeff Coughlin, and Tom Barclay for useful conversations and assistance vetting some of our candidates. We are grateful to BJ Fulton for providing us access to useful contour plotting tools, and also for allowing for the reproduction of a plot from another paper. Special thanks to Ellen Price for crucial assistance, time, and effort in setting up `vespa`. Finally, A.W.M. wishes to thank Prof. David Charbonneau and the classmates of Astronomy 99 for their regular support and feedback.

A.W.M, A.V., and E.J.G are supported by the NSF Graduate Research Fellowship grant nos. DGE 1752814, 1144152, and 1339067, respectively. This work was performed in part under contract with the California Institute of Technology (Caltech)/Jet Propulsion Laboratory (JPL) funded by NASA through the Sagan Fellowship Program executed by the NASA Exoplanet Science Institute. A.V. and D.W.L. acknowledge partial support from the TESS mission through a sub-award from the Massachusetts Institute of Technology to the Smithsonian Astrophysical Observatory.

[35] https://exoplanetarchive.ipac.caltech.edu/
[36] https://archive.stsci.edu/k2/published_planets/search.php

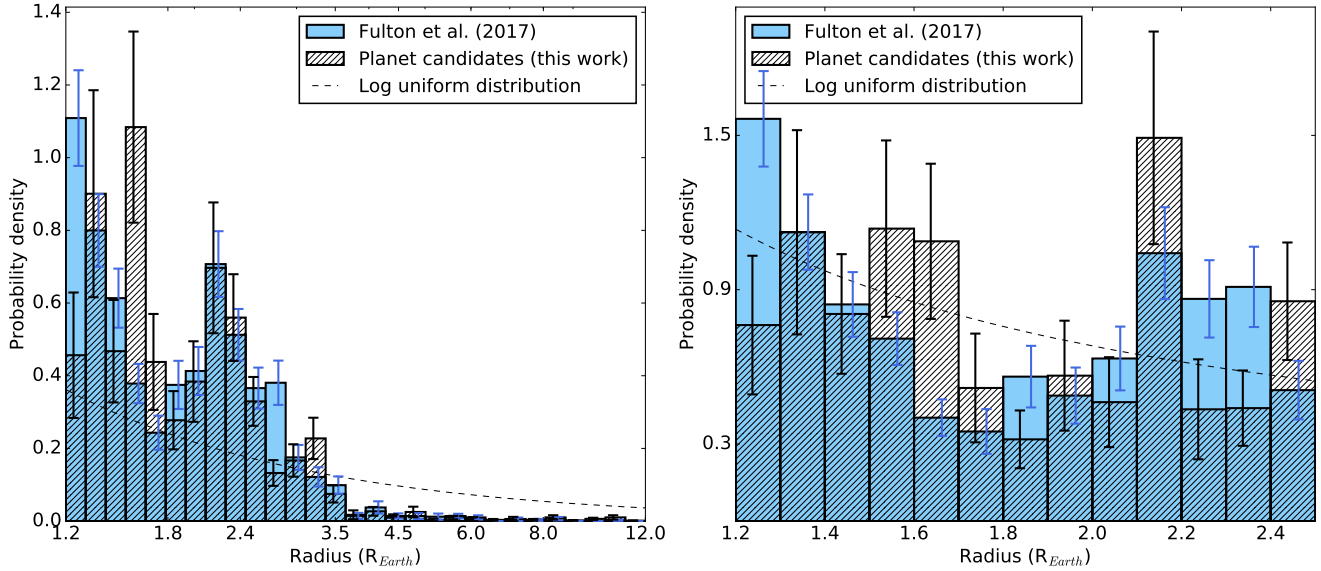

Figure 14. Left: Completeness-corrected comparison of the radius distribution between $1.2 - 12.0$ $R_\oplus$ for all candidate planets identified in this work (thatched), the planet sample analyzed in Fulton et al. (2017, blue), and a normalized log-uniform distribution (dashed line). Right: Comparison of the same distributions as the left panel, now focused on planet candidates with radii between $1.2 - 2.5$ $R_\oplus$. The frequency gap identified by Fulton et al. (2017) can clearly be seen in their distribution. A similar gap tentatively appears in our sample (near 1.8 to 2.0 $R_\oplus$), although a log-uniform distribution provides a fit to our sample roughly as good as the Fulton et al. (2017) distribution.

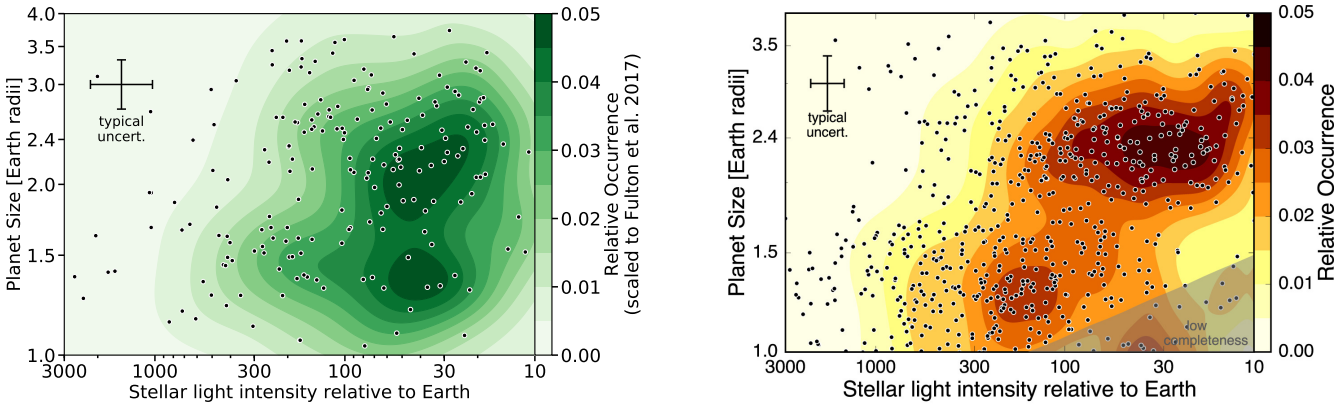

Figure 15. Left: Contour plot of incident stellar flux versus planetary radius. The black points are the 275 candidates in our sample and the typical uncertainty is plotted in the top left. The contours are completeness-corrected and roughly scaled to the same height as those in Fig. 10 from Fulton et al. (2017). The contours show tentative visual evidence of a gap in the radius frequency near 1.6 to 1.8 $R_\oplus$. Right: Top panel of Fig. 10 from Fulton et al. (2017, taken with permission), with a similar gap near 1.6 to 1.8 $R_\oplus$.

Some observations in the paper made use of the NN-EXPLORE Exoplanet and Stellar Speckle Imager (NESSI). NESSI was funded by the NASA Exoplanet Exploration Program and the NASA Ames Research Center. NESSI was built at the Ames Research Center by Steve B. Howell, Nic Scott, Elliott P. Horch, and Emmett Quigley. The NESSI data were obtained at the WIYN Observatory from telescope time allocated to NN-EXPLORE through the scientific partnership of the National Aeronautics and Space Administration, the National Science Foundation, and the National Optical Astronomy Observatory.

This paper includes data collected by the *Kepler*/K2 mission. Funding for the *Kepler* mission is provided by the NASA Science Mission directorate. Some of the data presented in this paper were obtained from the Mikulski Archive for Space Telescopes (MAST). STScI is operated by the Association of Universities for Research in Astronomy, Inc., under NASA contract NAS5–26555. Support for MAST for non–HST data is provided by the NASA Office of Space Science via grant NNX13AC07G and by other grants and contracts. Support from the Kepler Participating Scientist Program was provided via NASA grant NNX14AE11G. The authors are honored to be permitted to conduct observations on Iolkam Duag (Kitt Peak), a mountain within the Tohono O'odham Nation with particular significance to the Tohono O'odham people. Some of the data presented herein were obtained at the WM Keck Observatory (which is operated as a scientific partnership among Caltech, UC, and NASA). The authors wish to recognize and acknowledge the very significant cultural role and reverence that the summit of Mauna Kea has always had within the indigenous Hawaiian community. We are most fortunate to have the opportunity to conduct observations from this mountain.

Facilities: Kepler, FLWO:1.5m (TRES), WIYN (DSSI, NESSI), Gemini:Gillett (DSSI, NIRI), Gemini:South (DSSI), Keck:II (NIRC2), Hale (PHARO), LBT (LMIRCam), Gaia, HIPPARCOS, Exoplanet Archive, ADS, MAST

APPENDIX

CALIBRATING TRES TO MEASURE THE MT. WILSON $S_{\rm HK}$ INDEX

Our work involved the analysis of many spectra collected with the Tillinghast Reflector Echelle Spectrograph (TRES) on the 1.5-m Tillinghast telescope at the Whipple Observatory on Mt. Hopkins. In addition to using TRES spectra to derive spectroscopic parameters and measure radial velocities, we also used TRES to measure the Mt. Wilson $S_{\rm HK}$ activity indicator. $S_{\rm HK}$ is a ratio between the flux in the cores of the Calcium II H and K spectral features (at 3933.66 ± 1.09 and 3968.47 ± 1.09 Å) and the flux in two nearby continuum regions (one slightly redward of the Ca II lines called R and one slightly blueward called V). $S_{\rm HK}$ is commonly used as a proxy for a star's chromospheric activity (Isaacson & Fischer 2010). Because $S_{\rm HK}$ depends on ratios of fluxes at different wavelengths, it is sensitively affected by a spectrograph's blaze function. The effect of the spectrograph's blaze function must therefore be carefully calibrated and quantified in order to standardize measurements of $S_{\rm HK}$ from different instruments. In this appendix, we describe how we calibrated the TRES spectrograph to place measurements of $S_{\rm HK}$ on the Mt. Wilson scale, and present our measurements of $S_{\rm HK}$ for a handful of bright K2 planet candidate hosts for which we were able to measure $S_{\rm HK}$ reliably. These measurements are listed in Table 3.

To calibrate TRES to measure $S_{\rm HK}$ on the Mt. Wilson scale, we closely followed the procedure of Isaacson & Fischer (2010). We based our calibration on a sample of stars that were both observed by TRES (prior to 2016 June 1) and were included in the Duncan et al. (1991) catalog of Mt. Wilson $S_{\rm HK}$ measurements. Additionally, the following cuts were applied to improve the sample quality:

1. TRES spectra for the star in question were only used if the photon count in the R continuum region (4001.07 ± 10 Å) was greater than 174,000. (The cutoff is actually at 150,000 ADU, which is converted using a gain of 1.16 for TRES.) This conservative cutoff was imposed to remove spectra with only low or moderate SNR from the calibration.

2. The star was not in a close binary or multiple system. We only included widely separated ($\gtrsim 5''$) visual binaries in order to prevent flux from the companion star(s) being blended with flux of the intended target.

3. One rapidly rotating star (HD 30780, or 'VB123' in the TRES database) was removed from the calibration set as the H and K emission cores were clearly broadened and smeared with other spectral features ($v \sin i \simeq 180$ km s^{-1}).

After these cuts, our calibration sample included 118 stars with a total of 1204 individual TRES observations. The calibration was done in the same way as Isaacson & Fischer (2010), by determining values of $K_{\rm coeff}$, $V_{\rm coeff}$, m, and b that minimize the differences between the Mt. Wilson survey's measurement of $S_{\rm HK}$ for each star (Duncan et al. 1991) and $S_{\rm HK}$ calculated from the TRES spectra using the following equation:

$$S_{\rm HK,TRES} = m \times \frac{H + K_{\rm coeff} K}{R + V_{\rm coeff} V} + b \qquad \text{(A1)}$$

where H and K are fluxes in the cores of the Ca II H and K lines[37], R and V are continuum fluxes [38], $K_{\rm coeff}$ is a coefficient that scales the magnitude of K fluxes to match the magnitude of H fluxes, $V_{\rm coeff}$ is a coefficient that scales the magnitude of V fluxes to match the magnitude of R fluxes, and m and b are free parameters.

$K_{\rm coeff}$ was calculated through a linear regression between H and K for our TRES spectra, so as to scale the magnitude of K to match that of H. The same process was performed for R and V in order to calculate $V_{\rm coeff}$. This was done to mirror the approach taken by Isaacson

[37] The H and K fluxes were calculated by integrating the spectrum over triangular-shaped bandpasses centered at 3933.66 and 3968.47 Å respectively, each with a FWHM of 1.09 Å.

[38] The R and V fluxes were calculated by integrating the spectrum over 20 Å wide box-shaped bandpasses centered at 4001.07 Å and 3901.07 Å, respectively, following Duncan et al. (1991).

& Fischer (2010) in their calibration of the Keck HIRES instrument.

We estimated m and b by minimizing the differences between $S_{\rm HK,Mt.Wilson}$ from the Mt. Wilson survey (Duncan et al. 1991) and $S_{\rm HK,TRES}$ determined from TRES spectra with Equation A1 using a Markov chain Monte Carlo (MCMC) algorithm with affine invariant ensemble sampling (Foreman-Mackey et al. 2013). We calculated the likelihood, $\mathcal{L}$, using the following function:

$$\ln(\mathcal{L}) = -0.5 \sum \left(\frac{(S_{\rm HK,TRES} - S_{\rm HK,Mt.Wilson})^2}{\sigma^2} + \ln \sigma^2 \right) \tag{A2}$$

where σ is a "jitter" term that absorbs uncertainties in both measurements of $S_{\rm HK}$ as well as uncertainties due to factors including astrophysical variability in the $S_{\rm HK}$ index of a single star over time. We imposed uniform priors on m and b, and imposed a Jeffreys prior on σ.

It is important to note that for a given star, there could be both multiple TRES spectra and multiple Mt. Wilson $S_{\rm HK}$ measurements. So if a star had more than one TRES spectrum or Mt. Wilson $S_{\rm HK}$ measurement that star was simply represented as a grid of TRES and Mt. Wilson measurements in the MCMC process. With this in mind, the total number of data points in the fitting process was 3108. This implicitly gives higher weight in our calibration to stars with multiple observations, which helps average out astrophysical variability in $S_{\rm HK}$.

Our MCMC process used 200 chains of 50,000 steps each in order to explore parameter space and determine best-fit parameters and uncertainties. The resulting ensemble was well converged according to the Gelman-Rubin statistic (Gelman & Rubin 1992), which in this case was less than 1.04 for all parameters. The last 500 samples of the MCMC process are visualized in Figure 16 with a posterior corner plot (Foreman-Mackey 2016). We found the following parameter values from our model fit:

$$K_{\rm coeff} = 0.876$$

$$V_{\rm coeff} = 0.775$$

$$m = 15.496^{+0.068}_{-0.069}$$

$$b = -0.0031 \pm 0.0015$$

$$\ln(\text{jitter}) = -3.119 \pm 0.013$$

There was also significant covariance between m and b (see Fig. 16), which we estimated to be $\mathrm{Cov}(m, b) = -8.571 \times 10^{-5}$.

Statistical uncertainties, $\sigma_{\rm random}$, for $S_{\rm HK}$ were calculated by propagating sample draws from four Poisson distributions representing R, V, H, and K through draws from the m and b posterior distributions and the $K_{\rm coeff}$ and $V_{\rm coeff}$ values. We also included a systematic error term, $\sigma_{\rm systematic}$, in our uncertainty estimates. We estimated the systematic uncertainties for TRES $S_{\rm HK}$ measurements using 6 high signal-to-noise spectra of the bright star Tau Ceti collected with TRES on the night of 2013 October 24. We assumed that $S_{\rm HK}$ for Tau Ceti remained constant over the course of a single night, and estimated a systematic error term based on the scatter

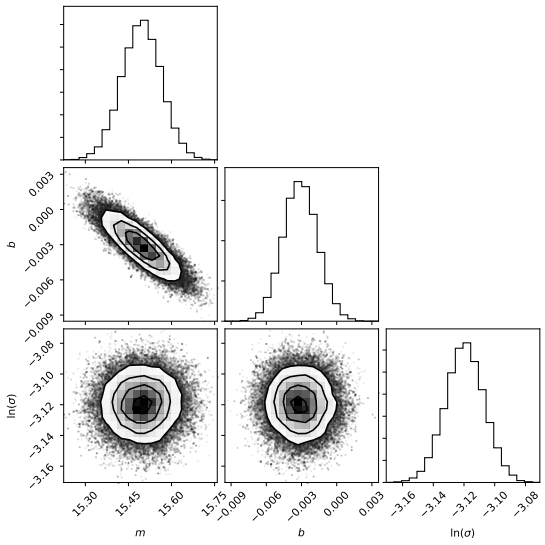

Figure 16. Corner plot for three parameters in our calibration of the Tillinghast Reflector Echelle Spectrograph for $S_{\rm HK}$, an indicator of stellar activity: a line slope (m) and a line y-intercept (b) in our $S_{\rm HK}$ equation, as well as a noise parameter ($\ln(\sigma)$) to account for error bars and stellar variability.

between individual $S_{\rm HK}$ measurements. Our final error estimates, $\sigma_{\rm total}$ came from assuming the statistical uncertainties and systematic uncertainties were independent and could be added in quadrature as follows:

$$\sigma^2_{\rm total} = \sigma^2_{\rm systematic} + \sigma^2_{\rm random} \tag{A3}$$

We note that our calibration for $S_{\rm HK}$ is only valid over specifics ranges in parameter values. Our calibration was performed over a range of 0.244 to 1.629 in B-V and yielded $S_{\rm HK}$ values ranging from 0.055 to 2.070. Based on tests with simulated data and with real low signal-to-noise data, we are cautious of $S_{\rm HK}$ measurements on spectra with fewer than 290,000 photon counts (or 250,000 ADU) in the R and V continuum regions combined. We also note that $S_{\rm HK}$ measurements can be affected by rapid stellar rotation. We found by artificially broadening the lines of slowly rotating stars that $S_{\rm HK}$ measurements for stars with $v \sin i$ above 20 km s^{-1} can be skewed compared to the values that would have been measured if the stars were slowly rotating.

We tested our calibration by comparing $S_{\rm HK}$ measurements derived from TRES with a "test set" of $S_{\rm HK}$ measurements from literature (in particular, we focused on stars observed by Isaacson & Fischer 2010). We constructed the test data set by identifying stars observed by TRES with the following properties:

1. The stars were not included in our calibration set (stars observed both by Duncan et al. 1991 and TRES).

2. The TRES spectra for the star in question have photon counts in the R continuum region greater than 174,000 (or 150,000 ADU).

3. The star had at least one $S_{\rm HK}$ measurement from Keck HIRES that had been reported in Isaacson & Fischer (2010).

After applying these cuts we were left with a test set of 121 stars, which had been observed a total of 4308 times by TRES.

We show the results of our $S_{\rm HK}$ calibration in Figure 17, which compares TRES $S_{\rm HK}$ measurements from our calibration set with measurements from the Mt. Wilson survey, and in Figure 18, which compares TRES $S_{\rm HK}$ measurements from our test set with values from Isaacson & Fischer (2010).

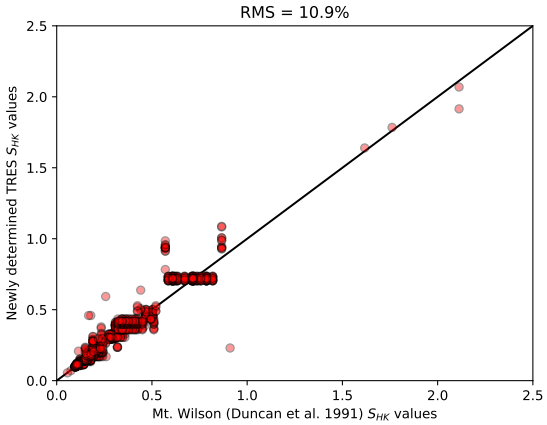

Figure 17. A comparison of our $S_{\rm HK}$ calibration for TRES against the Duncan et al. (1991) catalog for our calibration data set of 118 stars (with 1204 TRES spectra). Each red point denotes a unique pair of observations from TRES and Mt. Wilson for a given star. The fractional RMS scatter on the calibration set is 11.0%.

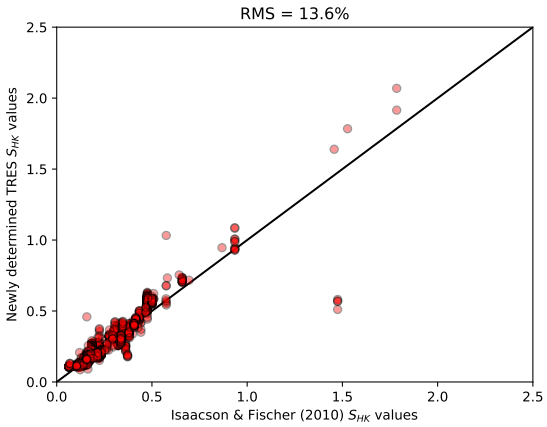

Figure 18. A comparison of our $S_{\rm HK}$ calibration for TRES against the Isaacson & Fischer (2010) catalog for our test data set of 121 stars (with 4308 TRES spectra). Each red point denotes a unique pair of observations from TRES and Mt. Wilson for a given star. The fractional RMS scatter on the calibration set is 13.6%.

For the calibration set, there is an 10.9% fractional RMS scatter about the one-to-one line. The only noticeable outlier appears to be at approximately (0.9,0.2), corresponding to the single TRES spectrum (and Mt. Wilson measurement) of HD 120477, a variable star observed in July 2015 by TRES and observed no later than 1991 at Mt. Wilson. The reason for this outlier could not be identified, but its presence in the calibration set did not significantly change the calibration so it was left in (removing the point maintained a fractional RMS scatter of 10.9%.)

As for the test set, there is a 13.6% fractional RMS scatter about the one-to-one line, slightly larger than for the calibration set (which is to be expected). There does appear to a slight systematic offset between TRES and Keck HIRES such that $S_{\rm HK}$ values from Keck HIRES tend to be smaller than those from TRES. However, this is to be expected, since the same systematic underestimation with Keck HIRES compared to Mt. Wilson can be seen in Fig. 4 of Isaacson & Fischer (2010). There are also a few obviously errant data points in this figure, centered around (1.5, 0.5). These data points correspond to four TRES spectra of the star GJ 570B, a spectroscopic binary. The test data set, because it was not used for calibration, was not clipped of binary stars; thus, GJ 570B is a clear example of how calculating $S_{\rm HK}$ for close binaries can go wrong. However, the presence of those four spectra has very little effect on the results; removing them only reduced the fractional RMS scatter of the test set to 13.5%.

Table 3
Stellar S_{HK} Activity Index

EPIC	Date	S_{HK}
201437844	2017-01-08	$0.1666^{+0.0030}_{-0.0031}$
201437844	2017-03-09	0.1698 ± 0.0032
201437844	2017-03-09	0.1589 ± 0.0031
201437844	2017-03-09	0.1712 ± 0.0031
201437844	2017-03-09	$0.1651^{+0.0030}_{-0.0029}$
201437844	2017-03-09	0.1624 ± 0.0030
201437844	2017-03-09	$0.1633^{+0.0030}_{-0.0029}$
201437844	2017-03-09	0.1614 ± 0.0029
201437844	2017-03-09	0.1692 ± 0.0029
201437844	2017-03-09	$0.1622^{+0.0030}_{-0.0029}$
201437844	2017-03-09	0.1635 ± 0.0028
201437844	2017-03-09	$0.1593^{+0.0029}_{-0.0027}$
201437844	2017-03-09	$0.1615^{+0.0028}_{-0.0029}$
201437844	2017-03-09	$0.1680^{+0.0028}_{-0.0029}$
201437844	2017-03-09	0.1646 ± 0.0029
201437844	2017-03-09	0.1639 ± 0.0028
201437844	2017-03-09	0.1651 ± 0.0028
201437844	2017-03-09	0.1656 ± 0.0029
201437844	2017-03-09	0.1693 ± 0.0029
201437844	2017-03-09	0.1641 ± 0.0029
201437844	2017-03-09	0.1680 ± 0.0029
205904628	2015-07-24	$0.1550^{+0.0029}_{-0.0030}$
205904628	2015-09-06	$0.1453^{+0.0031}_{-0.0033}$
211424769	2015-12-09	$0.3255^{+0.0040}_{-0.0039}$
211424769	2016-01-01	$0.3144^{+0.0040}_{-0.0039}$
211993818	2015-11-27	$0.4189^{+0.0044}_{-0.0045}$
211993818	2016-02-29	$0.3851^{+0.0031}_{-0.0030}$
211993818	2016-03-02	$0.3115^{+0.0027}_{-0.0028}$

REFERENCES

Adams, E. R., Jackson, B., & Endl, M. 2016, AJ, 152, 47
Barros, S. C. C., Demangeon, O., & Deleuil, M. 2016, A&A, 594, A100
Batalha, N. M., Rowe, J. F., Gilliland, R. L., et al. 2010a, ApJ, 713, L103
Batalha, N. M., Borucki, W. J., Koch, D. G., et al. 2010b, ApJ, 713, L109
Borucki, W., Koch, D., Basri, G., et al. 2008, in IAU Symposium, Vol. 249, Exoplanets: Detection, Formation and Dynamics, ed. Y.-S. Sun, S. Ferraz-Mello, & J.-L. Zhou, 17–24
Brown, T. M., Latham, D. W., Everett, M. E., & Esquerdo, G. A. 2011, AJ, 142, 112
Buchhave, L. A., Latham, D. W., Johansen, A., et al. 2012, Nature, 486, 375
Cabrera, J., Barros, S. C. C., Armstrong, D., et al. 2017, ArXiv e-prints, arXiv:1707.08007
Carter, J. A., Fabrycky, D. C., Ragozzine, D., et al. 2011, Science, 331, 562
Christiansen, J. L., Clarke, B. D., Burke, C. J., et al. 2016, ApJ, 828, 99
Christiansen, J. L., Vanderburg, A., Burt, J., et al. 2017, AJ, 154, 122
Ciardi, D. R., Beichman, C. A., Horch, E. P., & Howell, S. B. 2015, ApJ, 805, 16
Coughlin, J. L., Thompson, S. E., Bryson, S. T., et al. 2014, AJ, 147, 119
Coughlin, J. L., Mullally, F., Thompson, S. E., et al. 2016, ApJS, 224, 12
Crossfield, I. J. M., Petigura, E., Schlieder, J. E., et al. 2015, ApJ, 804, 10
Crossfield, I. J. M., Ciardi, D. R., Petigura, E. A., et al. 2016, ApJS, 226, 7
Crossfield, I. J. M., Ciardi, D. R., Isaacson, H., et al. 2017, AJ, 153, 255
Cutri, R. M., Skrutskie, M. F., van Dyk, S., et al. 2003, VizieR Online Data Catalog, 2246
David, T. J., Hillenbrand, L. A., Petigura, E. A., et al. 2016, Nature, 534, 658
Dressing, C. D., & Charbonneau, D. 2015, ApJ, 807, 45
Dressing, C. D., Newton, E. R., Schlieder, J. E., et al. 2017a, ApJ, 836, 167
Dressing, C. D., Vanderburg, A., Schlieder, J. E., et al. 2017b, AJ, 154, 207
Duncan, D. K., Vaughan, A. H., Wilson, O. C., et al. 1991, ApJS, 76, 383
Foreman-Mackey, D. 2016, The Journal of Open Source Software, 24, doi:10.21105/joss.00024
Foreman-Mackey, D., Hogg, D. W., Lang, D., & Goodman, J. 2013, PASP, 125, 306
Foreman-Mackey, D., Montet, B. T., Hogg, D. W., et al. 2015, ApJ, 806, 215
Fulton, B. J., Petigura, E. A., Howard, A. W., et al. 2017, AJ, 154, 109
Furlan, E., Ciardi, D. R., Everett, M. E., et al. 2017, AJ, 153, 71
Gaia Collaboration, Brown, A. G. A., Vallenari, A., et al. 2016a, A&A, 595, A2
Gaia Collaboration, Prusti, T., de Bruijne, J. H. J., et al. 2016b, A&A, 595, A1
Gelman, A., & Rubin, D. B. 1992, Statistical Science, 7, 16
Goodman, J., & Weare, J. 2010, Commun. Appl. Math. Comput. Sci., 5, 65
Hayward, T. L., Brandl, B., Pirger, B., et al. 2001, PASP, 113, 105
Hirano, T., Dai, F., Gandolfi, D., et al. 2017, ArXiv e-prints, arXiv:1710.03239
Hirsch, L. A., Ciardi, D. R., Howard, A. W., et al. 2017, AJ, 153, 117
Hodapp, K.-W., Irwin, E. M., Yamada, H., et al. 2003, in Proc. SPIE, Vol. 4841, Instrument Design and Performance for Optical/Infrared Ground-based Telescopes, ed. M. Iye & A. F. M. Moorwood, 869–880
Horch, E. P., Veillette, D. R., Baena Gallé, R., et al. 2009, AJ, 137, 5057
Howell, S. B., Everett, M. E., Sherry, W., Horch, E., & Ciardi, D. R. 2011, AJ, 142, 19
Howell, S. B., Rowe, J. F., Bryson, S. T., et al. 2012, ApJ, 746, 123
Howell, S. B., Sobeck, C., Haas, M., et al. 2014, PASP, 126, 398
Huber, D., Bryson, S. T., Haas, M. R., et al. 2016, ApJS, 224, 2
Isaacson, H., & Fischer, D. 2010, ApJ, 725, 875
Jenkins, J. M., Caldwell, D. A., Chandrasekaran, H., et al. 2010, ApJ, 713, L87
Kipping, D. M. 2013, MNRAS, 435, 2152
Kovács, G., Zucker, S., & Mazeh, T. 2002, A&A, 391, 369
Kreidberg, L. 2015, PASP, 127, 1161
Kurucz, R. L. 1992, in IAU Symposium, Vol. 149, The Stellar Populations of Galaxies, ed. B. Barbuy & A. Renzini, 225
Latham, D. W., Stefanik, R. P., Mazeh, T., Mayor, M., & Burki, G. 1989, Nature, 339, 38
Latham, D. W., Rowe, J. F., Quinn, S. N., et al. 2011, ApJ, 732, L24
Lee, E. J., & Chiang, E. 2016, ApJ, 817, 90
Lee, E. J., Chiang, E., & Ormel, C. W. 2014, ApJ, 797, 95
Leisenring, J. M., Skrutskie, M. F., Hinz, P. M., et al. 2012, in Proc. SPIE, Vol. 8446, Ground-based and Airborne Instrumentation for Astronomy IV, 84464F
Lissauer, J. J., Marcy, G. W., Rowe, J. F., et al. 2012, ApJ, 750, 112
Lopez, E. D., & Rice, K. 2016, ArXiv e-prints, arXiv:1610.09390
López-Morales, M., Haywood, R. D., Coughlin, J. L., et al. 2016, AJ, 152, 204
Mandel, K., & Agol, E. 2002, ApJ, 580, L171
Mann, A. W., Newton, E. R., Rizzuto, A. C., et al. 2016, AJ, 152, 61
Mann, A. W., Gaidos, E., Vanderburg, A., et al. 2017, AJ, 153, 64
Markwardt, C. B. 2009, in Astronomical Society of the Pacific Conference Series, Vol. 411, Astronomical Data Analysis Software and Systems XVIII, ed. D. A. Bohlender, D. Durand, & P. Dowler, 251
Martinez, A. O., Crossfield, I. J. M., Schlieder, J. E., et al. 2017, ApJ, 837, 72
Martins, J. H. C., Santos, N. C., Figueira, P., et al. 2015, A&A, 576, A134
Mayor, M., & Queloz, D. 1995, Nature, 378, 355
Montet, B. T., Morton, T. D., Foreman-Mackey, D., et al. 2015, ApJ, 809, 25
Morton, T. D. 2012, ApJ, 761, 6
—. 2015a, isochrones: Stellar model grid package, Astrophysics Source Code Library, ascl:1503.010
—. 2015b, VESPA: False positive probabilities calculator, Astrophysics Source Code Library, ascl:1503.011
Niraula, P., Redfield, S., Dai, F., et al. 2017, ArXiv e-prints, arXiv:1709.01527
Osborn, H. P., Santerne, A., Barros, S. C. C., et al. 2017, A&A, 604, A19
Owen, J. E., & Wu, Y. 2013, ApJ, 775, 105
—. 2017, ApJ, 847, 29
Perryman, M. A. C., Lindegren, L., Kovalevsky, J., et al. 1997, A&A, 323, L49
Petigura, E. A., Howard, A. W., & Marcy, G. W. 2013, Proceedings of the National Academy of Science, 110, 19273
Petigura, E. A., Schlieder, J. E., Crossfield, I. J. M., et al. 2015, ApJ, 811, 102
Petigura, E. A., Crossfield, I. J. M., Isaacson, H., et al. 2017, ArXiv e-prints, arXiv:1711.06377
Pope, B. J. S., Parviainen, H., & Aigrain, S. 2016, MNRAS, 461, 3399
Ricker, G. R., Winn, J. N., Vanderspek, R., et al. 2015, Journal of Astronomical Telescopes, Instruments, and Systems, 1, 014003
Rodriguez, J. E., Vanderburg, A., Eastman, J. D., et al. 2017a, ArXiv e-prints, arXiv:1709.01957
Rodriguez, J. E., Zhou, G., Vanderburg, A., et al. 2017b, AJ, 153, 256
Schlieder, J. E., Crossfield, I. J. M., Petigura, E. A., et al. 2016, ApJ, 818, 87
Shporer, A., Zhou, G., Vanderburg, A., et al. 2017, ArXiv e-prints, arXiv:1708.08455
Sinukoff, E., Howard, A. W., Petigura, E. A., et al. 2016, ApJ, 827, 78
Skrutskie, M. F., Cutri, R. M., Stiening, R., et al. 2006, AJ, 131, 1163

Stassun, K. G., Oelkers, R. J., Pepper, J., et al. 2017, ArXiv e-prints, arXiv:1706.00495
Sullivan, P. W., Winn, J. N., Berta-Thompson, Z. K., et al. 2015, ApJ, 809, 77
Thompson, S. E., Coughlin, J. L., Hoffman, K., et al. 2017, ArXiv e-prints, arXiv:1710.06758
Van Eylen, V., Agentoft, C., Lundkvist, M. S., et al. 2017, ArXiv e-prints, arXiv:1710.05398
Vanderburg, A., & Johnson, J. A. 2014, PASP, 126, 948
Vanderburg, A., Johnson, J. A., Rappaport, S., et al. 2015a, Nature, 526, 546
Vanderburg, A., Montet, B. T., Johnson, J. A., et al. 2015b, ApJ, 800, 59
Vanderburg, A., Latham, D. W., Buchhave, L. A., et al. 2016a, ApJS, 222, 14
Vanderburg, A., Bieryla, A., Duev, D. A., et al. 2016b, ApJ, 829, L9
Zhou, G., Rodriguez, J. E., Collins, K. A., et al. 2016, AJ, 152, 136
Ziegler, C., Law, N. M., Morton, T., et al. 2017, AJ, 153, 66

Table 4
Planet Candidate Parameters

New K2 Name	EPIC	T_0 (BJD-2454833)	P (d)	a/R_*	i (deg)	R_p/R_*	R_p ($R_\oplus$)	R_* ($R_\odot$)	M_* ($M_\odot$)	K_p	FPP	Disposition	Notes
K2-156 b	201110617.01	2750.1409 ± 0.0028	$0.813149^{+0.000050}_{-0.000049}$	$4.4^{+0.7}_{-1.1}$	$84.0^{+4.3}_{-7.6}$	$0.0170^{+0.0014}_{-0.0011}$	$1.14^{+0.10}_{-0.08}$	$0.616^{+0.019}_{-0.016}$	$0.642^{+0.022}_{-0.019}$	12.947	$< 1.00e-04$	Planet	
	201111557.01	2750.1621 ± 0.0021	$2.30237^{+0.00011}_{-0.00010}$	$12.6^{+2.8}_{-8.0}$	$87.4^{+1.9}_{-9.5}$	$0.0169^{+0.0067}_{-0.0015}$	$1.31^{+0.52}_{-0.12}$	$0.711^{+0.019}_{-0.020}$	0.746 ± 0.023	11.363	$1.22e-03$	Candidate	
	201127519.01	$2752.5513^{+0.0011}_{-0.0012}$	$6.17837^{+0.00019}_{-0.00017}$	$17.3^{+1.1}_{-2.0}$	$88.8^{+0.8}_{-1.0}$	$0.1151^{+0.0049}_{-0.0034}$	$9.91^{+0.53}_{-0.36}$	$0.789^{+0.025}_{-0.017}$	$0.857^{+0.021}_{-0.023}$	11.558	–	Candidate	c
K2-157 b	201130233.01	$2749.8239^{+0.0032}_{-0.0033}$	0.365257 ± 0.000029	$1.88^{+0.32}_{-0.38}$	$77.0^{+10.0}_{-18.0}$	$0.0110^{+0.0014}_{-0.0010}$	$1.06^{+0.15}_{-0.10}$	$0.876^{+0.045}_{-0.025}$	$0.940^{+0.023}_{-0.027}$	12.604	$< 1.00e-04$	Planet	
K2-158 b	201132684.01	$2757.4817^{+0.0096}_{-0.0092}$	$10.0621^{+0.0023}_{-0.0022}$	$17.6^{+2.9}_{-5.8}$	$88.4^{+1.2}_{-2.4}$	$0.0271^{+0.0027}_{-0.0020}$	$2.63^{+0.35}_{-0.22}$	$0.892^{+0.074}_{-0.036}$	$0.933^{+0.027}_{-0.030}$	11.678	$< 1.00e-04$	Planet	
	201166680.01	$2765.193^{+0.021}_{-0.016}$	$18.105^{+0.010}_{-0.013}$	$26.3^{+5.3}_{-8.9}$	$88.9^{+0.8}_{-1.7}$	$0.0157^{+0.0017}_{-0.0012}$	$2.10^{+0.31}_{-0.20}$	$1.22^{+0.12}_{-0.07}$	$1.192^{+0.033}_{-0.030}$	10.897	$1.73e-03$	Candidate	
	201211526.01	2755.4780 ± 0.0040	$21.0702^{+0.0024}_{-0.0023}$	$34.0^{+5.0}_{-11.0}$	$89.2^{+0.6}_{-1.2}$	$0.0170^{+0.0031}_{-0.0013}$	$1.65^{+0.32}_{-0.14}$	$0.891^{+0.056}_{-0.037}$	$0.936^{+0.032}_{-0.031}$	11.696	$2.10e-03$	Candidate	
K2-159 b	201225286.01	$2753.5147^{+0.0034}_{-0.0037}$	12.4211 ± 0.0010	$26.1^{+2.8}_{-6.0}$	$89.1^{+0.7}_{-1.1}$	$0.0244^{+0.0023}_{-0.0013}$	$2.21^{+0.24}_{-0.14}$	$0.830^{+0.045}_{-0.029}$	$0.886^{+0.027}_{-0.032}$	11.729	$3.53e-04$	Planet	
K2-160 b	201227197.01	$2752.66637^{+0.00081}_{-0.00079}$	$3.705871^{+0.000074}_{-0.000076}$	$14.7^{+1.5}_{-3.7}$	$88.3^{+1.2}_{-2.1}$	$0.0319^{+0.0017}_{-0.0011}$	$3.18^{+0.21}_{-0.15}$	$0.914^{+0.037}_{-0.026}$	$0.983^{+0.023}_{-0.025}$	12.486	$7.54e-04$	Planet	
K2-161 b	201231064.01	$2754.8476^{+0.0077}_{-0.0073}$	$9.2832^{+0.0021}_{-0.0023}$	$10.8^{+1.8}_{-4.7}$	$87.3^{+2.0}_{-5.6}$	$0.0218^{+0.0052}_{-0.0018}$	$6.1^{+1.6}_{-0.8}$	$2.57^{+0.31}_{-0.25}$	$0.987^{+0.082}_{-0.060}$	12.358	$7.97e-04$	Planet	
	201295312.01	1978.7201 ± 0.0026	$5.65630^{+0.00037}_{-0.00032}$	$9.4^{+0.9}_{-2.3}$	$87.4^{+1.9}_{-3.3}$	$0.01726^{+0.00070}_{-0.00054}$	$2.94^{+0.50}_{-0.38}$	$1.56^{+0.26}_{-0.19}$	$1.050^{+0.068}_{-0.045}$	12.126	$< 1.00e-04$	Planet	
	201299088.01	$2767.3429^{+0.0081}_{-0.0080}$	$21.2047^{+0.0053}_{-0.0055}$	$7.26^{+0.90}_{-0.66}$	$83.5^{+1.1}_{-1.0}$	$0.0474^{+0.0020}_{-0.0018}$	$9.1^{+1.2}_{-1.0}$	$1.76^{+0.21}_{-0.17}$	$0.848^{+0.023}_{-0.010}$	11.751	–	Candidate	a
	201352100.01	$2761.7920^{+0.0020}_{-0.0021}$	$13.38363^{+0.00076}_{-0.00073}$	$34.9^{+4.0}_{-9.0}$	$89.25^{+0.53}_{-0.91}$	$0.0323^{+0.0019}_{-0.0015}$	$2.87^{+0.19}_{-0.14}$	$0.815^{+0.027}_{-0.018}$	$0.889^{+0.019}_{-0.024}$	12.798	–	Candidate	c
	201384232.01	$1994.4972^{+0.0044}_{-0.0043}$	$30.9446^{+0.0030}_{-0.0032}$	$41.6^{+4.1}_{-9.9}$	$89.42^{+0.43}_{-0.74}$	$0.0246^{+0.0015}_{-0.0009}$	$2.31^{+0.17}_{-0.12}$	$0.863^{+0.034}_{-0.030}$	$0.930^{+0.029}_{-0.030}$	12.510	$< 1.00e-04$	Planet	
K2-162 b	201390048.01	$2750.9089^{+0.0064}_{-0.0054}$	9.4577 ± 0.0014	$22.6^{+3.8}_{-7.0}$	$88.8^{+0.9}_{-1.8}$	$0.0188^{+0.0021}_{-0.0014}$	$1.49^{+0.17}_{-0.12}$	0.726 ± 0.020	$0.777^{+0.025}_{-0.026}$	11.961	$< 1.00e-04$	Planet	
	201403446.01	$1982.3364^{+0.0051}_{-0.0052}$	19.1545 ± 0.0028	$18.8^{+2.1}_{-4.9}$	$88.6^{+1.0}_{-1.7}$	$0.0170^{+0.0013}_{-0.0008}$	$2.47^{+0.35}_{-0.30}$	$1.33^{+0.16}_{-0.15}$	$1.015^{+0.054}_{-0.046}$	11.995	$< 1.00e-04$	Planet	
K2-163 b	201427874.01	2749.8484 ± 0.0019	$6.67312^{+0.00032}_{-0.00030}$	$15.7^{+2.1}_{-4.4}$	$88.3^{+1.3}_{-2.2}$	$0.0297^{+0.0030}_{-0.0014}$	$2.47^{+0.26}_{-0.12}$	$0.762^{+0.018}_{-0.013}$	$0.826^{+0.019}_{-0.023}$	12.819	$< 1.00e-04$	Planet	
	201437844.01	2753.5434 ± 0.0044	$9.5545^{+0.0013}_{-0.0014}$	$18.3^{+2.5}_{-4.8}$	$88.5^{+1.1}_{-2.7}$	$0.0168^{+0.0010}_{-0.0007}$	$2.33^{+0.35}_{-0.26}$	$1.27^{+0.17}_{-0.12}$	$1.119^{+0.055}_{-0.043}$	9.234	$< 1.00e-04$	Planet	
	201437844.02	$2757.0745^{+0.0033}_{-0.0035}$	$21.0575^{+0.0022}_{-0.0020}$	$33.0^{+3.1}_{-7.2}$	$89.26^{+0.53}_{-0.83}$	$0.03091^{+0.00099}_{-0.00078}$	$4.29^{+0.60}_{-0.45}$	$1.27^{+0.17}_{-0.13}$	$1.119^{+0.055}_{-0.043}$	9.234	$< 1.00e-04$	Planet	
	201441872.01	$1979.8713^{+0.0067}_{-0.0072}$	$4.44126^{+0.00088}_{-0.00094}$	$11.0^{+3.1}_{-7.8}$	$87.0^{+2.0}_{-15.0}$	$0.0124^{+0.0093}_{-0.0013}$	$1.12^{+0.85}_{-0.31}$	$0.834^{+0.050}_{-0.031}$	$0.885^{+0.029}_{-0.031}$	12.088	–	Candidate	b
K2-164 b	201460826.01	$1983.7370^{+0.0084}_{-0.0091}$	$17.3551^{+0.0041}_{-0.0038}$	$13.9^{+2.3}_{-5.4}$	$87.9^{+1.5}_{-3.7}$	$0.01357^{+0.00097}_{-0.00074}$	$3.25^{+0.52}_{-0.41}$	$2.20^{+0.31}_{-0.25}$	$1.181^{+0.093}_{-0.061}$	11.130	$< 1.00e-04$	Planet	
	201505350.01	1984.27514 ± 0.00082	11.90762 ± 0.00024	$23.4^{+1.9}_{-4.0}$	$89.04^{+0.67}_{-0.95}$	$0.0445^{+0.0019}_{-0.0009}$	$4.05^{+0.25}_{-0.15}$	$0.834^{+0.036}_{-0.026}$	$0.895^{+0.026}_{-0.030}$	12.806	$< 1.00e-04$	Planet	
	201505350.02	1980.38334 ± 0.00026	$7.919493^{+0.000047}_{-0.000049}$	$19.6^{+0.5}_{-1.2}$	$89.37^{+0.45}_{-0.68}$	$0.0742^{+0.0014}_{-0.0010}$	$6.75^{+0.32}_{-0.23}$	$0.834^{+0.036}_{-0.026}$	$0.895^{+0.026}_{-0.030}$	12.806	$< 1.00e-04$	Planet	
	201505350.03	$1978.4307^{+0.0060}_{-0.0065}$	$2.50828^{+0.00031}_{-0.00030}$	$7.6^{+1.3}_{-2.2}$	$86.6^{+2.5}_{-5.1}$	$0.0127^{+0.0011}_{-0.0008}$	$1.16^{+0.11}_{-0.08}$	$0.834^{+0.036}_{-0.026}$	$0.895^{+0.026}_{-0.030}$	12.806	$< 1.00e-04$	Planet	
K2-165 b	201528828.01	$2751.4827^{+0.0047}_{-0.0046}$	$2.35499^{+0.00025}_{-0.00026}$	$9.2^{+1.6}_{-2.9}$	$87.1^{+2.2}_{-4.4}$	$0.0145^{+0.0014}_{-0.0010}$	$1.27^{+0.14}_{-0.10}$	$0.804^{+0.045}_{-0.029}$	$0.835^{+0.031}_{-0.030}$	11.415	$< 1.00e-04$	Planet	
K2-165 c	201528828.02	2751.2131 ± 0.0048	$4.38274^{+0.00051}_{-0.00054}$	$10.5^{+1.9}_{-4.2}$	$87.1^{+2.1}_{-5.0}$	$0.0177^{+0.0022}_{-0.0011}$	$1.55^{+0.21}_{-0.11}$	$0.804^{+0.045}_{-0.029}$	$0.835^{+0.031}_{-0.030}$	11.415	$< 1.00e-04$	Planet	
K2-165 d	201528828.03	2753.7581 ± 0.0022	14.1014 ± 0.0011	$27.7^{+3.6}_{-7.4}$	$89.0^{+0.7}_{-1.2}$	$0.0302^{+0.0023}_{-0.0013}$	$2.65^{+0.25}_{-0.15}$	$0.804^{+0.045}_{-0.029}$	$0.835^{+0.031}_{-0.030}$	11.415	$< 1.00e-04$	Planet	
	201546283.01	$1979.84469^{+0.00042}_{-0.00040}$	$6.771389^{+0.000059}_{-0.000062}$	$18.2^{+1.2}_{-2.5}$	$88.9^{+0.8}_{-1.0}$	$0.0491^{+0.0016}_{-0.0009}$	$4.58^{+0.25}_{-0.16}$	$0.855^{+0.038}_{-0.025}$	$0.920^{+0.023}_{-0.025}$	12.428	–	Candidate	c
	201577035.01	$1986.5775^{+0.0011}_{-0.0010}$	$19.30704^{+0.00057}_{-0.00060}$	$38.6^{+2.2}_{-5.5}$	$89.50^{+0.35}_{-0.53}$	$0.0380^{+0.0010}_{-0.0007}$	$3.73^{+0.24}_{-0.15}$	$0.902^{+0.054}_{-0.032}$	$0.958^{+0.026}_{-0.029}$	12.296	$< 1.00e-04$	Planet	
	201595106.01	$2750.0454^{+0.0027}_{-0.0026}$	0.877183 ± 0.000057	$5.2^{+1.0}_{-1.7}$	$84.7^{+3.8}_{-8.6}$	$0.0138^{+0.0018}_{-0.0011}$	$1.41^{+0.21}_{-0.13}$	$0.932^{+0.064}_{-0.038}$	$0.980^{+0.026}_{-0.029}$	11.678	$1.55e-03$	Candidate	
	201613023.01	$1982.3701^{+0.0028}_{-0.0029}$	$8.28246^{+0.00052}_{-0.00051}$	$13.0^{+2.3}_{-6.3}$	$87.6^{+1.8}_{-5.4}$	$0.0200^{+0.0024}_{-0.0009}$	$2.19^{+0.37}_{-0.22}$	$1.01^{+0.12}_{-0.09}$	$0.936^{+0.032}_{-0.033}$	12.137	$< 1.00e-04$	Planet	
K2-166 b	201615463.01	$2753.7668^{+0.0093}_{-0.0086}$	8.5272 ± 0.0020	$10.4^{+1.3}_{-3.3}$	$87.4^{+1.9}_{-3.9}$	$0.0140^{+0.0011}_{-0.0007}$	$1.82^{+0.30}_{-0.23}$	$1.20^{+0.18}_{-0.14}$	1.073 ± 0.034	11.964	$< 1.00e-04$	Planet	
	201713348.01	$1979.84015^{+0.00072}_{-0.00073}$	$5.340883^{+0.000088}_{-0.000089}$	$12.0^{+20.0}_{-3.0}$	$85.5^{+3.9}_{-3.3}$	$0.04^{+0.17}_{-0.01}$	$4.0^{+14.0}_{-1.0}$	$0.746^{+0.019}_{-0.021}$	$0.800^{+0.023}_{-0.027}$	11.531	$7.00e-03$	Candidate	
	201713348.02	1977.8914 ± 0.0013	1.422619 ± 0.000039	$8.0^{+1.4}_{-3.0}$	$86.3^{+2.7}_{-6.2}$	$0.0180^{+0.0026}_{-0.0013}$	$1.47^{+0.22}_{-0.11}$	$0.746^{+0.019}_{-0.021}$	$0.800^{+0.023}_{-0.027}$	11.531	$< 1.00e-04$	Planet	
	201828749.01	$1980.1544^{+0.0033}_{-0.0031}$	33.5136 ± 0.0028	$45.0^{+9.0}_{-18.0}$	$89.3^{+0.5}_{-1.1}$	$0.0264^{+0.0034}_{-0.0015}$	$2.47^{+0.34}_{-0.17}$	$0.858^{+0.045}_{-0.032}$	$0.915^{+0.029}_{-0.030}$	11.564	–	Candidate	c
	201855371.01	$1984.9438^{+0.0033}_{-0.0034}$	17.9691 ± 0.0014	$46.0^{+7.0}_{-14.0}$	$89.40^{+0.42}_{-0.82}$	$0.0297^{+0.0030}_{-0.0019}$	$1.95^{+0.21}_{-0.14}$	$0.601^{+0.017}_{-0.015}$	$0.625^{+0.020}_{-0.019}$	12.997	$< 1.00e-04$	Planet	
	201920032.01	$2000.2014^{+0.0048}_{-0.0058}$	$28.2718^{+0.0037}_{-0.0038}$	$43.0^{+8.0}_{-17.0}$	$89.3^{+0.5}_{-1.2}$	$0.0266^{+0.0046}_{-0.0020}$	$2.71^{+0.53}_{-0.24}$	$0.934^{+0.090}_{-0.047}$	0.954 ± 0.027	12.890	$9.73e-03$	Candidate	
	202089657.01	$1939.7758^{+0.0025}_{-0.0026}$	$1.31444^{+0.00019}_{-0.00018}$	$5.2^{+0.8}_{-1.9}$	$85.0^{+3.7}_{-9.9}$	$0.0193^{+0.0037}_{-0.0016}$	$3.10^{+0.76}_{-0.54}$	1.47 ± 0.22	$1.116^{+0.057}_{-0.074}$	11.600	–	Candidate	b
	202091388.01	1940.3832 ± 0.0026	$6.4797^{+0.0013}_{-0.0012}$	$15.5^{+2.3}_{-5.4}$	$88.1^{+1.3}_{-2.9}$	$0.0331^{+0.0032}_{-0.0019}$	$3.33^{+0.39}_{-0.23}$	$0.922^{+0.062}_{-0.032}$	$0.976^{+0.024}_{-0.026}$	13.500	–	Candidate	f
	202675839.01	$2065.8485^{+0.0036}_{-0.0037}$	$15.4667^{+0.0015}_{-0.0016}$	$13.5^{+5.2}_{-1.5}$	85.5 ± 1.8	$0.12^{+0.30}_{-0.06}$	$16.0^{+41.0}_{-8.0}$	$1.23^{+0.19}_{-0.13}$	$1.141^{+0.050}_{-0.039}$	12.362	–	Candidate	a
	202821899.01	$2062.6880^{+0.0029}_{-0.0031}$	$4.47451^{+0.00030}_{-0.00031}$	$13.5^{+2.4}_{-5.1}$	$87.8^{+1.6}_{-3.6}$	$0.0337^{+0.0056}_{-0.0025}$	$8.2^{+1.7}_{-1.3}$	$2.22^{+0.28}_{-0.30}$	$1.53^{+0.09}_{-0.10}$	12.577	–	Candidate	b
	202900527.01	$2072.75711^{+0.00057}_{-0.00053}$	13.00838 ± 0.00021	$19.3^{+0.9}_{-1.2}$	$89.03^{+0.59}_{-0.53}$	$0.1010^{+0.0022}_{-0.0013}$	$15.7^{+3.0}_{-2.3}$	$1.42^{+0.27}_{-0.21}$	$1.004^{+0.086}_{-0.047}$	12.303	–	Candidate	a,d,e
	203771098.01	$2082.62484^{+0.00057}_{-0.00055}$	$42.36398^{+0.00076}_{-0.00080}$	$49.8^{+3.3}_{-4.5}$	$89.57^{+0.28}_{-0.25}$	$0.0611^{+0.0017}_{-0.0011}$	$7.12^{+0.68}_{-0.35}$	$1.068^{+0.097}_{-0.050}$	$1.095^{+0.028}_{-0.029}$	11.648	$< 1.00e-04$	Planet	
	203771098.02	$2072.79594^{+0.00087}_{-0.00080}$	$20.88502^{+0.00041}_{-0.00044}$	$26.5^{+3.6}_{-4.2}$	$88.87^{+0.71}_{-0.67}$	$0.0451^{+0.0023}_{-0.0016}$	$5.26^{+0.55}_{-0.31}$	$1.068^{+0.097}_{-0.050}$	$1.095^{+0.028}_{-0.029}$	11.648	$< 1.00e-04$	Planet	
	203826436.01	$2065.8559^{+0.0021}_{-0.0020}$	$6.42958^{+0.00029}_{-0.00031}$	$15.3^{+2.1}_{-4.9}$	$88.2^{+1.4}_{-2.7}$	$0.0291^{+0.0035}_{-0.0014}$	$2.60^{+0.33}_{-0.15}$	$0.818^{+0.032}_{-0.025}$	$0.887^{+0.025}_{-0.031}$	12.241	$< 1.00e-04$	Planet	
	203826436.02	$2074.2360^{+0.0026}_{-0.0024}$	$14.0910^{+0.0010}_{-0.0011}$	$34.0^{+5.0}_{-11.0}$	$89.2^{+0.6}_{-1.2}$	$0.0270^{+0.0036}_{-0.0015}$	$2.41^{+0.33}_{-0.15}$	$0.818^{+0.032}_{-0.025}$	$0.887^{+0.025}_{-0.031}$	12.241	$< 1.00e-04$	Planet	
	203826436.03	$2065.1129^{+0.0046}_{-0.0042}$	$4.44377^{+0.00045}_{-0.00050}$	$10.8^{+1.4}_{-3.1}$	$87.5^{+1.8}_{-3.4}$	$0.0171^{+0.0019}_{-0.0010}$	$1.53^{+0.18}_{-0.10}$	$0.818^{+0.032}_{-0.025}$	$0.887^{+0.025}_{-0.031}$	12.241	$< 1.00e-04$	Planet	
	204750116.01	$2065.8359^{+0.0040}_{-0.0037}$	$23.4469^{+0.0019}_{-0.0021}$	$27.9^{+3.8}_{-8.2}$	$89.0^{+0.7}_{-1.3}$	$0.0269^{+0.0026}_{-0.0013}$	$2.90^{+0.32}_{-0.18}$	$0.987^{+0.051}_{-0.039}$	$1.037^{+0.026}_{-0.030}$	11.526	–	Candidate	c
	205029914.01	$2061.7314^{+0.0014}_{-0.0015}$	4.98184 ± 0.00017	$8.6^{+1.4}_{-3.4}$	$86.4^{+2.6}_{-6.0}$	$0.0224^{+0.0026}_{-0.0009}$	$2.39^{+0.38}_{-0.17}$	$0.98^{+0.11}_{-0.06}$	$0.983^{+0.029}_{-0.034}$	12.183	–	Candidate	c
	205071984.01	$2067.92671^{+0.00060}_{-0.00063}$	8.99194 ± 0.00016	$20.2^{+1.0}_{-2.3}$	$89.12^{+0.61}_{-0.86}$	$0.0565^{+0.0013}_{-0.0010}$	$5.17^{+0.20}_{-0.16}$	$0.839^{+0.026}_{-0.021}$	$0.916^{+0.020}_{-0.026}$	12.005	$< 1.00e-04$	Planet	
	205071984.02	$2070.7929^{+0.0024}_{-0.0025}$	$31.7151^{+0.0026}_{-0.0022}$	$45.0^{+6.0}_{-15.0}$	$89.35^{+0.47}_{-0.91}$	$0.0373^{+0.0025}_{-0.0013}$	$3.41^{+0.26}_{-0.14}$	$0.839^{+0.026}_{-0.021}$	$0.916^{+0.020}_{-0.026}$	12.005	$< 1.00e-04$	Planet	
	205071984.03	$2066.4221^{+0.0036}_{-0.0039}$	$20.6616^{+0.0018}_{-0.0017}$	$33.5^{+3.2}_{-8.0}$	$89.27^{+0.51}_{-0.91}$	$0.0340^{+0.0016}_{-0.0010}$	$3.12^{+0.18}_{-0.12}$	$0.839^{+0.026}_{-0.021}$	$0.916^{+0.020}_{-0.026}$	12.005	$< 1.00e-04$	Planet	

Table 4 — *Continued*

New K2 Name	EPIC	T_0 (BJD-2454833)	P (d)	a/R_*	i (deg)	R_p/R_*	R_p ($R_\oplus$)	R_* ($R_\odot$)	M_* ($M_\odot$)	K_p	FPP	Disposition	Notes
K2-167 b	205904628.01	$2146.9368^{+0.0025}_{-0.0024}$	9.9775 ± 0.0010	$19.4^{+2.5}_{-5.9}$	$88.6^{+1.0}_{-2.0}$	$0.0141^{+0.0013}_{-0.0007}$	$2.82^{+0.52}_{-0.45}$	$1.83^{+0.29}_{-0.28}$	$1.02^{+0.12}_{-0.09}$	8.220	$8.64e-04$	Planet	
	205944181.01	$2148.81517^{+0.00094}_{-0.00085}$	$2.475641^{+0.000057}_{-0.000054}$	$8.0^{+15.0}_{-2.0}$	$82.2^{+6.9}_{-4.0}$	$0.06^{+0.19}_{-0.03}$	$5.0^{+17.0}_{-3.0}$	$0.825^{+0.046}_{-0.026}$	$0.872^{+0.026}_{-0.033}$	12.410	$9.49e-01$	Candidate	
K2-168 b	205950854.01	$2157.8877^{+0.0027}_{-0.0026}$	15.8540 ± 0.0014	$27.9^{+4.1}_{-8.6}$	$88.9^{+0.7}_{-1.3}$	$0.0225^{+0.0013}_{-0.0010}$	$2.14^{+0.21}_{-0.14}$	$0.874^{+0.068}_{-0.039}$	$0.907^{+0.029}_{-0.032}$	12.105	$7.10e-04$	Planet	
	205957328.01	$2148.5855^{+0.0035}_{-0.0032}$	$14.3534^{+0.0014}_{-0.0015}$	$31.0^{+6.0}_{-13.0}$	$89.0^{+0.7}_{-1.8}$	$0.0239^{+0.0044}_{-0.0018}$	$2.16^{+0.41}_{-0.17}$	$0.828^{+0.033}_{-0.021}$	$0.892^{+0.022}_{-0.027}$	12.464	$3.97e-03$	Candidate	
K2-169 b	206007892.01	$2149.0097^{+0.0036}_{-0.0038}$	$6.38080^{+0.00078}_{-0.00070}$	$13.6^{+2.2}_{-5.1}$	$87.8^{+1.6}_{-3.6}$	$0.01270^{+0.00083}_{-0.00065}$	$1.27^{+0.11}_{-0.08}$	$0.919^{+0.049}_{-0.030}$	$0.986^{+0.028}_{-0.026}$	12.023	$< 1.00e-04$	Planet	
K2-170 c	206008091.01	$2152.6669^{+0.0047}_{-0.0046}$	$12.4000^{+0.0017}_{-0.0019}$	$20.9^{+3.0}_{-7.6}$	$88.7^{+1.0}_{-2.3}$	$0.0168^{+0.0013}_{-0.0008}$	$1.80^{+0.25}_{-0.16}$	$0.98^{+0.11}_{-0.07}$	0.964 ± 0.032	12.506	$< 1.00e-04$	Planet	
K2-170 b	206008091.02	$2153.1855^{+0.0069}_{-0.0074}$	$7.5765^{+0.0018}_{-0.0017}$	$14.3^{+2.3}_{-5.3}$	$88.0^{+1.4}_{-3.3}$	$0.0132^{+0.0012}_{-0.0008}$	$1.42^{+0.20}_{-0.13}$	$0.98^{+0.11}_{-0.07}$	0.964 ± 0.032	12.506	$< 1.00e-04$	Planet	
	206011496.01	$2148.64577^{+0.00095}_{-0.00098}$	$2.369008^{+0.000056}_{-0.000059}$	$7.3^{+0.7}_{-1.8}$	$86.6^{+2.4}_{-4.3}$	$0.0171^{+0.0011}_{-0.0005}$	$1.66^{+0.16}_{-0.08}$	$0.889^{+0.061}_{-0.030}$	$0.940^{+0.025}_{-0.027}$	10.916	–	Candidate	c
	206026904.01	$2146.92339^{+0.00086}_{-0.00090}$	7.05248 ± 0.00016	$24.8^{+3.4}_{-7.8}$	$88.9^{+0.8}_{-1.6}$	$0.0296^{+0.0030}_{-0.0013}$	$2.59^{+0.28}_{-0.13}$	$0.803^{+0.034}_{-0.020}$	$0.858^{+0.022}_{-0.027}$	12.150	$< 1.00e-04$	Planet	
	206026904.02	2146.5862 ± 0.0014	$2.537071^{+0.000096}_{-0.000093}$	$7.9^{+1.3}_{-3.4}$	$86.1^{+2.8}_{-7.3}$	$0.0185^{+0.0028}_{-0.0009}$	$1.63^{+0.26}_{-0.09}$	$0.803^{+0.034}_{-0.020}$	$0.858^{+0.022}_{-0.027}$	12.150	$< 1.00e-04$	Planet	
	206026904.03	$2165.0672^{+0.0029}_{-0.0028}$	$22.8816^{+0.0021}_{-0.0022}$	$49.0^{+6.0}_{-15.0}$	$89.43^{+0.41}_{-0.81}$	$0.0200^{+0.0021}_{-0.0009}$	$1.75^{+0.20}_{-0.09}$	$0.803^{+0.034}_{-0.020}$	$0.858^{+0.022}_{-0.027}$	12.150	$< 1.00e-04$	Planet	
	206044803.01	2147.6401 ± 0.0024	$2.57341^{+0.00016}_{-0.00017}$	$6.6^{+0.9}_{-2.1}$	$86.0^{+2.9}_{-6.4}$	$0.0174^{+0.0022}_{-0.0009}$	$1.93^{+0.32}_{-0.15}$	$1.02^{+0.11}_{-0.06}$	1.030 ± 0.029	12.975	$2.16e-04$	Planet	
K2-171 b	206049764.01	2146.4671 ± 0.0071	$5.6285^{+0.0017}_{-0.0015}$	$5.5^{+0.7}_{-2.1}$	$85.0^{+3.7}_{-9.6}$	$0.0143^{+0.0011}_{-0.0007}$	$2.69^{+0.40}_{-0.33}$	$1.72^{+0.22}_{-0.19}$	$0.892^{+0.060}_{-0.027}$	12.445	$< 1.00e-04$	Planet	
K2-172 c	206082454.01	$2160.5398^{+0.0011}_{-0.0012}$	29.6268 ± 0.0016	$44.2^{+3.4}_{-7.8}$	$89.50^{+0.35}_{-0.53}$	$0.0338^{+0.0013}_{-0.0009}$	$3.21^{+0.19}_{-0.14}$	$0.869^{+0.038}_{-0.029}$	$0.934^{+0.026}_{-0.027}$	12.308	$< 1.00e-04$	Planet	
K2-172 b	206082454.02	2149.2949 ± 0.0034	14.3169 ± 0.0014	$25.1^{+3.1}_{-8.5}$	$88.9^{+0.8}_{-1.7}$	$0.0176^{+0.0015}_{-0.0008}$	$1.67^{+0.16}_{-0.10}$	$0.869^{+0.038}_{-0.029}$	$0.934^{+0.026}_{-0.027}$	12.308	$< 1.00e-04$	Planet	
	206096602.01	$2149.68564^{+0.00097}_{-0.00098}$	$6.67177^{+0.00018}_{-0.00017}$	$29.9^{+3.8}_{-8.6}$	$89.1^{+0.6}_{-1.2}$	$0.0272^{+0.0017}_{-0.0011}$	$1.93^{+0.13}_{-0.10}$	$0.648^{+0.021}_{-0.018}$	$0.684^{+0.022}_{-0.023}$	12.045	$< 1.00e-04$	Planet	
	206096602.02	2158.5448 ± 0.0016	$16.19720^{+0.00083}_{-0.00082}$	$77.0^{+13.0}_{-32.0}$	$89.61^{+0.29}_{-0.71}$	$0.0268^{+0.0027}_{-0.0014}$	$1.89^{+0.20}_{-0.11}$	$0.648^{+0.021}_{-0.018}$	$0.684^{+0.022}_{-0.023}$	12.045	$< 1.00e-04$	Planet	
	206114630.01	$2152.3896^{+0.0014}_{-0.0013}$	7.44503 ± 0.00030	$55.0^{+18.0}_{-37.0}$	$89.3^{+0.4}_{-2.7}$	$0.025^{+0.034}_{-0.003}$	$2.3^{+3.1}_{-0.3}$	$0.825^{+0.021}_{-0.019}$	$0.897^{+0.030}_{-0.024}$	11.032	$9.91e-01$	Candidate	
	206119924.01	2146.9496 ± 0.0043	4.65534 ± 0.00051	$13.8^{+2.9}_{-5.4}$	$87.8^{+1.6}_{-3.6}$	$0.0096^{+0.0012}_{-0.0007}$	$0.719^{+0.089}_{-0.057}$	$0.687^{+0.015}_{-0.017}$	$0.727^{+0.020}_{-0.021}$	10.310	–	Candidate	b
	206144956.01	$2153.3277^{+0.0015}_{-0.0016}$	$12.64781^{+0.00067}_{-0.00072}$	$28.9^{+3.0}_{-8.5}$	$89.1^{+0.6}_{-1.3}$	$0.0189^{+0.0033}_{-0.0011}$	$1.38^{+0.25}_{-0.09}$	$0.669^{+0.023}_{-0.021}$	$0.702^{+0.025}_{-0.023}$	10.396	$< 1.00e-04$	Planet	
	206146957.01	2146.8699 ± 0.0033	5.76136 ± 0.00052	$16.9^{+2.5}_{-6.0}$	$88.3^{+1.2}_{-2.7}$	$0.0140^{+0.0013}_{-0.0008}$	$1.37^{+0.15}_{-0.09}$	$0.902^{+0.048}_{-0.034}$	$0.956^{+0.031}_{-0.030}$	11.379	$5.22e-03$	Candidate	
	206159027.01	$2149.3259^{+0.0019}_{-0.0020}$	$8.05479^{+0.00045}_{-0.00044}$	$19.9^{+2.3}_{-4.2}$	$88.7^{+0.9}_{-1.3}$	$0.0239^{+0.0017}_{-0.0011}$	$1.83^{+0.14}_{-0.10}$	0.702 ± 0.021	$0.751^{+0.025}_{-0.026}$	12.597	$< 1.00e-04$	Planet	
	206169375.01	$2146.53588^{+0.00072}_{-0.00069}$	0.3674730 ± 0.0000070	$2.5^{+1.4}_{-1.1}$	$72.0^{+15.0}_{-34.0}$	$0.03^{+0.15}_{-0.00}$	$4.0^{+20.0}_{-1.0}$	$1.26^{+0.22}_{-0.15}$	$1.096^{+0.056}_{-0.047}$	12.559	$9.25e-01$	Candidate	
	206181769.01	$2151.4441^{+0.0012}_{-0.0011}$	$13.97852^{+0.00056}_{-0.00057}$	$29.6^{+2.9}_{-7.8}$	$89.1^{+0.6}_{-1.1}$	$0.03157^{+0.00099}_{-0.00076}$	$2.75^{+0.15}_{-0.10}$	$0.799^{+0.034}_{-0.021}$	$0.848^{+0.023}_{-0.028}$	12.770	$< 1.00e-04$	Planet	
	206192335.01	2146.9471 ± 0.0020	$3.59905^{+0.00020}_{-0.00018}$	$13.4^{+2.1}_{-4.5}$	$87.9^{+1.4}_{-3.2}$	$0.0176^{+0.0015}_{-0.0010}$	$1.59^{+0.16}_{-0.11}$	$0.826^{+0.039}_{-0.028}$	$0.883^{+0.029}_{-0.030}$	11.870	–	Candidate	c
	206245553.01	$2147.1766^{+0.0014}_{-0.0013}$	7.49569 ± 0.00028	$15.1^{+1.4}_{-3.2}$	$88.4^{+1.1}_{-1.8}$	$0.0229^{+0.0013}_{-0.0006}$	$2.63^{+0.36}_{-0.19}$	$1.05^{+0.13}_{-0.07}$	$1.043^{+0.026}_{-0.027}$	11.745	$< 1.00e-04$	Planet	
	206268299.01	$2164.9999^{+0.0023}_{-0.0027}$	$19.5656^{+0.0019}_{-0.0017}$	$26.1^{+3.3}_{-5.9}$	$88.9^{+0.7}_{-1.0}$	$0.0250^{+0.0018}_{-0.0011}$	$2.96^{+0.43}_{-0.33}$	$1.09^{+0.14}_{-0.11}$	0.987 ± 0.040	12.430	$5.17e-04$	Planet	
	206348688.01	$2150.4293^{+0.0037}_{-0.0039}$	$7.81795^{+0.00078}_{-0.00075}$	$10.6^{+1.3}_{-4.1}$	$87.4^{+1.9}_{-5.0}$	$0.0189^{+0.0012}_{-0.0007}$	$2.55^{+0.37}_{-0.23}$	$1.24^{+0.16}_{-0.11}$	$1.174^{+0.048}_{-0.041}$	12.566	$< 1.00e-04$	Planet	
	206348688.02	$2159.7472^{+0.0067}_{-0.0097}$	$18.2861^{+0.0057}_{-0.0046}$	$21.4^{+2.4}_{-6.3}$	$88.8^{+0.9}_{-1.8}$	$0.0194^{+0.0011}_{-0.0008}$	$2.63^{+0.37}_{-0.25}$	$1.24^{+0.16}_{-0.11}$	$1.174^{+0.048}_{-0.041}$	12.566	$< 1.00e-04$	Planet	
	206439513.01	$2159.8681^{+0.0082}_{-0.0080}$	$18.4151^{+0.0067}_{-0.0065}$	$2.72^{+0.30}_{-0.22}$	$64.3^{+4.8}_{-7.2}$	$0.18^{+0.34}_{-0.11}$	$69.0^{+130.0}_{-42.0}$	$3.47^{+0.48}_{-0.44}$	$1.62^{+0.07}_{-0.10}$	11.437	–	Candidate	a
	206535016.01	$2163.3684^{+0.0028}_{-0.0030}$	20.3981 ± 0.0019	$73.0^{+16.0}_{-39.0}$	$89.6^{+0.3}_{-1.2}$	$0.0304^{+0.0088}_{-0.0026}$	$2.58^{+0.76}_{-0.24}$	$0.777^{+0.038}_{-0.028}$	$0.815^{+0.032}_{-0.029}$	11.644	$1.92e-01$	Candidate	
	210363145.01	$2237.8065^{+0.0015}_{-0.0014}$	$8.19981^{+0.00036}_{-0.00037}$	$23.5^{+2.5}_{-7.1}$	$88.9^{+0.8}_{-1.7}$	$0.0292^{+0.0012}_{-0.0010}$	$2.50^{+0.13}_{-0.09}$	$0.784^{+0.024}_{-0.014}$	$0.852^{+0.019}_{-0.024}$	11.896	$< 1.00e-04$	Planet	
	210365511.01	2234.617 ± 0.010	$3.9520^{+0.0012}_{-0.0013}$	$1.47^{+0.50}_{-0.11}$	38.9 ± 9.2	$0.11^{+0.38}_{-0.07}$	$8.0^{+29.0}_{-6.0}$	$0.692^{+0.020}_{-0.021}$	$0.730^{+0.024}_{-0.023}$	12.439	–	Candidate	a
	210402237.01	2237.2465 ± 0.0020	$10.99395^{+0.00060}_{-0.00063}$	$17.7^{+1.6}_{-4.1}$	$88.6^{+1.0}_{-1.7}$	$0.0278^{+0.0015}_{-0.0009}$	$3.15^{+0.33}_{-0.18}$	$1.038^{+0.092}_{-0.050}$	$1.062^{+0.029}_{-0.026}$	11.801	$< 1.00e-04$	Planet	
	210403955.01	$2244.5926^{+0.0056}_{-0.0055}$	$19.0999^{+0.0041}_{-0.0040}$	$29.0^{+5.0}_{-11.0}$	$89.0^{+0.7}_{-1.6}$	$0.0230^{+0.0032}_{-0.0013}$	$2.11^{+0.30}_{-0.13}$	$0.841^{+0.031}_{-0.022}$	$0.913^{+0.030}_{-0.024}$	12.388	$< 1.00e-04$	Planet	
	210403955.02	$2233.4860^{+0.0037}_{-0.0038}$	$5.60531^{+0.00064}_{-0.00063}$	$13.3^{+1.9}_{-4.5}$	$87.9^{+1.5}_{-3.3}$	$0.0162^{+0.0020}_{-0.0010}$	$1.49^{+0.19}_{-0.10}$	$0.841^{+0.031}_{-0.022}$	$0.913^{+0.021}_{-0.024}$	12.388	$< 1.00e-04$	Planet	
K2-80 d	210403955.03	$2249.9371^{+0.0036}_{-0.0045}$	$28.8673^{+0.0051}_{-0.0046}$	$46.0^{+6.0}_{-13.0}$	$89.40^{+0.43}_{-0.77}$	$0.0278^{+0.0028}_{-0.0013}$	$2.55^{+0.28}_{-0.14}$	$0.841^{+0.031}_{-0.022}$	$0.913^{+0.021}_{-0.024}$	12.388	$< 1.00e-04$	Planet	
	210423938.01	$2239.0161^{+0.0043}_{-0.0037}$	$19.8605^{+0.0020}_{-0.0022}$	$34.0^{+9.0}_{-18.0}$	$89.0^{+0.8}_{-2.3}$	$0.0274^{+0.0071}_{-0.0027}$	$2.08^{+0.54}_{-0.22}$	$0.697^{+0.021}_{-0.020}$	$0.741^{+0.024}_{-0.026}$	12.655	$8.45e-02$	Candidate	
K2-173 b	210512842.01	$2234.1411^{+0.0029}_{-0.0028}$	$5.86870^{+0.00045}_{-0.00041}$	$13.0^{+1.8}_{-3.9}$	$87.8^{+1.5}_{-2.9}$	$0.0175^{+0.0013}_{-0.0008}$	$1.61^{+0.16}_{-0.11}$	$0.843^{+0.039}_{-0.031}$	$0.882^{+0.034}_{-0.036}$	12.106	$7.20e-04$	Planet	
K2-174 b	210558622.01	$2231.2161^{+0.0011}_{-0.0012}$	$19.56274^{+0.00076}_{-0.00073}$	$23.5^{+2.2}_{-4.2}$	$88.94^{+0.71}_{-0.96}$	$0.0357^{+0.0023}_{-0.0009}$	$2.49^{+0.18}_{-0.10}$	$0.639^{+0.020}_{-0.019}$	$0.668^{+0.022}_{-0.021}$	12.034	$< 1.00e-04$	Planet	
	210609658.01	2241.4056 ± 0.0011	$14.14524^{+0.00044}_{-0.00047}$	$8.07^{+0.75}_{-0.51}$	$86.5^{+1.7}_{-0.9}$	$0.0633^{+0.0015}_{-0.0019}$	$14.9^{+1.8}_{-1.5}$	$2.15^{+0.26}_{-0.21}$	$1.009^{+0.081}_{-0.049}$	12.587	–	Candidate	a
	210629082.01	$2253.0149^{+0.0051}_{-0.0052}$	$27.3531^{+0.0073}_{-0.0075}$	$25.7^{+3.1}_{-8.0}$	$89.0^{+0.7}_{-1.5}$	$0.0193^{+0.0029}_{-0.0012}$	$3.05^{+0.69}_{-0.43}$	$1.45^{+0.25}_{-0.18}$	$1.256^{+0.078}_{-0.058}$	11.580	$2.09e-03$	Candidate	
K2-175 b	210643811.01	$2240.2768^{+0.0045}_{-0.0044}$	$9.5260^{+0.0012}_{-0.0013}$	$11.1^{+1.3}_{-3.0}$	$87.5^{+1.7}_{-3.0}$	$0.0132^{+0.0013}_{-0.0007}$	$2.04^{+0.36}_{-0.27}$	$1.42^{+0.21}_{-0.17}$	$1.095^{+0.057}_{-0.039}$	10.632	$5.26e-04$	Planet	
K2-176 b	210667381.01	$2233.7859^{+0.0037}_{-0.0038}$	$5.32944^{+0.00061}_{-0.00071}$	$13.8^{+2.0}_{-4.4}$	$88.1^{+1.4}_{-2.9}$	$0.0158^{+0.0012}_{-0.0009}$	$1.49^{+0.12}_{-0.09}$	$0.864^{+0.033}_{-0.020}$	$0.939^{+0.020}_{-0.025}$	12.674	$5.38e-04$	Planet	
	210707130.01	$2231.68219^{+0.00074}_{-0.00072}$	0.684553 ± 0.000013	$5.7^{+0.7}_{-1.5}$	$85.5^{+3.3}_{-6.1}$	$0.0181^{+0.0014}_{-0.0010}$	$1.28^{+0.11}_{-0.08}$	$0.647^{+0.020}_{-0.019}$	$0.678^{+0.021}_{-0.022}$	12.099	$< 1.00e-04$	Planet	
	210718708.01	2237.0169 ± 0.0035	$8.77586^{+0.00090}_{-0.00089}$	$20.3^{+3.4}_{-7.2}$	$88.6^{+1.0}_{-2.2}$	$0.0251^{+0.0031}_{-0.0017}$	$1.98^{+0.26}_{-0.15}$	$0.722^{+0.035}_{-0.025}$	$0.757^{+0.028}_{-0.029}$	12.801	$< 1.00e-04$	Planet	
	210775710.01	2231.69728 ± 0.00013	59.84857 ± 0.00018	$114.7^{+4.2}_{-6.7}$	$89.854^{+0.098}_{-0.090}$	$0.1008^{+0.0019}_{-0.0011}$	$10.8^{+1.2}_{-0.6}$	$0.98^{+0.10}_{-0.05}$	$1.003^{+0.026}_{-0.027}$	11.827	$1.55e-03$	Candidate	
	210848071.01	2235.5288 ± 0.0028	41.6886 ± 0.0034	$55.0^{+6.0}_{-13.0}$	$89.53^{+0.33}_{-0.54}$	$0.0226^{+0.0018}_{-0.0009}$	$2.36^{+0.31}_{-0.17}$	$0.956^{+0.099}_{-0.055}$	$0.964^{+0.030}_{-0.032}$	11.040	$1.62e-03$	Candidate	
K2-177 b	210857328.01	$2237.0802^{+0.0071}_{-0.0069}$	$14.1552^{+0.0032}_{-0.0030}$	$10.6^{+1.6}_{-3.4}$	$87.2^{+2.0}_{-3.7}$	$0.0160^{+0.0018}_{-0.0009}$	$2.12^{+0.28}_{-0.16}$	$1.214^{+0.087}_{-0.061}$	$1.211^{+0.032}_{-0.038}$	12.584	$1.19e-04$	Planet	
	210894022.01	$2234.9691^{+0.0046}_{-0.0045}$	$5.35140^{+0.00060}_{-0.00061}$	$10.4^{+1.8}_{-3.7}$	$87.0^{+2.1}_{-4.3}$	$0.0121^{+0.0013}_{-0.0007}$	$1.22^{+0.20}_{-0.12}$	$0.92^{+0.11}_{-0.08}$	$0.877^{+0.036}_{-0.041}$	12.300	$< 1.00e-04$	Planet	
	210957318.01	$2234.90560^{+0.00024}_{-0.00025}$	$4.098492^{+0.000027}_{-0.000028}$	$11.71^{+0.59}_{-0.50}$	$86.56^{+0.40}_{-0.37}$	$0.1276^{+0.0028}_{-0.0034}$	$12.65^{+0.81}_{-0.53}$	$0.909^{+0.054}_{-0.029}$	$0.970^{+0.024}_{-0.027}$	13.171	–	Candidate	a
K2-178 b	210965800.01	2237.3366 ± 0.0015	8.74782 ± 0.00036	$18.5^{+1.9}_{-4.4}$	$88.6^{+1.0}_{-1.6}$	$0.0368^{+0.0011}_{-0.0009}$	$3.56^{+0.20}_{-0.14}$	$0.887^{+0.044}_{-0.026}$	$0.951^{+0.023}_{-0.028}$	12.134	$3.47e-04$	Planet	

Table 4 — *Continued*

New K2 Name	EPIC	T_0 (BJD-2454833)	P (d)	a/R_*	i (deg)	R_p/R_*	R_p ($R_\oplus$)	R_* ($R_\odot$)	M_* ($M_\odot$)	K_p	FPP	Disposition	Notes
K2-179 b	211048999.01	$2233.5803^{+0.0014}_{-0.0015}$	5.17219 ± 0.00020	$20.1^{+2.3}_{-5.1}$	$88.8^{+0.9}_{-1.6}$	$0.0300^{+0.0018}_{-0.0013}$	$2.51^{+0.16}_{-0.12}$	$0.768^{+0.022}_{-0.018}$	$0.824^{+0.022}_{-0.027}$	12.659	$4.97e-04$	Planet	
	211089792.01	2231.43152 ± 0.00010	3.2588240 ± 0.0000090	$10.99^{+0.61}_{-0.41}$	$86.97^{+0.62}_{-0.44}$	0.1289 ± 0.0035	$12.06^{+0.65}_{-0.47}$	$0.858^{+0.040}_{-0.024}$	$0.923^{+0.023}_{-0.026}$	12.914	–	Candidate	b,c
	211106187.01	$2239.2745^{+0.0030}_{-0.0028}$	$14.6431^{+0.0013}_{-0.0014}$	$55.0^{+15.0}_{-30.0}$	$89.4^{+0.5}_{-1.7}$	$0.046^{+0.026}_{-0.005}$	$66.0^{+43.0}_{-15.0}$	$13.2^{+4.6}_{-2.7}$	$1.10^{+0.47}_{-0.18}$	13.124	–	Candidate	a,b,d
	211147528.01	$2232.4082^{+0.0012}_{-0.0013}$	$2.349515^{+0.000080}_{-0.000077}$	$6.4^{+1.6}_{-1.1}$	$84.1^{+4.3}_{-3.0}$	$0.0905^{+0.0067}_{-0.0078}$	$53.0^{+6.0}_{-11.0}$	$5.4^{+0.5}_{-1.0}$	$2.02^{+0.05}_{-0.13}$	11.832	–	Candidate	a,c
K2-180 b	211319617.01	2310.3955 ± 0.0016	$8.86593^{+0.00032}_{-0.00033}$	$21.6^{+2.8}_{-6.3}$	$88.7^{+1.0}_{-1.7}$	$0.0324^{+0.0026}_{-0.0013}$	$2.41^{+0.21}_{-0.11}$	$0.681^{+0.021}_{-0.016}$	$0.730^{+0.020}_{-0.022}$	12.393	$< 1.00e-04$	Planet	
	211351816.01	$2309.0552^{+0.0052}_{-0.0046}$	8.4053 ± 0.0012	$8.7^{+2.0}_{-3.8}$	$85.9^{+2.9}_{-6.4}$	$0.0250^{+0.0032}_{-0.0016}$	$8.0^{+1.4}_{-1.0}$	$2.95^{+0.37}_{-0.30}$	$1.054^{+0.089}_{-0.067}$	12.409	–	Candidate	a
K2-181 b	211355342.01	$2310.7936^{+0.0026}_{-0.0025}$	6.89425 ± 0.00043	$18.4^{+2.2}_{-4.8}$	$88.6^{+1.0}_{-1.8}$	$0.0248^{+0.0021}_{-0.0013}$	$2.71^{+0.31}_{-0.18}$	$0.999^{+0.077}_{-0.041}$	$1.044^{+0.024}_{-0.029}$	12.637	$9.95e-04$	Planet	
K2-182 b	211359660.01	$2308.20586^{+0.00064}_{-0.00065}$	$4.736884^{+0.000071}_{-0.000075}$	$13.4^{+1.1}_{-2.3}$	$88.3^{+1.2}_{-1.7}$	$0.0321^{+0.0015}_{-0.0008}$	$2.77^{+0.17}_{-0.10}$	$0.790^{+0.032}_{-0.021}$	$0.847^{+0.024}_{-0.031}$	11.742	$5.97e-04$	Planet	
	211391664.01	$2312.9800^{+0.0015}_{-0.0016}$	$10.13680^{+0.00042}_{-0.00039}$	$14.6^{+1.0}_{-2.4}$	$88.5^{+1.0}_{-1.5}$	$0.0304^{+0.0012}_{-0.0007}$	$5.01^{+0.76}_{-0.74}$	1.51 ± 0.22	$1.156^{+0.082}_{-0.069}$	12.102	$2.65e-04$	Planet	
	211401787.01	$2318.0685^{+0.0025}_{-0.0024}$	13.7738 ± 0.0011	$20.1^{+2.5}_{-7.5}$	$88.6^{+1.0}_{-2.4}$	$0.0180^{+0.0019}_{-0.0007}$	$3.29^{+0.62}_{-0.47}$	$1.68^{+0.27}_{-0.23}$	$1.20^{+0.10}_{-0.09}$	9.709	$3.65e-03$	Candidate	
	211418290.01	$2308.80704^{+0.00081}_{-0.00086}$	5.03207 ± 0.00010	$4.92^{+0.05}_{-0.11}$	$88.4^{+1.1}_{-1.4}$	$0.09133^{+0.00069}_{-0.00063}$	$36.7^{+5.4}_{-3.9}$	$3.69^{+0.54}_{-0.39}$	$0.915^{+0.068}_{-0.051}$	11.504	–	Candidate	a
	211424769.01	2311.49837 ± 0.00031	$5.176243^{+0.000040}_{-0.000041}$	$12.5^{+1.1}_{-0.9}$	$85.1^{+0.9}_{-1.2}$	$0.16^{+0.20}_{-0.06}$	$19.0^{+25.0}_{-8.0}$	$1.12^{+0.11}_{-0.07}$	$1.102^{+0.041}_{-0.037}$	9.438	–	Candidate	a,e
	211491383.01	$2308.5884^{+0.0074}_{-0.0092}$	$4.1454^{+0.0010}_{-0.0008}$	$8.8^{+1.9}_{-3.1}$	$86.7^{+2.4}_{-5.2}$	$0.0084^{+0.0012}_{-0.0008}$	$1.20^{+0.26}_{-0.18}$	$1.31^{+0.22}_{-0.16}$	$1.101^{+0.053}_{-0.050}$	11.785	$2.40e-03$	Candidate	
	211525389.01	$2314.99178^{+0.00064}_{-0.00068}$	$8.26679^{+0.00014}_{-0.00013}$	$17.9^{+1.1}_{-2.1}$	$88.87^{+0.74}_{-0.94}$	$0.03437^{+0.00086}_{-0.00066}$	$3.41^{+0.23}_{-0.15}$	$0.909^{+0.058}_{-0.036}$	$0.965^{+0.031}_{-0.029}$	11.687	$< 1.00e-04$	Planet	
K2-183 c	211562654.01	$2314.7749^{+0.0031}_{-0.0028}$	$10.79347^{+0.00080}_{-0.00073}$	$19.0^{+3.0}_{-5.1}$	$88.4^{+1.1}_{-1.7}$	$0.0264^{+0.0025}_{-0.0012}$	$2.51^{+0.26}_{-0.14}$	$0.873^{+0.037}_{-0.023}$	$0.942^{+0.021}_{-0.025}$	12.754	$< 1.00e-04$	Planet	
K2-183 d	211562654.02	$2311.1552^{+0.0034}_{-0.0037}$	$22.6295^{+0.0018}_{-0.0019}$	$45.0^{+6.0}_{-14.0}$	$89.38^{+0.45}_{-0.84}$	$0.0267^{+0.0027}_{-0.0014}$	$2.54^{+0.28}_{-0.15}$	$0.873^{+0.037}_{-0.023}$	$0.942^{+0.021}_{-0.025}$	12.754	$< 1.00e-04$	Planet	
K2-183 b	211562654.03	$2307.6034^{+0.0019}_{-0.0021}$	$0.469269^{+0.000026}_{-0.000024}$	$1.40^{+0.93}_{-0.29}$	$25.0^{+56.0}_{-10.0}$	$0.03^{+0.27}_{-0.01}$	$3.0^{+26.0}_{-1.0}$	$0.873^{+0.037}_{-0.023}$	$0.942^{+0.021}_{-0.025}$	12.754	$< 1.00e-04$	Planet	
K2-184 b	211594205.01	2315.5008 ± 0.0014	$16.99344^{+0.00079}_{-0.00078}$	$48.0^{+6.0}_{-13.0}$	$89.47^{+0.40}_{-0.71}$	$0.0184^{+0.0016}_{-0.0009}$	$1.54^{+0.15}_{-0.09}$	$0.764^{+0.028}_{-0.025}$	$0.819^{+0.028}_{-0.030}$	10.680	$< 1.00e-04$	Planet	
	211606790.01	$2317.08969^{+0.00050}_{-0.00057}$	$37.24687^{+0.00085}_{-0.00069}$	$32.3^{+2.1}_{-1.9}$	$88.20^{+0.20}_{-0.23}$	$0.148^{+0.056}_{-0.031}$	$23.8^{+9.7}_{-5.6}$	$1.48^{+0.22}_{-0.17}$	$0.947^{+0.073}_{-0.032}$	12.673	–	Candidate	a,e
K2-185 b	211611158.01	$2311.7371^{+0.0060}_{-0.0054}$	$10.6166^{+0.0016}_{-0.0018}$	$27.0^{+5.0}_{-10.0}$	$88.9^{+0.8}_{-1.9}$	$0.0132^{+0.0021}_{-0.0011}$	$1.31^{+0.22}_{-0.12}$	$0.914^{+0.044}_{-0.033}$	0.976 ± 0.028	12.414	$7.24e-04$	Planet	
	211611158.02	$2326.1581^{+0.0025}_{-0.0024}$	$52.7141^{+0.0038}_{-0.0036}$	$48.0^{+33.0}_{-17.0}$	$89.00^{+0.79}_{-0.78}$	$0.0280^{+0.0044}_{-0.0043}$	$2.80^{+0.46}_{-0.44}$	$0.914^{+0.044}_{-0.033}$	0.976 ± 0.028	12.414	$4.16e-03$	Candidate	
	211682544.01	$2312.5676^{+0.0017}_{-0.0018}$	$50.8193^{+0.0024}_{-0.0025}$	$104.0^{+15.0}_{-34.0}$	$89.72^{+0.20}_{-0.40}$	$0.0237^{+0.0019}_{-0.0010}$	$2.17^{+0.21}_{-0.12}$	$0.837^{+0.040}_{-0.027}$	$0.898^{+0.027}_{-0.031}$	11.407	$2.92e-03$	Candidate	
	211733267.01	2311.93174 ± 0.00015	8.658168 ± 0.000030	$23.0^{+1.4}_{-1.0}$	$87.36^{+0.37}_{-0.39}$	$0.19^{+0.11}_{-0.06}$	$17.0^{+10.0}_{-5.0}$	$0.819^{+0.040}_{-0.028}$	$0.872^{+0.027}_{-0.029}$	12.150	$4.40e-01$	Candidate	
	211736671.01	2312.0974 ± 0.0013	4.73379 ± 0.00015	$8.6^{+1.7}_{-2.6}$	$86.1^{+2.7}_{-4.0}$	$0.0301^{+0.0030}_{-0.0014}$	$7.6^{+1.5}_{-1.2}$	$2.31^{+0.38}_{-0.35}$	1.29 ± 0.11	12.160	$8.45e-03$	Candidate	
	211743874.01	$2315.2087^{+0.0051}_{-0.0049}$	$12.2823^{+0.0017}_{-0.0018}$	$19.1^{+2.7}_{-6.3}$	$88.5^{+1.1}_{-2.2}$	$0.0164^{+0.0013}_{-0.0010}$	2.53 ± 0.38	$1.41^{+0.18}_{-0.19}$	$1.128^{+0.056}_{-0.040}$	12.486	–	Candidate	c
	211763214.01	$2313.5930^{+0.0056}_{-0.0067}$	$21.1918^{+0.0033}_{-0.0030}$	$30.0^{+5.0}_{-10.0}$	$89.0^{+0.7}_{-1.5}$	$0.0154^{+0.0016}_{-0.0011}$	$1.32^{+0.16}_{-0.10}$	$0.782^{+0.043}_{-0.028}$	$0.826^{+0.030}_{-0.031}$	12.529	$5.33e-03$	Candidate	
	211770696.01	$2312.9686^{+0.0051}_{-0.0048}$	16.2728 ± 0.0024	$14.8^{+1.8}_{-4.1}$	$88.1^{+1.3}_{-2.3}$	$0.0182^{+0.0016}_{-0.0009}$	$2.11^{+0.31}_{-0.25}$	$1.06^{+0.12}_{-0.11}$	$0.872^{+0.037}_{-0.035}$	12.253	–	Candidate	c
	211800191.01	$2307.74930^{+0.00036}_{-0.00035}$	1.1061750 ± 0.0000090	$2.68^{+0.26}_{-0.22}$	$67.3^{+3.1}_{-3.2}$	$0.089^{+0.060}_{-0.033}$	$8.8^{+6.0}_{-3.3}$	$0.906^{+0.091}_{-0.053}$	$0.917^{+0.036}_{-0.040}$	12.443	–	Candidate	a
	211818569.01	2310.56048 ± 0.00010	5.185759 ± 0.000014	$20.1^{+0.9}_{-1.3}$	$89.03^{+0.57}_{-0.54}$	$0.1021^{+0.0040}_{-0.0023}$	$7.64^{+0.37}_{-0.29}$	$0.686^{+0.020}_{-0.021}$	$0.727^{+0.025}_{-0.024}$	12.935	$< 1.00e-04$	Planet	
	211886472.01	$2319.37961^{+0.00015}_{-0.00017}$	$19.640123^{+0.000091}_{-0.000083}$	$36.4^{+2.1}_{-1.8}$	88.33 ± 0.21	$0.180^{+0.079}_{-0.052}$	$34.0^{+16.0}_{-11.0}$	$1.74^{+0.32}_{-0.27}$	$1.39^{+0.11}_{-0.08}$	11.126	–	Candidate	a,c,e
K2-186 b	211906650.01	$2321.8454^{+0.0019}_{-0.0020}$	$41.4742^{+0.0033}_{-0.0043}$	$49.0^{+4.0}_{-11.0}$	$89.52^{+0.33}_{-0.59}$	$0.02965^{+0.00093}_{-0.00087}$	$3.17^{+0.26}_{-0.16}$	$0.981^{+0.075}_{-0.041}$	$1.019^{+0.023}_{-0.027}$	12.193	$< 1.00e-04$	Planet	
	211913977.01	$2319.6820^{+0.0022}_{-0.0023}$	$14.67721^{+0.00085}_{-0.00082}$	$29.0^{+6.0}_{-12.0}$	$88.9^{+0.8}_{-2.0}$	$0.0261^{+0.0036}_{-0.0014}$	$2.19^{+0.31}_{-0.12}$	$0.770^{+0.022}_{-0.015}$	$0.833^{+0.020}_{-0.024}$	12.619	$4.27e-03$	Candidate	
	211941472.01	$2310.6169^{+0.0079}_{-0.0080}$	5.7819 ± 0.0013	$10.2^{+1.8}_{-2.7}$	$87.6^{+1.7}_{-3.5}$	$0.0096^{+0.0011}_{-0.0008}$	$1.44^{+0.26}_{-0.21}$	$1.38^{+0.19}_{-0.16}$	$1.020^{+0.043}_{-0.033}$	11.788	–	Candidate	c
	211945201.01	$2325.82591^{+0.00066}_{-0.00067}$	$19.49179^{+0.00052}_{-0.00051}$	$39.0^{+4.2}_{-9.1}$	$89.33^{+0.49}_{-0.73}$	$0.0380^{+0.0026}_{-0.0010}$	$5.85^{+0.95}_{-0.78}$	$1.41^{+0.21}_{-0.18}$	$1.143^{+0.059}_{-0.040}$	10.115	$1.64e-01$	Candidate	
	211978988.01	$2319.7054^{+0.0031}_{-0.0025}$	$36.5563^{+0.0036}_{-0.0042}$	$40.0^{+5.0}_{-11.0}$	$89.32^{+0.47}_{-0.81}$	$0.0263^{+0.0020}_{-0.0011}$	$2.97^{+0.44}_{-0.27}$	$1.04^{+0.13}_{-0.09}$	$0.988^{+0.028}_{-0.030}$	12.588	$2.57e-03$	Candidate	
	211993818.01	$2316.02846^{+0.00028}_{-0.00029}$	$8.986648^{+0.000068}_{-0.000067}$	$10.17^{+0.31}_{-0.23}$	$83.7^{+1.0}_{-1.3}$	$0.31^{+0.23}_{-0.10}$	$143.0^{+108.0}_{-50.0}$	$4.26^{+0.68}_{-0.52}$	$1.11^{+0.13}_{-0.06}$	7.218	–	Candidate	d
	212006318.01	$2314.326^{+0.011}_{-0.010}$	$14.4606^{+0.0037}_{-0.0047}$	$13.9^{+2.2}_{-4.6}$	$88.0^{+1.5}_{-3.1}$	$0.0151^{+0.0017}_{-0.0011}$	$1.76^{+0.31}_{-0.19}$	$1.07^{+0.14}_{-0.09}$	$1.030^{+0.027}_{-0.028}$	12.909	$1.13e-03$	Candidate	
	212008766.01	$2312.1114^{+0.0026}_{-0.0025}$	14.1334 ± 0.0010	$26.6^{+3.5}_{-9.8}$	$89.0^{+0.7}_{-1.9}$	$0.0285^{+0.0064}_{-0.0019}$	$2.32^{+0.53}_{-0.17}$	$0.748^{+0.026}_{-0.021}$	$0.805^{+0.026}_{-0.027}$	12.802	$1.50e-03$	Candidate	
	212012119.01	$2309.1345^{+0.0022}_{-0.0021}$	3.28086 ± 0.00017	$12.3^{+1.4}_{-3.3}$	$88.0^{+1.4}_{-2.9}$	$0.0268^{+0.0017}_{-0.0013}$	$2.13^{+0.15}_{-0.12}$	$0.727^{+0.023}_{-0.021}$	$0.760^{+0.028}_{-0.025}$	11.753	$2.26e-03$	Candidate	
	212110888.01	$2308.351088^{+0.000090}_{-0.000088}$	2.9956460 ± 0.0000060	$6.88^{+0.16}_{-0.14}$	$83.23^{+0.27}_{-0.24}$	$0.0880^{+0.0017}_{-0.0010}$	$14.0^{+2.0}_{-1.9}$	$1.45^{+0.21}_{-0.20}$	$1.120^{+0.053}_{-0.044}$	11.441	$9.17e-04$	Planet	
	212132195.01	$2331.3908^{+0.0016}_{-0.0017}$	$26.1970^{+0.0023}_{-0.0022}$	$55.0^{+7.0}_{-18.0}$	$89.52^{+0.35}_{-0.77}$	$0.0313^{+0.0021}_{-0.0014}$	$2.36^{+0.17}_{-0.13}$	$0.692^{+0.021}_{-0.020}$	$0.737^{+0.025}_{-0.024}$	11.670	$2.29e-03$	Candidate	
	212138198.01	$2309.37287^{+0.00056}_{-0.00060}$	$3.209149^{+0.000047}_{-0.000042}$	$15.0^{+15.0}_{-5.0}$	$86.5^{+3.0}_{-3.3}$	$0.06^{+0.18}_{-0.01}$	$5.0^{+17.0}_{-1.0}$	$0.839^{+0.038}_{-0.028}$	$0.898^{+0.027}_{-0.029}$	12.902	–	Candidate	c
K2-187 d	212157262.01	2313.3285 ± 0.0020	$7.14908^{+0.00036}_{-0.00037}$	$14.8^{+4.2}_{-6.6}$	$87.5^{+1.9}_{-3.9}$	$0.0330^{+0.0050}_{-0.0023}$	$3.22^{+0.51}_{-0.25}$	$0.895^{+0.041}_{-0.026}$	$0.967^{+0.025}_{-0.024}$	12.864	$< 1.00e-04$	Planet	
K2-187 e	212157262.02	$2308.4722^{+0.0050}_{-0.0055}$	$13.6083^{+0.0017}_{-0.0016}$	$26.3^{+3.4}_{-7.3}$	$89.0^{+0.8}_{-1.3}$	$0.0231^{+0.0020}_{-0.0012}$	$2.26^{+0.22}_{-0.13}$	$0.895^{+0.041}_{-0.026}$	$0.967^{+0.025}_{-0.024}$	12.864	$< 1.00e-04$	Planet	
K2-187 c	212157262.03	$2308.7638^{+0.0036}_{-0.0039}$	2.87179 ± 0.00026	$7.6^{+1.2}_{-3.0}$	$86.1^{+2.8}_{-7.0}$	$0.0174^{+0.0024}_{-0.0011}$	$1.70^{+0.25}_{-0.11}$	$0.895^{+0.041}_{-0.026}$	$0.967^{+0.025}_{-0.024}$	12.864	$< 1.00e-04$	Planet	
K2-187 b	212157262.04	$2308.0935^{+0.0028}_{-0.0030}$	$0.773981^{+0.000052}_{-0.000050}$	$3.38^{+0.48}_{-0.98}$	$82.0^{+6.0}_{-12.0}$	$0.0142^{+0.0015}_{-0.0008}$	$1.38^{+0.16}_{-0.09}$	$0.895^{+0.041}_{-0.026}$	$0.967^{+0.025}_{-0.024}$	12.864	$< 1.00e-04$	Planet	
K2-188 b	212164470.01	$2309.2133^{+0.0050}_{-0.0047}$	1.74298 ± 0.00026	$4.7^{+0.8}_{-1.7}$	$83.9^{+4.4}_{-9.9}$	$0.01041^{+0.00090}_{-0.00072}$	$1.26^{+0.16}_{-0.11}$	$1.11^{+0.11}_{-0.06}$	$1.107^{+0.031}_{-0.025}$	12.704	$< 1.00e-04$	Planet	
K2-188 c	212164470.02	2311.8660 ± 0.0026	$7.80760^{+0.00056}_{-0.00060}$	$15.2^{+2.1}_{-4.8}$	$88.1^{+1.4}_{-2.6}$	$0.0217^{+0.0014}_{-0.0008}$	$2.63^{+0.31}_{-0.18}$	$1.11^{+0.16}_{-0.06}$	$1.107^{+0.041}_{-0.025}$	12.704	$< 1.00e-04$	Planet	
	212303338.01	$2385.3925^{+0.0034}_{-0.0033}$	$0.595621^{+0.000044}_{-0.000046}$	$4.7^{+1.6}_{-1.7}$	$84.0^{+4.0}_{-10.0}$	$0.0062^{+0.0011}_{-0.0007}$	$0.58^{+0.11}_{-0.07}$	$0.863^{+0.053}_{-0.030}$	$0.915^{+0.025}_{-0.029}$	9.957	–	Candidate	c
	212357477.01	$2388.2300^{+0.0013}_{-0.0012}$	6.32667 ± 0.00020	$21.9^{+3.3}_{-7.6}$	$88.7^{+1.0}_{-2.0}$	$0.0205^{+0.0018}_{-0.0009}$	$2.12^{+0.23}_{-0.12}$	$0.947^{+0.058}_{-0.033}$	$1.000^{+0.024}_{-0.028}$	10.215	$3.04e-03$	Candidate	
K2-189 b	212394689.01	$2420.2044^{+0.0019}_{-0.0017}$	$5.17630^{+0.00041}_{-0.00043}$	$14.9^{+2.3}_{-5.0}$	$88.1^{+1.4}_{-2.8}$	$0.0161^{+0.0015}_{-0.0009}$	$1.51^{+0.15}_{-0.10}$	$0.862^{+0.038}_{-0.027}$	$0.928^{+0.024}_{-0.027}$	12.206	$< 1.00e-04$	Planet	
K2-189 c	212394689.02	$2390.4181^{+0.0014}_{-0.0016}$	6.67934 ± 0.00024	$17.0^{+2.9}_{-7.3}$	$88.2^{+1.3}_{-3.3}$	$0.0264^{+0.0031}_{-0.0012}$	$2.48^{+0.32}_{-0.14}$	$0.862^{+0.038}_{-0.027}$	$0.928^{+0.024}_{-0.027}$	12.206	$< 1.00e-04$	Planet	

Table 4 — *Continued*

New K2 Name	EPIC	T_0 (BJD-2454833)	P (d)	a/R_*	i (deg)	R_p/R_*	R_p ($R_\oplus$)	R_* ($R_\odot$)	M_* ($M_\odot$)	K_p	FPP	Disposition	Notes
	212460519.01	$2390.7941^{+0.0016}_{-0.0015}$	7.38707 ± 0.00028	$20.3^{+2.4}_{-5.3}$	$88.7^{+1.0}_{-1.6}$	$0.0280^{+0.0020}_{-0.0011}$	$1.80^{+0.14}_{-0.08}$	$0.589^{+0.016}_{-0.014}$	$0.610^{+0.019}_{-0.018}$	12.445	$< 1.00e-04$	Planet	
K2-190 b	212480208.01	2391.7679 ± 0.0026	$10.09886^{+0.00062}_{-0.00064}$	$17.2^{+2.4}_{-5.5}$	$88.4^{+1.2}_{-2.3}$	$0.0136^{+0.0010}_{-0.0006}$	$1.36^{+0.18}_{-0.10}$	$0.912^{+0.096}_{-0.058}$	$0.905^{+0.033}_{-0.036}$	10.892	$< 1.00e-04$	Planet	
K2-190 c	212480208.02	$2395.6926^{+0.0065}_{-0.0073}$	$21.5740^{+0.0057}_{-0.0043}$	$28.0^{+5.0}_{-10.0}$	$89.0^{+0.7}_{-1.6}$	$0.0110^{+0.0010}_{-0.0006}$	$1.09^{+0.15}_{-0.09}$	$0.912^{+0.096}_{-0.058}$	$0.905^{+0.033}_{-0.036}$	10.892	$< 1.00e-04$	Planet	
K2-191 b	212496592.01	2386.5570 ± 0.0029	$2.85865^{+0.00017}_{-0.00018}$	$8.6^{+1.2}_{-2.7}$	$87.1^{+2.1}_{-4.9}$	$0.0172^{+0.0028}_{-0.0013}$	$1.58^{+0.27}_{-0.13}$	$0.840^{+0.036}_{-0.026}$	$0.901^{+0.026}_{-0.028}$	12.966	$< 1.00e-04$	Planet	
	212521166.01	$2386.87440^{+0.00072}_{-0.00068}$	$13.86391^{+0.00022}_{-0.00023}$	$32.3^{+2.1}_{-5.7}$	$89.36^{+0.43}_{-0.75}$	$0.0334^{+0.0018}_{-0.0007}$	$2.52^{+0.16}_{-0.10}$	$0.692^{+0.024}_{-0.023}$	$0.724^{+0.025}_{-0.024}$	11.590	$< 1.00e-04$	Planet	
	212534729.01	$2390.5239^{+0.0044}_{-0.0056}$	$13.4850^{+0.0015}_{-0.0014}$	$31.6^{+4.5}_{-7.5}$	$89.3^{+0.5}_{-1.0}$	$0.0170^{+0.0016}_{-0.0012}$	$1.57^{+0.19}_{-0.13}$	$0.843^{+0.064}_{-0.034}$	$0.879^{+0.029}_{-0.032}$	13.066	–	Candidate	c
K2-192 b	212555594.01	$2387.4424^{+0.0020}_{-0.0021}$	$4.16322^{+0.00021}_{-0.00020}$	$17.4^{+2.7}_{-5.2}$	$88.4^{+1.1}_{-2.1}$	$0.0174^{+0.0014}_{-0.0011}$	$1.57^{+0.15}_{-0.11}$	$0.828^{+0.042}_{-0.027}$	$0.873^{+0.024}_{-0.031}$	12.482	$1.71e-04$	Planet	
	212562715.01	$2387.4693^{+0.0028}_{-0.0030}$	$13.5247^{+0.0011}_{-0.0009}$	$37.0^{+6.0}_{-11.0}$	$89.3^{+0.5}_{-1.1}$	$0.0235^{+0.0019}_{-0.0013}$	$2.28^{+0.21}_{-0.15}$	$0.888^{+0.038}_{-0.027}$	$0.955^{+0.022}_{-0.026}$	13.046	$4.03e-03$	Candidate	
	212577658.01	$2388.3213^{+0.0022}_{-0.0023}$	$14.06976^{+0.00072}_{-0.00071}$	$31.0^{+5.0}_{-11.0}$	$89.0^{+0.7}_{-1.4}$	$0.0192^{+0.0015}_{-0.0009}$	$1.87^{+0.18}_{-0.11}$	$0.890^{+0.052}_{-0.033}$	$0.945^{+0.027}_{-0.031}$	11.541	–	Candidate	c
K2-193 b	212580872.01	2391.2591 ± 0.0011	$14.78721^{+0.00043}_{-0.00047}$	$25.2^{+1.6}_{-3.5}$	$89.19^{+0.56}_{-0.76}$	$0.0385^{+0.0014}_{-0.0008}$	$4.01^{+0.34}_{-0.21}$	$0.957^{+0.074}_{-0.045}$	$0.994^{+0.029}_{-0.027}$	13.047	$< 1.00e-04$	Planet	
	212586030.01	$2387.8833^{+0.0035}_{-0.0039}$	$7.78523^{+0.00075}_{-0.00065}$	$9.0^{+21.0}_{-2.0}$	$83.5^{+5.9}_{-4.5}$	$0.04^{+0.18}_{-0.02}$	$8.0^{+36.0}_{-3.0}$	$1.82^{+0.22}_{-0.15}$	$1.007^{+0.077}_{-0.043}$	11.689	–	Candidate	c
	212587672.01	$2404.0437^{+0.0037}_{-0.0039}$	$23.2260^{+0.0031}_{-0.0032}$	$45.0^{+7.0}_{-16.0}$	$89.4^{+0.4}_{-1.0}$	$0.0216^{+0.0036}_{-0.0018}$	$2.24^{+0.40}_{-0.21}$	$0.953^{+0.057}_{-0.043}$	$0.987^{+0.034}_{-0.033}$	12.188	$1.57e-02$	Candidate	
	212639319.01	$2389.4365^{+0.0028}_{-0.0029}$	$13.84372^{+0.00095}_{-0.00087}$	$29.0^{+33.0}_{-13.0}$	$88.2^{+1.6}_{-2.9}$	$0.04^{+0.30}_{-0.01}$	$7.0^{+53.0}_{-2.0}$	$1.64^{+0.26}_{-0.23}$	$1.051^{+0.097}_{-0.073}$	12.471	$9.96e-01$	Candidate	
	212645891.01	2385.04150 ± 0.00018	0.3281520 ± 0.0000010	$1.441^{+0.066}_{-0.048}$	$41.6^{+5.4}_{-4.9}$	$0.14^{+0.11}_{-0.06}$	$15.0^{+12.0}_{-6.0}$	$0.990^{+0.072}_{-0.040}$	1.033 ± 0.026	12.641	–	Candidate	a
K2-194 b	212672300.01	2410.0070 ± 0.0043	$39.7214^{+0.0057}_{-0.0056}$	$31.0^{+4.0}_{-10.0}$	$89.1^{+0.6}_{-1.3}$	$0.0261^{+0.0025}_{-0.0010}$	$3.64^{+0.62}_{-0.50}$	$1.28^{+0.18}_{-0.17}$	$1.110^{+0.046}_{-0.035}$	12.846	$< 1.00e-04$	Planet	
	212686205.01	$2388.4481^{+0.0034}_{-0.0032}$	$5.67581^{+0.00041}_{-0.00043}$	$20.5^{+2.9}_{-7.1}$	$88.7^{+1.0}_{-2.2}$	$0.0170^{+0.0013}_{-0.0009}$	$1.20^{+0.10}_{-0.07}$	$0.651^{+0.021}_{-0.017}$	$0.687^{+0.023}_{-0.022}$	12.256	$< 1.00e-04$	Planet	
K2-195 b	212689874.01	$2392.0460^{+0.0017}_{-0.0018}$	$15.85354^{+0.00079}_{-0.00075}$	$24.1^{+2.0}_{-6.9}$	$89.0^{+0.7}_{-1.6}$	$0.0297^{+0.0013}_{-0.0007}$	$2.94^{+0.20}_{-0.13}$	$0.906^{+0.047}_{-0.033}$	$0.963^{+0.028}_{-0.032}$	12.330	$< 1.00e-04$	Planet	
K2-195 c	212689874.02	$2410.0089^{+0.0061}_{-0.0055}$	$28.4828^{+0.0064}_{-0.0073}$	$28.0^{+9.0}_{-15.0}$	$88.5^{+1.1}_{-2.7}$	$0.0261^{+0.0024}_{-0.0012}$	$2.58^{+0.27}_{-0.15}$	$0.906^{+0.047}_{-0.033}$	$0.963^{+0.028}_{-0.032}$	12.330	$< 1.00e-04$	Planet	
K2-196 b	212691422.01	2394.8907 ± 0.0051	$48.3242^{+0.0085}_{-0.0087}$	$23.0^{+9.0}_{-10.0}$	$88.3^{+1.4}_{-2.3}$	$0.0214^{+0.0017}_{-0.0013}$	$3.60^{+0.60}_{-0.50}$	$1.54^{+0.23}_{-0.19}$	$1.162^{+0.075}_{-0.045}$	11.923	$< 1.00e-04$	Planet	
	212697709.01	2385.28702 ± 0.00010	$3.9516260^{+0.0000080}_{-0.0000090}$	$10.27^{+0.43}_{-0.35}$	$85.09^{+0.30}_{-0.28}$	$0.0949^{+0.0033}_{-0.0030}$	$10.77^{+0.97}_{-0.66}$	$1.040^{+0.087}_{-0.054}$	$1.068^{+0.035}_{-0.032}$	12.193	$3.49e-04$	Planet	
	212703473.01	2389.7255 ± 0.0023	$6.78908^{+0.00036}_{-0.00035}$	$16.1^{+2.3}_{-4.9}$	$88.2^{+1.3}_{-2.3}$	$0.01507^{+0.00082}_{-0.00053}$	$1.61^{+0.14}_{-0.09}$	$0.978^{+0.068}_{-0.039}$	$1.020^{+0.025}_{-0.027}$	10.729	–	Candidate	c
	212703473.02	2388.1642 ± 0.0025	$18.51732^{+0.00092}_{-0.00093}$	$43.0^{+8.0}_{-16.0}$	$89.3^{+0.5}_{-1.1}$	$0.0174^{+0.0012}_{-0.0007}$	$1.86^{+0.18}_{-0.11}$	$0.978^{+0.068}_{-0.039}$	$1.020^{+0.025}_{-0.027}$	10.729	–	Candidate	c
K2-197 b	212735333.01	$2385.1830^{+0.0016}_{-0.0017}$	8.35795 ± 0.00028	$17.0^{+1.8}_{-4.3}$	$88.5^{+1.1}_{-1.9}$	$0.0252^{+0.0015}_{-0.0008}$	$2.50^{+0.19}_{-0.12}$	$0.910^{+0.042}_{-0.031}$	$0.975^{+0.025}_{-0.029}$	11.977	$< 1.00e-04$	Planet	
K2-198 b	212768333.01	$2388.61179^{+0.00073}_{-0.00074}$	$17.04318^{+0.00032}_{-0.00031}$	$42.0^{+4.1}_{-8.4}$	$89.40^{+0.41}_{-0.60}$	$0.0485^{+0.0023}_{-0.0014}$	$4.12^{+0.26}_{-0.17}$	$0.778^{+0.031}_{-0.024}$	0.836 ± 0.029	11.022	$2.74e-04$	Planet	
	212772313.01	$2393.3740^{+0.0090}_{-0.0079}$	$37.362^{+0.015}_{-0.016}$	$20.0^{+33.0}_{-11.0}$	$87.3^{+2.4}_{-5.1}$	$0.02^{+0.24}_{-0.01}$	$3.0^{+30.0}_{-1.0}$	$1.12^{+0.16}_{-0.13}$	0.972 ± 0.026	10.471	$3.23e-02$	Candidate	
K2-199 b	212779596.01	$2385.73787^{+0.00097}_{-0.00093}$	$3.225423^{+0.000067}_{-0.000071}$	$10.7^{+1.6}_{-3.8}$	$87.2^{+2.1}_{-4.2}$	$0.0259^{+0.0024}_{-0.0009}$	$1.88^{+0.19}_{-0.19}$	$0.667^{+0.020}_{-0.019}$	$0.706^{+0.024}_{-0.023}$	11.930	$< 1.00e-04$	Planet	
K2-199 c	212779596.02	$2389.93002^{+0.00067}_{-0.00063}$	$7.37450^{+0.00012}_{-0.00013}$	$22.1^{+2.0}_{-4.8}$	$88.9^{+0.8}_{-1.3}$	$0.0390^{+0.0021}_{-0.0011}$	$2.84^{+0.17}_{-0.11}$	$0.667^{+0.020}_{-0.019}$	$0.706^{+0.024}_{-0.023}$	11.930	$< 1.00e-04$	Planet	
	212803289.01	$2400.8260^{+0.0011}_{-0.0012}$	$18.24871^{+0.00063}_{-0.00057}$	$11.4^{+1.3}_{-1.6}$	$87.6^{+1.6}_{-1.4}$	$0.0424^{+0.0012}_{-0.0008}$	$10.5^{+1.5}_{-1.2}$	$2.28^{+0.32}_{-0.26}$	$1.42^{+0.10}_{-0.11}$	11.014	–	Candidate	a
K2-200 b	212828909.01	2385.5609 ± 0.0029	$2.84988^{+0.00019}_{-0.00018}$	$13.2^{+2.2}_{-4.3}$	$88.0^{+1.4}_{-3.2}$	$0.0158^{+0.0016}_{-0.0011}$	$1.36^{+0.14}_{-0.11}$	$0.792^{+0.024}_{-0.022}$	$0.860^{+0.023}_{-0.027}$	12.244	$1.11e-04$	Planet	
	213546283.01	2469.3568 ± 0.0015	$9.77019^{+0.00031}_{-0.00032}$	$22.9^{+2.4}_{-5.4}$	$88.9^{+0.8}_{-1.3}$	$0.0294^{+0.0015}_{-0.0010}$	$3.19^{+0.42}_{-0.33}$	$0.99^{+0.12}_{-0.10}$	0.911 ± 0.035	12.031	–	Candidate	c
	213817056.01	$2478.9450^{+0.0048}_{-0.0050}$	$13.6136^{+0.0017}_{-0.0016}$	23.0 ± 13.0	$88.0^{+1.5}_{-4.5}$	$0.04^{+0.19}_{-0.01}$	$3.0^{+11.0}_{-1.0}$	$0.781^{+0.030}_{-0.022}$	$0.817^{+0.027}_{-0.026}$	12.964	$3.60e-01$	Candidate	
	214234110.01	2470.8794 ± 0.0015	$4.63791^{+0.00016}_{-0.00015}$	$28.8^{+5.4}_{-9.5}$	$89.0^{+0.7}_{-1.4}$	$0.0174^{+0.0021}_{-0.0015}$	$1.87^{+0.27}_{-0.18}$	$0.985^{+0.077}_{-0.042}$	$1.032^{+0.028}_{-0.031}$	11.624	$2.47e-01$	Candidate	
	214254518.01	$2471.2170^{+0.0043}_{-0.0045}$	5.05903 ± 0.00049	$14.4^{+2.3}_{-4.4}$	$88.1^{+1.4}_{-2.7}$	$0.0153^{+0.0015}_{-0.0011}$	$1.04^{+0.10}_{-0.08}$	$0.624^{+0.019}_{-0.018}$	$0.653^{+0.022}_{-0.021}$	11.874	$1.47e-02$	Candidate	
	215171927.01	$2468.8706^{+0.0037}_{-0.0035}$	$4.13571^{+0.00031}_{-0.00034}$	$13.1^{+2.4}_{-4.7}$	$87.7^{+1.7}_{-3.5}$	$0.0192^{+0.0018}_{-0.0012}$	$1.60^{+0.16}_{-0.11}$	$0.764^{+0.025}_{-0.018}$	$0.811^{+0.024}_{-0.026}$	12.692	–	Candidate	b
	215171927.02	$2473.8953^{+0.0068}_{-0.0072}$	6.6312 ± 0.0011	$17.8^{+3.7}_{-5.8}$	$88.4^{+1.6}_{-2.3}$	$0.0163^{+0.0016}_{-0.0013}$	$1.36^{+0.14}_{-0.11}$	$0.764^{+0.025}_{-0.018}$	$0.811^{+0.024}_{-0.026}$	12.692	–	Candidate	b
	215502661.01	$2473.223^{+0.011}_{-0.010}$	$21.5216^{+0.0051}_{-0.0061}$	$21.0^{+15.0}_{-14.0}$	$87.7^{+1.9}_{-8.5}$	$0.02^{+0.19}_{-0.00}$	$2.0^{+24.0}_{-1.0}$	$1.16^{+0.17}_{-0.14}$	$0.978^{+0.029}_{-0.027}$	12.032	$9.78e-01$	Candidate	
	215854715.01	$2477.0811^{+0.0046}_{-0.0055}$	$11.1237^{+0.0015}_{-0.0012}$	$21.1^{+2.9}_{-6.0}$	$88.7^{+0.9}_{-1.7}$	$0.0192^{+0.0014}_{-0.0012}$	$1.72^{+0.14}_{-0.12}$	$0.821^{+0.029}_{-0.023}$	$0.885^{+0.023}_{-0.028}$	12.611	–	Candidate	b
K2-201 b	216008129.01	2468.9841 ± 0.0019	$1.059790^{+0.000043}_{-0.000044}$	$4.7^{+0.6}_{-1.1}$	$84.4^{+4.1}_{-6.7}$	$0.0146^{+0.0013}_{-0.0007}$	$1.40^{+0.14}_{-0.08}$	$0.878^{+0.029}_{-0.021}$	$0.956^{+0.020}_{-0.021}$	11.966	$< 1.00e-04$	Planet	
K2-201 c	216008129.02	$2486.7830^{+0.0023}_{-0.0022}$	$22.7799^{+0.0020}_{-0.0019}$	$41.0^{+6.0}_{-13.0}$	$89.27^{+0.52}_{-0.92}$	$0.0343^{+0.0040}_{-0.0017}$	$3.29^{+0.40}_{-0.18}$	$0.878^{+0.029}_{-0.021}$	$0.956^{+0.020}_{-0.021}$	11.966	$2.71e-04$	Planet	
	216050437.01	$2475.24064^{+0.00083}_{-0.00082}$	14.94897 ± 0.00032	$15.8^{+1.4}_{-1.1}$	$85.77^{+0.82}_{-0.91}$	$0.22^{+0.23}_{-0.11}$	$37.0^{+39.0}_{-19.0}$	$1.52^{+0.28}_{-0.16}$	$1.381^{+0.094}_{-0.070}$	12.326	–	Candidate	a,c,d
	216114172.01	$2470.2127^{+0.0081}_{-0.0084}$	$13.1252^{+0.0022}_{-0.0023}$	$22.0^{+3.7}_{-8.4}$	$88.7^{+0.9}_{-2.3}$	$0.0157^{+0.0026}_{-0.0013}$	$1.68^{+0.29}_{-0.15}$	$0.977^{+0.061}_{-0.039}$	$1.029^{+0.028}_{-0.027}$	12.603	–	Candidate	b
	216166748.01	2470.3619 ± 0.0025	$19.6794^{+0.0011}_{-0.0010}$	$29.0^{+6.0}_{-12.0}$	$88.8^{+0.9}_{-1.8}$	$0.0212^{+0.0036}_{-0.0013}$	$2.32^{+0.42}_{-0.18}$	$1.002^{+0.061}_{-0.046}$	$1.050^{+0.030}_{-0.034}$	11.884	–	Candidate	b,d
	216387101.01	$2470.0120^{+0.0086}_{-0.0079}$	$9.7619^{+0.0018}_{-0.0017}$	$12.7^{+4.7}_{-9.0}$	$87.0^{+2.0}_{-15.0}$	$0.018^{+0.079}_{-0.002}$	$3.0^{+15.0}_{-1.0}$	$1.77^{+0.23}_{-0.21}$	$0.990^{+0.041}_{-0.038}$	12.897	$3.00e-02$	Candidate	
K2-202 b	216405287.01	$2471.2515^{+0.0016}_{-0.0017}$	$3.40516^{+0.00013}_{-0.00012}$	$11.9^{+1.5}_{-3.4}$	$87.7^{+1.6}_{-2.9}$	$0.0232^{+0.0013}_{-0.0010}$	$2.30^{+0.18}_{-0.13}$	$0.911^{+0.051}_{-0.034}$	$0.971^{+0.030}_{-0.028}$	12.997	$< 1.00e-04$	Planet	
	216468514.01	2471.52446 ± 0.00013	3.313921 ± 0.000010	$5.93^{+0.14}_{-0.11}$	$82.36^{+0.34}_{-0.26}$	$0.0827^{+0.0017}_{-0.0011}$	$12.0^{+1.6}_{-1.0}$	$1.33^{+0.18}_{-0.10}$	$1.258^{+0.051}_{-0.046}$	12.749	–	Candidate	a,c
	216494238.01	$2474.5834^{+0.0060}_{-0.0056}$	$19.8946^{+0.0027}_{-0.0029}$	$17.5^{+1.7}_{-3.7}$	$88.6^{+1.0}_{-1.5}$	$0.0479^{+0.0023}_{-0.0019}$	$5.55^{+0.45}_{-0.33}$	$1.064^{+0.069}_{-0.047}$	$1.101^{+0.025}_{-0.028}$	12.302	–	Candidate	c
	217192839.01	$2471.8448^{+0.0041}_{-0.0042}$	7.93926 ± 0.00080	$29.0^{+8.0}_{-20.0}$	$88.9^{+0.8}_{-5.4}$	$0.015^{+0.013}_{-0.002}$	$1.08^{+0.94}_{-0.13}$	$0.646^{+0.021}_{-0.019}$	$0.678^{+0.023}_{-0.022}$	12.601	–	Candidate	c
	217192839.02	2471.2912 ± 0.0018	$16.03505^{+0.00080}_{-0.00081}$	$31.0^{+9.0}_{-16.0}$	$88.8^{+0.9}_{-2.3}$	$0.0292^{+0.0081}_{-0.0035}$	$2.06^{+0.57}_{-0.25}$	$0.646^{+0.021}_{-0.019}$	$0.678^{+0.023}_{-0.022}$	12.601	–	Candidate	c
	217192839.03	2474.9123 ± 0.0031	26.8050 ± 0.0024	$56.0^{+9.0}_{-18.0}$	$89.48^{+0.38}_{-0.73}$	$0.0217^{+0.0039}_{-0.0017}$	$1.53^{+0.28}_{-0.13}$	$0.646^{+0.021}_{-0.019}$	$0.678^{+0.023}_{-0.022}$	12.601	–	Candidate	c
	217855533.01	$2487.3845^{+0.0063}_{-0.0060}$	$21.5873^{+0.0047}_{-0.0053}$	$31.3^{+4.7}_{-9.4}$	$89.1^{+0.6}_{-1.2}$	$0.01113^{+0.00095}_{-0.00070}$	$1.78^{+0.32}_{-0.25}$	$1.47^{+0.23}_{-0.18}$	$1.203^{+0.089}_{-0.062}$	10.043	$1.24e-03$	Candidate	
	217941732.01	$2470.2003^{+0.0022}_{-0.0021}$	2.49416 ± 0.00012	$10.0^{+1.5}_{-2.5}$	$87.6^{+1.7}_{-3.4}$	$0.0151^{+0.0016}_{-0.0012}$	$1.06^{+0.12}_{-0.09}$	$0.644^{+0.020}_{-0.018}$	0.675 ± 0.021	12.283	$< 1.00e-04$	Planet	
	217977895.01	$2481.3702^{+0.0041}_{-0.0042}$	$21.6976^{+0.0023}_{-0.0022}$	$26.0^{+12.0}_{-16.0}$	$88.3^{+1.4}_{-4.7}$	$0.029^{+0.064}_{-0.006}$	$2.8^{+6.1}_{-0.6}$	$0.882^{+0.038}_{-0.028}$	$0.948^{+0.025}_{-0.028}$	12.745	$4.00e-02$	Candidate	

Table 4 — *Continued*

New K2 Name	EPIC	T_0 (BJD-2454833)	P (d)	a/R_*	i (deg)	R_p/R_*	R_p ($R_\oplus$)	R_* ($R_\odot$)	M_* ($M_\odot$)	K_p	FPP	Disposition	Notes
	218131080.01	2468.80843 ± 0.00026	3.142846 ± 0.000018	$4.78^{+0.29}_{-0.21}$	$83.1^{+1.4}_{-1.0}$	$0.0626^{+0.0008}_{-0.0010}$	$8.8^{+1.6}_{-0.8}$	$1.29^{+0.24}_{-0.12}$	$1.214^{+0.064}_{-0.049}$	12.700	–	Candidate	a,c
	218170789.01	$2470.4022^{+0.0049}_{-0.0051}$	3.04162 ± 0.00032	$2.01^{+0.26}_{-0.18}$	$57.3^{+6.2}_{-6.6}$	$0.09^{+0.16}_{-0.05}$	$9.0^{+15.0}_{-5.0}$	$0.874^{+0.051}_{-0.049}$	$0.858^{+0.028}_{-0.024}$	12.890	–	Candidate	a
	218304292.01	$2473.8158^{+0.0024}_{-0.0023}$	$8.42166^{+0.00038}_{-0.00040}$	86.0 ± 29.0	$89.68^{+0.22}_{-0.53}$	$0.0258^{+0.0050}_{-0.0026}$	$3.46^{+0.84}_{-0.53}$	$1.23^{+0.17}_{-0.14}$	$0.918^{+0.057}_{-0.043}$	12.511	$8.32e-01$	Candidate	
	218668602.01	$2469.0913^{+0.0030}_{-0.0031}$	1.86598 ± 0.00012	$6.3^{+1.1}_{-2.5}$	$85.3^{+3.4}_{-8.6}$	$0.0207^{+0.0032}_{-0.0015}$	$1.86^{+0.30}_{-0.14}$	$0.825^{+0.027}_{-0.019}$	$0.899^{+0.021}_{-0.023}$	12.411	$1.57e-03$	Candidate	
	218916923.01	2492.81728 ± 0.00036	$28.38207^{+0.00028}_{-0.00027}$	$45.8^{+2.1}_{-2.5}$	$89.56^{+0.26}_{-0.20}$	$0.0974^{+0.0023}_{-0.0020}$	$9.27^{+0.42}_{-0.31}$	$0.872^{+0.034}_{-0.023}$	$0.949^{+0.024}_{-0.022}$	11.470	–	Candidate	a,c
	219388192.01	2470.98880 ± 0.00028	5.292605 ± 0.000031	$13.35^{+0.19}_{-0.43}$	$89.30^{+0.49}_{-0.66}$	$0.09434^{+0.00085}_{-0.00070}$	$9.98^{+0.91}_{-0.47}$	$0.970^{+0.088}_{-0.045}$	$1.004^{+0.026}_{-0.025}$	12.336	–	Candidate	a
K2-203 b	220170303.01	2563.6388 ± 0.0058	9.6951 ± 0.0013	$19.0^{+3.8}_{-8.5}$	$88.4^{+1.2}_{-3.3}$	$0.0165^{+0.0032}_{-0.0014}$	$1.37^{+0.28}_{-0.12}$	$0.763^{+0.030}_{-0.024}$	$0.794^{+0.033}_{-0.028}$	12.114	$< 1.00e-04$	Planet	
K2-204 b	220186645.01	$2563.5086^{+0.0037}_{-0.0038}$	$7.05578^{+0.00065}_{-0.00064}$	$11.0^{+1.3}_{-3.2}$	$87.6^{+1.7}_{-3.3}$	$0.02371^{+0.00094}_{-0.00082}$	$3.05^{+0.43}_{-0.37}$	$1.18^{+0.16}_{-0.14}$	$1.009^{+0.031}_{-0.027}$	12.961	$< 1.00e-04$	Planet	
	220192485.01	$2576.22330^{+0.00040}_{-0.00037}$	$50.69364^{+0.00057}_{-0.00055}$	$75.6^{+5.0}_{-3.4}$	$89.481^{+0.082}_{-0.054}$	$0.1004^{+0.0017}_{-0.0025}$	$8.68^{+0.46}_{-0.38}$	$0.793^{+0.040}_{-0.028}$	$0.840^{+0.027}_{-0.031}$	11.758	–	Candidate	c
	220207765.01	$2563.4263^{+0.0041}_{-0.0042}$	$7.11986^{+0.00062}_{-0.00064}$	$27.7^{+5.3}_{-7.5}$	$89.1^{+0.7}_{-1.3}$	$0.0202^{+0.0021}_{-0.0016}$	$1.88^{+0.21}_{-0.16}$	$0.852^{+0.033}_{-0.023}$	$0.927^{+0.025}_{-0.023}$	12.170	$5.27e-03$	Candidate	
K2-205 b	220211923.01	$2580.4191^{+0.0045}_{-0.0061}$	$26.6723^{+0.0042}_{-0.0037}$	$31.0^{+4.4}_{-9.3}$	$89.1^{+0.7}_{-1.2}$	$0.0170^{+0.0011}_{-0.0009}$	$2.00^{+0.27}_{-0.23}$	$1.08^{+0.13}_{-0.11}$	$0.951^{+0.038}_{-0.036}$	12.250	$< 1.00e-04$	Planet	
K2-206 b	220216730.01	$2563.5766^{+0.0039}_{-0.0043}$	$18.2945^{+0.0017}_{-0.0016}$	$28.3^{+3.0}_{-7.6}$	$89.1^{+0.6}_{-1.2}$	$0.0338^{+0.0023}_{-0.0014}$	$2.80^{+0.22}_{-0.15}$	$0.758^{+0.032}_{-0.027}$	$0.789^{+0.030}_{-0.028}$	12.826	$< 1.00e-04$	Planet	
K2-207 b	220218012.01	$2570.6446^{+0.0036}_{-0.0039}$	12.4875 ± 0.0012	$21.2^{+3.2}_{-5.9}$	$88.6^{+1.0}_{-1.6}$	$0.0257^{+0.0026}_{-0.0015}$	$2.61^{+0.37}_{-0.21}$	$0.928^{+0.092}_{-0.051}$	0.942 ± 0.028	12.971	$1.86e-04$	Planet	
K2-208 b	220225178.01	$2563.5116^{+0.0025}_{-0.0023}$	$4.19095^{+0.00023}_{-0.00025}$	$14.2^{+2.1}_{-4.0}$	$88.0^{+1.4}_{-2.5}$	$0.0178^{+0.0016}_{-0.0012}$	$1.68^{+0.16}_{-0.12}$	$0.862^{+0.034}_{-0.030}$	0.925 ± 0.030	12.302	$< 1.00e-04$	Planet	
K2-209 b	220241529.01	$2561.2331^{+0.0027}_{-0.0025}$	2.08061 ± 0.00013	$8.5^{+1.8}_{-3.5}$	$86.2^{+2.7}_{-6.3}$	$0.0112^{+0.0013}_{-0.0007}$	$0.87^{+0.10}_{-0.06}$	0.712 ± 0.020	$0.745^{+0.026}_{-0.024}$	10.717	$< 1.00e-04$	Planet	
	220245303.01	$2563.4771^{+0.0038}_{-0.0036}$	$3.68034^{+0.00036}_{-0.00032}$	$12.9^{+2.7}_{-4.3}$	$87.9^{+1.5}_{-3.3}$	$0.0126^{+0.0022}_{-0.0012}$	$1.06^{+0.19}_{-0.10}$	$0.775^{+0.023}_{-0.021}$	$0.837^{+0.024}_{-0.028}$	11.821	$1.22e-03$	Candidate	
K2-210 b	220250254.01	2560.9580 ± 0.0021	0.570233 ± 0.000028	$4.3^{+0.8}_{-1.3}$	$84.1^{+4.2}_{-9.0}$	$0.0088^{+0.0010}_{-0.0007}$	$0.82^{+0.10}_{-0.07}$	$0.852^{+0.042}_{-0.025}$	$0.912^{+0.023}_{-0.028}$	11.507	$2.31e-04$	Planet	
K2-211 b	220256496.01	$2560.8136^{+0.0021}_{-0.0022}$	0.669558 ± 0.000032	$3.4^{+0.6}_{-1.1}$	$82.0^{+6.0}_{-13.0}$	$0.0155^{+0.0018}_{-0.0011}$	$1.37^{+0.17}_{-0.10}$	$0.816^{+0.033}_{-0.019}$	$0.882^{+0.019}_{-0.027}$	12.872	$2.16e-04$	Planet	
	220292715.01	2574.48548 ± 0.00056	$41.55293^{+0.00077}_{-0.00087}$	$86.0^{+26.0}_{-23.0}$	89.55 ± 0.32	$0.0526^{+0.0045}_{-0.0033}$	$4.16^{+0.38}_{-0.29}$	$0.724^{+0.025}_{-0.022}$	$0.762^{+0.026}_{-0.025}$	12.213	$1.11e-01$	Candidate	
	220294712.01	$2580.7194^{+0.0030}_{-0.0027}$	$23.6079^{+0.0020}_{-0.0023}$	$27.7^{+3.4}_{-7.5}$	$89.0^{+0.7}_{-1.2}$	$0.0256^{+0.0024}_{-0.0011}$	$3.12^{+0.40}_{-0.21}$	$1.115^{+0.098}_{-0.058}$	$1.121^{+0.031}_{-0.030}$	12.264	–	Candidate	c
	220317172.01	2563.1520 ± 0.0028	$4.43572^{+0.00031}_{-0.00032}$	$33.0^{+7.0}_{-10.0}$	$89.2^{+0.6}_{-1.2}$	$0.0143^{+0.0016}_{-0.0012}$	$1.32^{+0.16}_{-0.12}$	$0.847^{+0.036}_{-0.023}$	$0.913^{+0.021}_{-0.026}$	12.107	$5.11e-02$	Candidate	
K2-212 b	220321605.01	2566.6413 ± 0.0011	9.79540 ± 0.00029	$28.4^{+2.5}_{-7.3}$	$89.2^{+0.6}_{-1.2}$	$0.0367^{+0.0019}_{-0.0011}$	$2.39^{+0.17}_{-0.09}$	$0.598^{+0.017}_{-0.014}$	$0.622^{+0.020}_{-0.018}$	12.588	$< 1.00e-04$	Planet	
K2-213 b	220341183.01	$2566.0026^{+0.0066}_{-0.0076}$	8.1309 ± 0.0018	$13.2^{+2.6}_{-5.0}$	$87.9^{+1.6}_{-3.7}$	$0.0115^{+0.0016}_{-0.0010}$	$1.51^{+0.30}_{-0.21}$	$1.20^{+0.17}_{-0.13}$	$1.070^{+0.055}_{-0.038}$	12.043	$< 1.00e-04$	Planet	
K2-214 b	220376054.01	$2563.5994^{+0.0024}_{-0.0028}$	$8.59653^{+0.00059}_{-0.00053}$	$15.6^{+2.3}_{-5.8}$	$88.1^{+1.3}_{-3.1}$	$0.0181^{+0.0020}_{-0.0008}$	$2.22^{+0.38}_{-0.26}$	$1.12^{+0.15}_{-0.12}$	$1.022^{+0.031}_{-0.028}$	11.597	$3.73e-04$	Planet	
	220383386.01	$2561.37357^{+0.00097}_{-0.00095}$	$0.959665^{+0.000020}_{-0.000021}$	$4.1^{+0.4}_{-1.0}$	$83.8^{+4.4}_{-8.2}$	$0.0178^{+0.0016}_{-0.0007}$	$1.62^{+0.17}_{-0.08}$	$0.837^{+0.048}_{-0.027}$	$0.890^{+0.026}_{-0.029}$	8.945	$2.90e-04$	Planet	
	220383386.02	2561.9795 ± 0.0016	29.8450 ± 0.0014	$42.0^{+6.0}_{-11.0}$	$89.33^{+0.49}_{-0.74}$	$0.0310^{+0.0029}_{-0.0012}$	$2.83^{+0.31}_{-0.14}$	$0.837^{+0.048}_{-0.027}$	$0.890^{+0.026}_{-0.029}$	8.945	$< 1.00e-04$	Planet	
	220397060.01	2570.2329 ± 0.0011	$12.09220^{+0.00038}_{-0.00036}$	$10.2^{+0.8}_{-1.2}$	87.7 ± 1.5	$0.0541^{+0.0022}_{-0.0013}$	$5.8^{+1.5}_{-0.5}$	$0.99^{+0.24}_{-0.09}$	$0.869^{+0.025}_{-0.020}$	12.835	–	Candidate	c,e
	220410754.01	$2570.2505^{+0.0073}_{-0.0071}$	$19.4966^{+0.0045}_{-0.0055}$	$25.0^{+6.0}_{-11.0}$	$88.9^{+0.8}_{-2.5}$	$0.0176^{+0.0027}_{-0.0015}$	$2.22^{+0.49}_{-0.32}$	$1.16^{+0.18}_{-0.13}$	$0.993^{+0.032}_{-0.033}$	12.843	$1.06e-03$	Candidate	
K2-215 b	220471666.01	$2561.3322^{+0.0023}_{-0.0024}$	$8.26965^{+0.00047}_{-0.00046}$	$28.1^{+4.3}_{-9.0}$	$89.0^{+0.7}_{-1.4}$	$0.0200^{+0.0015}_{-0.0011}$	$2.12^{+0.26}_{-0.16}$	$0.974^{+0.095}_{-0.049}$	$1.000^{+0.026}_{-0.027}$	12.798	$3.76e-04$	Planet	
K2-216 b	220481411.01	$2561.04171^{+0.00075}_{-0.00081}$	$2.174789^{+0.000039}_{-0.000038}$	$8.7^{+0.9}_{-2.1}$	$87.0^{+2.1}_{-3.5}$	$0.0231^{+0.0012}_{-0.0008}$	$1.68^{+0.10}_{-0.08}$	$0.666^{+0.022}_{-0.019}$	0.699 ± 0.023	12.100	$< 1.00e-04$	Planet	
K2-217 b	220487418.01	$2562.0045^{+0.0030}_{-0.0029}$	$14.07452^{+0.00099}_{-0.00094}$	$16.1^{+2.8}_{-6.2}$	$88.0^{+1.3}_{-3.0}$	$0.0246^{+0.0031}_{-0.0011}$	$3.58^{+0.49}_{-0.37}$	$1.33^{+0.20}_{-0.17}$	$1.103^{+0.046}_{-0.037}$	12.062	$3.56e-04$	Planet	
K2-218 b	220503236.01	2563.4591 ± 0.0019	$8.67989^{+0.00042}_{-0.00043}$	$16.0^{+1.6}_{-3.8}$	$88.5^{+1.1}_{-1.8}$	$0.0234^{+0.0017}_{-0.0009}$	$2.57^{+0.28}_{-0.15}$	$1.008^{+0.080}_{-0.046}$	$1.047^{+0.031}_{-0.028}$	12.713	$< 1.00e-04$	Planet	
	220555384.01	$2564.7712^{+0.0013}_{-0.0014}$	4.28452 ± 0.00014	$26.1^{+3.8}_{-7.2}$	$89.0^{+0.7}_{-1.4}$	$0.0192^{+0.0017}_{-0.0013}$	$1.30^{+0.12}_{-0.10}$	$0.622^{+0.020}_{-0.017}$	$0.650^{+0.021}_{-0.020}$	12.395	–	Candidate	c
K2-219 b	220592745.01	$2563.7453^{+0.0059}_{-0.0065}$	$3.90129^{+0.00066}_{-0.00068}$	$9.0^{+1.5}_{-3.1}$	$86.8^{+2.3}_{-4.8}$	$0.01039^{+0.00072}_{-0.00059}$	$1.35^{+0.20}_{-0.18}$	$1.19^{+0.16}_{-0.14}$	$1.022^{+0.034}_{-0.030}$	11.923	$< 1.00e-04$	Planet	
K2-219 c	220592745.02	$2565.4157^{+0.0090}_{-0.0075}$	$6.6677^{+0.0013}_{-0.0016}$	$10.3^{+1.7}_{-3.9}$	$87.3^{+2.0}_{-4.9}$	$0.01109^{+0.00074}_{-0.00060}$	$1.44^{+0.21}_{-0.19}$	$1.19^{+0.16}_{-0.14}$	$1.022^{+0.034}_{-0.030}$	11.923	$< 1.00e-04$	Planet	
K2-219 d	220592745.03	$2571.5943^{+0.0023}_{-0.0025}$	$11.13728^{+0.00081}_{-0.00079}$	$15.8^{+1.9}_{-4.1}$	$88.3^{+1.2}_{-2.0}$	$0.01986^{+0.00078}_{-0.00060}$	$2.58^{+0.36}_{-0.32}$	$1.19^{+0.16}_{-0.14}$	$1.022^{+0.034}_{-0.030}$	11.923	$< 1.00e-04$	Planet	
K2-220 b	220621788.01	$2568.2705^{+0.0020}_{-0.0022}$	$13.68251^{+0.00072}_{-0.00069}$	$28.0^{+5.0}_{-11.0}$	$88.9^{+0.8}_{-1.9}$	$0.0218^{+0.0016}_{-0.0009}$	$2.21^{+0.27}_{-0.14}$	$0.930^{+0.089}_{-0.044}$	$0.960^{+0.026}_{-0.029}$	11.752	$3.78e-04$	Planet	
	220643470.01	2560.8116 ± 0.0015	$2.653230^{+0.000084}_{-0.000089}$	$2.83^{+0.37}_{-0.20}$	$71.0^{+2.9}_{-1.8}$	$0.0416^{+0.0027}_{-0.0021}$	$62.0^{+11.0}_{-8.0}$	$13.7^{+2.3}_{-1.6}$	$0.97^{+0.22}_{-0.13}$	10.839	–	Candidate	c,f
	220648214.01	2583.6486 ± 0.0034	$29.4352^{+0.0053}_{-0.0051}$	$42.0^{+6.0}_{-14.0}$	$89.3^{+0.5}_{-1.0}$	$0.0223^{+0.0018}_{-0.0011}$	$2.92^{+0.48}_{-0.39}$	$1.20^{+0.17}_{-0.15}$	$1.012^{+0.033}_{-0.027}$	12.390	$6.32e-03$	Candidate	
K2-221 b	220650439.01	$2562.3558^{+0.0023}_{-0.0022}$	$2.39909^{+0.00013}_{-0.00012}$	$6.5^{+1.0}_{-2.0}$	$85.4^{+3.2}_{-5.8}$	$0.0162^{+0.0014}_{-0.0008}$	$1.68^{+0.17}_{-0.10}$	$0.948^{+0.045}_{-0.029}$	$1.011^{+0.024}_{-0.025}$	12.232	$< 1.00e-04$	Planet	
	220674823.01	2561.0108 ± 0.0012	0.571299 ± 0.000015	$2.65^{+0.30}_{-0.66}$	$80.0^{+7.0}_{-13.0}$	$0.0169^{+0.0014}_{-0.0007}$	$1.67^{+0.16}_{-0.09}$	$0.906^{+0.051}_{-0.029}$	$0.967^{+0.023}_{-0.028}$	11.958	$< 1.00e-04$	Planet	
	220674823.02	$2572.7341^{+0.0029}_{-0.0027}$	$13.3397^{+0.0010}_{-0.0011}$	$23.7^{+4.5}_{-9.9}$	$88.6^{+1.0}_{-2.3}$	$0.0274^{+0.0033}_{-0.0014}$	$2.70^{+0.36}_{-0.16}$	$0.906^{+0.051}_{-0.029}$	$0.967^{+0.023}_{-0.028}$	11.958	$< 1.00e-04$	Planet	
	220679255.01	$2567.9859^{+0.0052}_{-0.0051}$	$8.1332^{+0.0012}_{-0.0013}$	$26.0^{+6.0}_{-11.0}$	$88.9^{+0.8}_{-2.1}$	$0.0174^{+0.0026}_{-0.0016}$	$2.05^{+0.40}_{-0.23}$	$1.08^{+0.13}_{-0.07}$	$1.071^{+0.027}_{-0.032}$	11.975	$2.56e-02$	Candidate	
K2-222 b	220709978.01	$2566.0599^{+0.0021}_{-0.0022}$	$15.38883^{+0.00099}_{-0.00096}$	$23.4^{+3.2}_{-7.7}$	$88.8^{+0.9}_{-1.8}$	$0.0196^{+0.0018}_{-0.0007}$	$2.22^{+0.34}_{-0.22}$	$1.04^{+0.13}_{-0.10}$	$0.950^{+0.040}_{-0.036}$	9.443	$< 1.00e-04$	Planet	
K2-223 b	228721452.01	2750.0620 ± 0.0031	$0.505570^{+0.000037}_{-0.000036}$	$3.4^{+0.7}_{-1.2}$	$82.0^{+6.0}_{-14.0}$	$0.00823^{+0.00077}_{-0.00061}$	$0.910^{+0.099}_{-0.074}$	$1.013^{+0.055}_{-0.035}$	1.067 ± 0.026	11.325	$< 1.00e-04$	Planet	
K2-223 c	228721452.02	$2749.9734^{+0.0028}_{-0.0027}$	$4.56417^{+0.00028}_{-0.00030}$	$10.8^{+1.4}_{-3.6}$	$87.5^{+1.8}_{-3.9}$	$0.01465^{+0.00099}_{-0.00062}$	$1.62^{+0.14}_{-0.09}$	$1.013^{+0.055}_{-0.035}$	1.067 ± 0.026	11.325	$< 1.00e-04$	Planet	
K2-224 b	228725972.01	$2752.6741^{+0.0066}_{-0.0063}$	$4.47859^{+0.00061}_{-0.00064}$	$12.3^{+1.7}_{-3.3}$	$87.9^{+1.5}_{-2.8}$	$0.0182^{+0.0025}_{-0.0012}$	$1.66^{+0.24}_{-0.13}$	$0.840^{+0.038}_{-0.030}$	$0.902^{+0.028}_{-0.029}$	12.482	$< 1.00e-04$	Planet	
	228725972.02	$2755.4089^{+0.0023}_{-0.0024}$	$10.09607^{+0.00064}_{-0.00062}$	$19.4^{+2.1}_{-4.7}$	$88.7^{+0.9}_{-1.6}$	$0.0273^{+0.0031}_{-0.0015}$	$2.51^{+0.31}_{-0.16}$	$0.840^{+0.038}_{-0.030}$	$0.902^{+0.028}_{-0.029}$	12.482	–	Candidate	b,c
	228729473.01	$2752.7713^{+0.0039}_{-0.0037}$	16.7706 ± 0.0016	$7.8^{+0.7}_{-1.0}$	86.7 ± 2.1	$0.0422^{+0.0017}_{-0.0010}$	$13.2^{+1.8}_{-1.6}$	$2.88^{+0.38}_{-0.33}$	$1.00^{+0.11}_{-0.08}$	11.524	–	Candidate	a
	228732031.01	$2749.93557^{+0.00099}_{-0.00098}$	$0.3693110^{+0.0000080}_{-0.0000090}$	$2.30^{+0.37}_{-0.62}$	$77.0^{+9.0}_{-17.0}$	$0.0211^{+0.0025}_{-0.0014}$	$1.76^{+0.22}_{-0.13}$	$0.765^{+0.033}_{-0.026}$	$0.803^{+0.028}_{-0.030}$	11.937	$< 1.00e-04$	Planet	
	228734889.01	2800.07702 ± 0.00013	$48.24955^{+0.00016}_{-0.00017}$	$67.96^{+0.49}_{-0.48}$	$89.554^{+0.024}_{-0.021}$	$0.1726^{+0.0020}_{-0.0025}$	$18.0^{+1.0}_{-0.7}$	$0.956^{+0.054}_{-0.037}$	$1.008^{+0.027}_{-0.029}$	12.59	–	Candidate	a,d
K2-225 b	228734900.01	$2754.3682^{+0.0040}_{-0.0049}$	$15.8715^{+0.0021}_{-0.0017}$	$18.0^{+2.3}_{-6.4}$	$88.4^{+1.1}_{-2.5}$	$0.0202^{+0.0011}_{-0.0008}$	$2.66^{+0.46}_{-0.31}$	$1.21^{+0.20}_{-0.13}$	$1.115^{+0.054}_{-0.035}$	11.535	$< 1.00e-04$	Planet	

Table 4 — *Continued*

New K2 Name	EPIC	T_0 (BJD-2454833)	P (d)	a/R_*	i (deg)	R_p/R_*	R_p ($R_\oplus$)	R_* ($R_\odot$)	M_* ($M_\odot$)	K_p	FPP	Disposition	Notes
	228735255.01	2755.28503 ± 0.00012	$6.569213^{+0.000019}_{-0.000020}$	$15.30^{+0.08}_{-0.19}$	$89.64^{+0.25}_{-0.38}$	$0.11417^{+0.00056}_{-0.00043}$	$13.0^{+1.8}_{-1.0}$	$1.05^{+0.14}_{-0.08}$	$1.017^{+0.036}_{-0.034}$	12.483	–	Candidate	a,c
K2-226 b	228736155.01	2751.0261 ± 0.0044	3.27111 ± 0.00037	$9.2^{+1.4}_{-3.2}$	$86.7^{+2.1}_{-4.7}$	$0.0165^{+0.0019}_{-0.0011}$	$1.49^{+0.18}_{-0.11}$	$0.824^{+0.034}_{-0.027}$	$0.886^{+0.028}_{-0.030}$	12.042	$< 1.00e-04$	Planet	
	228737155.01	$2758.157^{+0.017}_{-0.019}$	$25.988^{+0.012}_{-0.011}$	$2.98^{+0.37}_{-0.24}$	$67.1^{+3.8}_{-4.2}$	$0.18^{+0.21}_{-0.10}$	$317.0^{+371.0}_{-179.0}$	$16.0^{+2.0}_{-1.4}$	$0.874^{+0.090}_{-0.046}$	11.081	–	Candidate	f
	228754001.01	$2757.1696^{+0.0062}_{-0.0064}$	$9.1739^{+0.0015}_{-0.0014}$	$8.4^{+0.8}_{-1.7}$	$87.0^{+2.1}_{-2.9}$	$0.0291^{+0.0015}_{-0.0010}$	$6.86^{+0.89}_{-0.69}$	$2.16^{+0.26}_{-0.20}$	$0.984^{+0.072}_{-0.039}$	11.651	–	Candidate	c
K2-227 b	228760097.01	$2759.2383^{+0.0097}_{-0.0094}$	$13.6218^{+0.0032}_{-0.0033}$	$21.0^{+6.0}_{-15.0}$	$88.4^{+1.2}_{-7.3}$	$0.017^{+0.013}_{-0.002}$	$1.7^{+1.2}_{-0.2}$	$0.891^{+0.041}_{-0.031}$	$0.951^{+0.028}_{-0.030}$	11.512	$< 1.00e-04$	Planet	
K2-228 b	228798746.01	2750.1928 ± 0.0022	$2.69837^{+0.00013}_{-0.00014}$	$11.4^{+1.8}_{-3.6}$	$87.5^{+1.8}_{-3.4}$	$0.0182^{+0.0012}_{-0.0010}$	$1.38^{+0.10}_{-0.09}$	$0.699^{+0.022}_{-0.020}$	$0.742^{+0.025}_{-0.023}$	12.66	$< 1.00e-04$	Planet	
K2-229 b	228801451.01	$2749.8861^{+0.0010}_{-0.0011}$	0.584240 ± 0.000014	$3.16^{+0.35}_{-0.80}$	$82.0^{+6.0}_{-11.0}$	$0.0143^{+0.0015}_{-0.0007}$	$1.25^{+0.14}_{-0.07}$	$0.802^{+0.034}_{-0.023}$	$0.858^{+0.025}_{-0.029}$	10.955	$< 1.00e-04$	Planet	
K2-229 c	228801451.02	$2753.3351^{+0.0017}_{-0.0016}$	$8.32801^{+0.00040}_{-0.00039}$	$22.0^{+6.0}_{-11.0}$	$88.3^{+1.2}_{-3.1}$	$0.0248^{+0.0051}_{-0.0019}$	$2.16^{+0.46}_{-0.18}$	$0.802^{+0.034}_{-0.023}$	$0.858^{+0.025}_{-0.029}$	10.955	$< 1.00e-04$	Planet	
K2-230 b	228804845.01	$2752.4496^{+0.0047}_{-0.0050}$	$2.86064^{+0.00031}_{-0.00029}$	$7.1^{+1.2}_{-2.3}$	$86.0^{+2.8}_{-5.9}$	$0.0150^{+0.0015}_{-0.0010}$	$1.93^{+0.30}_{-0.20}$	$1.18^{+0.14}_{-0.09}$	$1.131^{+0.041}_{-0.029}$	12.551	$< 1.00e-04$	Planet	
	228809391.01	$2763.8037^{+0.0041}_{-0.0043}$	$19.5757^{+0.0030}_{-0.0027}$	$47.0^{+10.0}_{-18.0}$	$89.3^{+0.5}_{-1.0}$	$0.0287^{+0.0042}_{-0.0021}$	$2.84^{+0.44}_{-0.22}$	$0.907^{+0.046}_{-0.028}$	$0.970^{+0.022}_{-0.026}$	12.595	$1.68e-03$	Candidate	
	228952747.01	$2750.0961^{+0.0015}_{-0.0016}$	$1.055785^{+0.000040}_{-0.000043}$	$36.0^{+29.0}_{-22.0}$	$89.1^{+0.7}_{-3.6}$	$0.024^{+0.035}_{-0.006}$	$1.5^{+2.3}_{-0.4}$	$0.593^{+0.017}_{-0.015}$	$0.615^{+0.019}_{-0.018}$	12.224	$3.54e-01$	Candidate	
	229004835.01	$2764.6247^{+0.0025}_{-0.0027}$	16.1404 ± 0.0012	$50.0^{+7.0}_{-15.0}$	$89.44^{+0.40}_{-0.72}$	$0.0194^{+0.0013}_{-0.0010}$	$2.06^{+0.23}_{-0.15}$	$0.975^{+0.088}_{-0.053}$	$0.990^{+0.034}_{-0.035}$	10.151	$1.83e-02$	Candidate	
	229039390.01	2749.62123 ± 0.00011	0.2516470 ± 0.0000010	$1.46^{+0.22}_{-0.08}$	$38.7^{+5.0}_{-5.5}$	$0.26^{+0.25}_{-0.11}$	$28.0^{+27.0}_{-12.0}$	$0.987^{+0.088}_{-0.048}$	$1.013^{+0.029}_{-0.031}$	12.735	–	Candidate	f
	229131722.01	2752.7053 ± 0.0064	15.4824 ± 0.0022	$26.1^{+3.3}_{-7.0}$	$89.0^{+0.7}_{-1.3}$	$0.0178^{+0.0021}_{-0.0013}$	$2.10^{+0.31}_{-0.19}$	$1.078^{+0.092}_{-0.053}$	$1.100^{+0.034}_{-0.028}$	12.515	$2.52e-03$	Candidate	
	229133720.01	2750.9645 ± 0.0011	4.03679 ± 0.00011	$11.2^{+2.3}_{-4.3}$	$87.0^{+2.2}_{-4.3}$	$0.0294^{+0.0056}_{-0.0023}$	$2.34^{+0.45}_{-0.19}$	$0.728^{+0.022}_{-0.021}$	$0.778^{+0.026}_{-0.027}$	11.477	–	Candidate	c

[a] Unless there is a deep secondary eclipse or ellipsoidal variations in the light curve, VESPA cannot distinguish between a planet-sized star and a planet. In this case, $R_p > 8R_\oplus$ and RV measurements cannot rule out the foreground eclipsing binary scenario. Therefore, a FPP value is not reported.
[b] Companion in aperture, therefore a FPP is not reported
[c] AO/Speckle companion, therefore a FPP is not reported
[d] Composite spectrum, therefore a FPP is not reported
[e] Large RV amplitude variations confirm a binary in the system, therefore a FPP is not reported
[f] VESPA failed to find a FPP

Table 5
Stellar Parameters

EPIC	$T_{\rm eff}$	$[m/{\rm H}]$	$\log g$	R_* ($R_\odot$)	M_* ($M_\odot$)	$K_{\rm p}$	Notes
201110617	4460.0 ± 50.0	-0.33 ± 0.08	4.68 ± 0.1	$0.616^{+0.019}_{-0.016}$	$0.642^{+0.022}_{-0.019}$	12.947	
201111557	4720.0 ± 50.0	-0.06 ± 0.08	4.5 ± 0.1	$0.711^{+0.019}_{-0.020}$	0.746 ± 0.023	11.363	
201127519	5015.0 ± 50.0	0.24 ± 0.08	4.67 ± 0.1	$0.789^{+0.025}_{-0.017}$	$0.857^{+0.021}_{-0.023}$	11.558	
201130233	5456.0 ± 50.0	0.13 ± 0.08	4.55 ± 0.1	$0.876^{+0.045}_{-0.025}$	$0.940^{+0.023}_{-0.027}$	12.604	
201132684	5489.0 ± 50.0	0.07 ± 0.08	4.46 ± 0.1	$0.892^{+0.074}_{-0.036}$	$0.933^{+0.027}_{-0.030}$	11.678	
201166680	6213.0 ± 50.0	0.14 ± 0.08	4.32 ± 0.1	$1.22^{+0.12}_{-0.07}$	$1.192^{+0.033}_{-0.030}$	10.897	
201211526	5728.0 ± 50.0	-0.2 ± 0.08	4.51 ± 0.1	$0.891^{+0.056}_{-0.037}$	$0.936^{+0.032}_{-0.031}$	11.696	
201225286	5419.0 ± 50.0	-0.1 ± 0.08	4.57 ± 0.1	$0.830^{+0.045}_{-0.029}$	$0.886^{+0.027}_{-0.032}$	11.729	
201227197	5649.0 ± 50.0	0.07 ± 0.08	4.61 ± 0.1	$0.914^{+0.037}_{-0.026}$	$0.983^{+0.023}_{-0.025}$	12.486	
201231064	4972.0 ± 50.0	-0.03 ± 0.08	3.63 ± 0.1	$2.57^{+0.31}_{-0.25}$	$0.987^{+0.082}_{-0.060}$	12.358	
201295312	5722.0 ± 50.0	0.04 ± 0.08	4.02 ± 0.1	$1.56^{+0.26}_{-0.19}$	$1.050^{+0.068}_{-0.045}$	12.126	
201299088	5154.0 ± 50.0	-0.26 ± 0.08	3.91 ± 0.1	$1.76^{+0.21}_{-0.17}$	$0.848^{+0.023}_{-0.010}$	11.751	
201352100	5216.0 ± 50.0	0.16 ± 0.08	4.7 ± 0.1	$0.815^{+0.027}_{-0.018}$	$0.889^{+0.019}_{-0.024}$	12.798	
201384232	5617.0 ± 53.0	-0.12 ± 0.08	4.67 ± 0.1	$0.863^{+0.034}_{-0.030}$	$0.930^{+0.029}_{-0.030}$	12.510	
201390048	4885.0 ± 50.0	-0.09 ± 0.08	4.71 ± 0.1	0.726 ± 0.020	$0.777^{+0.025}_{-0.026}$	11.961	
201403446	6114.0 ± 50.0	-0.32 ± 0.08	4.11 ± 0.1	$1.33^{+0.16}_{-0.15}$	$1.015^{+0.054}_{-0.046}$	11.995	
201427874	4937.0 ± 50.0	0.14 ± 0.08	4.71 ± 0.1	$0.762^{+0.018}_{-0.013}$	$0.826^{+0.019}_{-0.023}$	12.819	
201437844	6321.0 ± 50.0	-0.23 ± 0.08	4.19 ± 0.1	$1.27^{+0.17}_{-0.13}$	$1.119^{+0.055}_{-0.043}$	9.234	b
201441872	5450.0 ± 50.0	-0.13 ± 0.08	4.54 ± 0.1	$0.834^{+0.050}_{-0.031}$	$0.885^{+0.029}_{-0.031}$	12.088	
201460826	5791.0 ± 50.0	-0.23 ± 0.08	3.81 ± 0.1	$2.20^{+0.31}_{-0.25}$	$1.181^{+0.093}_{-0.061}$	11.130	
201505350	5391.0 ± 50.0	-0.03 ± 0.08	4.6 ± 0.1	$0.834^{+0.036}_{-0.026}$	$0.895^{+0.026}_{-0.030}$	12.806	
201528828	5185.0 ± 50.0	-0.05 ± 0.08	4.46 ± 0.1	$0.804^{+0.045}_{-0.029}$	$0.835^{+0.031}_{-0.030}$	11.415	
201546283	5368.0 ± 50.0	0.15 ± 0.08	4.58 ± 0.1	$0.855^{+0.038}_{-0.025}$	$0.920^{+0.023}_{-0.025}$	12.428	
201577035	5638.0 ± 50.0	-0.03 ± 0.08	4.53 ± 0.1	$0.902^{+0.054}_{-0.032}$	$0.958^{+0.026}_{-0.029}$	12.296	
201595106	5705.0 ± 50.0	-0.01 ± 0.08	4.48 ± 0.1	$0.932^{+0.064}_{-0.038}$	$0.980^{+0.026}_{-0.029}$	11.678	
201613023	5663.0 ± 50.0	-0.11 ± 0.08	4.3 ± 0.1	$1.01^{+0.12}_{-0.09}$	$0.936^{+0.032}_{-0.033}$	12.137	
201615463	5922.0 ± 57.0	0.05 ± 0.08	4.24 ± 0.102	$1.20^{+0.18}_{-0.14}$	1.073 ± 0.034	11.964	
201713348	4944.0 ± 50.0	-0.03 ± 0.08	4.7 ± 0.1	$0.746^{+0.019}_{-0.021}$	$0.800^{+0.023}_{-0.027}$	11.531	
201828749	5628.0 ± 50.0	-0.18 ± 0.08	4.57 ± 0.1	$0.858^{+0.045}_{-0.032}$	$0.915^{+0.029}_{-0.030}$	11.564	
201855371	4382.0 ± 50.0	-0.35 ± 0.08	4.71 ± 0.1	$0.601^{+0.017}_{-0.015}$	$0.625^{+0.020}_{-0.019}$	12.997	
201920032	5548.0 ± 50.0	0.13 ± 0.08	4.42 ± 0.1	$0.934^{+0.090}_{-0.047}$	0.954 ± 0.027	12.890	
202089657	6009.0 ± 53.0	-0.12 ± 0.08	4.09 ± 0.1	1.47 ± 0.22	$1.116^{+0.057}_{-0.074}$	11.600	
202091388	5586.0 ± 50.0	0.15 ± 0.08	4.5 ± 0.1	$0.922^{+0.062}_{-0.032}$	$0.976^{+0.024}_{-0.026}$	13.500	
202675839	5807.0 ± 50.0	0.45 ± 0.08	4.25 ± 0.1	$1.23^{+0.19}_{-0.13}$	$1.141^{+0.050}_{-0.039}$	12.362	
202821899	6081.0 ± 50.0	0.46 ± 0.08	3.88 ± 0.1	$2.22^{+0.28}_{-0.30}$	$1.53^{+0.09}_{-0.10}$	12.577	
202900527	5526.0 ± 58.0	0.44 ± 0.08	4.29 ± 0.1	$1.42^{+0.27}_{-0.21}$	$1.004^{+0.086}_{-0.047}$	12.303	
203771098	5744.0 ± 50.0	0.44 ± 0.08	4.41 ± 0.1	$1.068^{+0.097}_{-0.050}$	$1.095^{+0.028}_{-0.029}$	11.648	
203826436	5382.0 ± 57.0	-0.07 ± 0.08	4.66 ± 0.1	$0.818^{+0.032}_{-0.025}$	$0.887^{+0.025}_{-0.031}$	12.241	
204750116	5869.0 ± 53.0	0.02 ± 0.08	4.53 ± 0.1	$0.987^{+0.051}_{-0.039}$	$1.037^{+0.026}_{-0.030}$	11.526	
205029914	5774.0 ± 50.0	-0.08 ± 0.08	4.37 ± 0.1	$0.98^{+0.11}_{-0.06}$	$0.983^{+0.029}_{-0.034}$	12.183	
205071984	5415.0 ± 50.0	0.03 ± 0.08	4.73 ± 0.1	$0.839^{+0.026}_{-0.021}$	$0.916^{+0.020}_{-0.026}$	12.005	
205904628	5908.0 ± 50.0	-0.45 ± 0.08	3.88 ± 0.1	$1.83^{+0.29}_{-0.28}$	$1.02^{+0.12}_{-0.09}$	8.220	b
205944181	5257.0 ± 50.0	0.03 ± 0.08	4.49 ± 0.1	$0.825^{+0.046}_{-0.026}$	$0.872^{+0.026}_{-0.033}$	12.410	
205950854	5554.0 ± 50.0	-0.13 ± 0.08	4.46 ± 0.1	$0.874^{+0.068}_{-0.039}$	$0.907^{+0.029}_{-0.032}$	12.105	
205957328	5317.0 ± 50.0	0.04 ± 0.08	4.59 ± 0.1	$0.828^{+0.033}_{-0.021}$	$0.892^{+0.022}_{-0.027}$	12.464	
206007892	5548.0 ± 50.0	0.26 ± 0.08	4.56 ± 0.1	$0.919^{+0.049}_{-0.030}$	$0.986^{+0.028}_{-0.026}$	12.023	
206008091	5748.0 ± 50.0	-0.11 ± 0.08	4.34 ± 0.1	$0.98^{+0.11}_{-0.07}$	0.964 ± 0.032	12.506	
206011496	5509.0 ± 50.0	0.07 ± 0.08	4.49 ± 0.1	$0.889^{+0.061}_{-0.030}$	$0.940^{+0.025}_{-0.027}$	10.916	
206026904	5134.0 ± 50.0	0.11 ± 0.08	4.54 ± 0.1	$0.803^{+0.034}_{-0.020}$	$0.858^{+0.022}_{-0.027}$	12.150	
206044803	5761.0 ± 50.0	0.17 ± 0.08	4.38 ± 0.1	$1.02^{+0.11}_{-0.06}$	1.030 ± 0.029	12.975	
206049764	5250.0 ± 50.0	-0.09 ± 0.08	3.95 ± 0.1	$1.72^{+0.22}_{-0.19}$	$0.892^{+0.060}_{-0.027}$	12.445	
206082454	5569.0 ± 50.0	-0.06 ± 0.08	4.61 ± 0.1	$0.869^{+0.038}_{-0.029}$	$0.934^{+0.026}_{-0.027}$	12.308	
206096602	4636.0 ± 50.0	-0.29 ± 0.08	4.7 ± 0.1	$0.648^{+0.021}_{-0.018}$	$0.684^{+0.022}_{-0.023}$	12.045	
206114630	5277.0 ± 50.0	0.12 ± 0.08	4.65 ± 0.1	$0.825^{+0.030}_{-0.019}$	$0.897^{+0.021}_{-0.024}$	11.032	
206119924	4547.0 ± 50.0	0.01 ± 0.08	4.64 ± 0.1	$0.687^{+0.015}_{-0.017}$	$0.727^{+0.020}_{-0.021}$	10.310	
206144956	4799.0 ± 50.0	-0.34 ± 0.08	4.55 ± 0.1	$0.669^{+0.023}_{-0.021}$	$0.702^{+0.025}_{-0.023}$	10.396	
206146957	5744.0 ± 50.0	-0.14 ± 0.08	4.57 ± 0.1	$0.902^{+0.048}_{-0.034}$	$0.956^{+0.031}_{-0.030}$	11.379	

Table 5 — *Continued*

EPIC	$T_{\rm eff}$	$[m/{\rm H}]$	$\log g$	R_* ($R_\odot$)	M_* ($M_\odot$)	$K_{\rm p}$	Notes
206159027	4893.0 ± 50.0	-0.21 ± 0.08	4.74 ± 0.1	0.702 ± 0.021	$0.751^{+0.025}_{-0.026}$	12.597	
206169375	6060.0 ± 50.0	-0.08 ± 0.08	4.19 ± 0.1	$1.26^{+0.22}_{-0.15}$	$1.096^{+0.056}_{-0.047}$	12.559	
206181769	5131.0 ± 50.0	0.06 ± 0.08	4.53 ± 0.1	$0.799^{+0.034}_{-0.021}$	$0.848^{+0.023}_{-0.028}$	12.770	
206192335	5459.0 ± 50.0	-0.15 ± 0.08	4.59 ± 0.1	$0.826^{+0.039}_{-0.028}$	$0.883^{+0.029}_{-0.030}$	11.870	
206245553	5844.0 ± 50.0	0.09 ± 0.08	4.35 ± 0.1	$1.05^{+0.13}_{-0.07}$	$1.043^{+0.026}_{-0.027}$	11.745	
206268299	5929.0 ± 60.0	-0.21 ± 0.08	4.24 ± 0.11	$1.09^{+0.14}_{-0.11}$	0.987 ± 0.040	12.430	
206348688	6022.0 ± 51.0	0.3 ± 0.08	4.26 ± 0.1	$1.24^{+0.16}_{-0.11}$	$1.174^{+0.048}_{-0.041}$	12.566	
206439513	6211.0 ± 59.0	-0.25 ± 0.08	3.56 ± 0.104	$3.47^{+0.48}_{-0.44}$	$1.62^{+0.07}_{-0.10}$	11.437	
206535016	5199.0 ± 50.0	-0.17 ± 0.08	4.52 ± 0.1	$0.777^{+0.038}_{-0.028}$	$0.815^{+0.032}_{-0.029}$	11.644	
210363145	5070.0 ± 50.0	0.12 ± 0.08	4.67 ± 0.1	$0.784^{+0.024}_{-0.014}$	$0.852^{+0.019}_{-0.024}$	11.896	
210365511	4672.0 ± 50.0	-0.1 ± 0.08	4.63 ± 0.1	$0.692^{+0.020}_{-0.021}$	$0.730^{+0.024}_{-0.023}$	12.439	
210402237	5839.0 ± 51.0	0.2 ± 0.08	4.41 ± 0.1	$1.038^{+0.092}_{-0.050}$	$1.062^{+0.029}_{-0.026}$	11.801	
210403955	5377.0 ± 50.0	0.07 ± 0.08	4.65 ± 0.1	$0.841^{+0.031}_{-0.022}$	$0.913^{+0.021}_{-0.024}$	12.388	
210423938	4760.0 ± 50.0	-0.14 ± 0.08	4.69 ± 0.1	$0.697^{+0.021}_{-0.020}$	$0.741^{+0.024}_{-0.026}$	12.655	
210512842	5580.0 ± 70.0	-0.25 ± 0.08	4.52 ± 0.12	$0.843^{+0.058}_{-0.039}$	$0.882^{+0.034}_{-0.036}$	12.106	a
210558622	4500.0 ± 50.0	-0.24 ± 0.08	4.62 ± 0.1	$0.639^{+0.020}_{-0.019}$	$0.668^{+0.022}_{-0.021}$	12.034	
210609658	5016.0 ± 50.0	0.2 ± 0.08	3.81 ± 0.1	$2.15^{+0.26}_{-0.21}$	$1.009^{+0.081}_{-0.049}$	12.587	
210629082	6148.0 ± 50.0	0.28 ± 0.08	4.15 ± 0.1	$1.45^{+0.25}_{-0.18}$	$1.256^{+0.078}_{-0.058}$	11.580	
210643811	5909.0 ± 50.0	0.05 ± 0.08	4.11 ± 0.1	$1.42^{+0.21}_{-0.17}$	$1.095^{+0.057}_{-0.039}$	10.632	
210667381	5428.0 ± 50.0	0.15 ± 0.08	4.63 ± 0.1	$0.864^{+0.033}_{-0.020}$	$0.939^{+0.020}_{-0.025}$	12.674	
210707130	4441.0 ± 50.0	-0.14 ± 0.08	4.65 ± 0.1	$0.647^{+0.020}_{-0.019}$	$0.678^{+0.021}_{-0.022}$	12.099	
210718708	5129.0 ± 50.0	-0.35 ± 0.08	4.52 ± 0.1	$0.722^{+0.035}_{-0.025}$	$0.757^{+0.028}_{-0.029}$	12.801	
210775710	5738.0 ± 50.0	0.07 ± 0.08	4.4 ± 0.1	$0.98^{+0.10}_{-0.05}$	$1.003^{+0.026}_{-0.027}$	11.827	
210848071	5703.0 ± 50.0	-0.06 ± 0.08	4.38 ± 0.1	$0.956^{+0.099}_{-0.055}$	$0.964^{+0.030}_{-0.032}$	11.040	
210857328	6063.0 ± 50.0	0.41 ± 0.08	4.38 ± 0.1	$1.214^{+0.087}_{-0.061}$	$1.211^{+0.032}_{-0.038}$	12.584	
210894022	5741.0 ± 50.0	-0.36 ± 0.08	4.36 ± 0.1	$0.92^{+0.11}_{-0.08}$	$0.877^{+0.036}_{-0.041}$	12.300	
210957318	5574.0 ± 50.0	0.13 ± 0.08	4.53 ± 0.1	$0.909^{+0.054}_{-0.029}$	$0.970^{+0.024}_{-0.027}$	13.171	
210965800	5525.0 ± 50.0	0.09 ± 0.08	4.55 ± 0.1	$0.887^{+0.044}_{-0.026}$	$0.951^{+0.023}_{-0.028}$	12.134	
211048999	5015.0 ± 50.0	0.03 ± 0.08	4.63 ± 0.1	$0.768^{+0.022}_{-0.018}$	$0.824^{+0.022}_{-0.027}$	12.659	
211089792	5392.0 ± 50.0	0.13 ± 0.08	4.59 ± 0.1	$0.858^{+0.040}_{-0.024}$	$0.923^{+0.023}_{-0.026}$	12.914	
211106187	4883.0 ± 98.0	-1.1 ± 0.092	2.27 ± 0.162	$13.2^{+4.6}_{-2.7}$	$1.10^{+0.47}_{-0.18}$	13.124	a
211147528	6254.0 ± 98.0	0.15 ± 0.092	3.19 ± 0.161	$5.4^{+0.5}_{-1.0}$	$2.02^{+0.05}_{-0.13}$	11.832	a
211319617	5263.0 ± 50.0	-0.59 ± 0.08	4.7 ± 0.1	$0.681^{+0.021}_{-0.016}$	$0.730^{+0.020}_{-0.022}$	12.393	
211351816	4836.0 ± 50.0	0.27 ± 0.08	3.5 ± 0.1	$2.95^{+0.37}_{-0.30}$	$1.054^{+0.089}_{-0.067}$	12.409	
211355342	5609.0 ± 50.0	0.42 ± 0.08	4.46 ± 0.1	$0.999^{+0.077}_{-0.041}$	$1.044^{+0.024}_{-0.029}$	12.637	
211359660	5159.0 ± 50.0	-0.01 ± 0.08	4.59 ± 0.1	$0.790^{+0.032}_{-0.021}$	$0.847^{+0.024}_{-0.031}$	11.742	
211391664	6095.0 ± 50.0	-0.1 ± 0.08	4.09 ± 0.1	1.51 ± 0.22	$1.156^{+0.082}_{-0.069}$	12.102	
211401787	6114.0 ± 50.0	-0.15 ± 0.08	4.01 ± 0.1	$1.68^{+0.27}_{-0.23}$	$1.20^{+0.10}_{-0.09}$	9.709	
211418290	5070.0 ± 59.0	-0.43 ± 0.08	3.25 ± 0.104	$3.69^{+0.54}_{-0.39}$	$0.915^{+0.068}_{-0.051}$	11.504	
211424769	6185.0 ± 50.0	-0.12 ± 0.08	4.34 ± 0.1	$1.12^{+0.11}_{-0.07}$	$1.102^{+0.041}_{-0.037}$	9.438	b
211491383	6035.0 ± 50.0	-0.07 ± 0.08	4.16 ± 0.1	$1.31^{+0.22}_{-0.16}$	$1.101^{+0.053}_{-0.050}$	11.785	
211525389	5475.0 ± 50.0	0.26 ± 0.08	4.51 ± 0.1	$0.909^{+0.058}_{-0.036}$	$0.965^{+0.031}_{-0.029}$	11.687	
211562654	5482.0 ± 50.0	0.09 ± 0.08	4.6 ± 0.1	$0.873^{+0.037}_{-0.023}$	$0.942^{+0.021}_{-0.025}$	12.754	
211594205	5252.0 ± 50.0	-0.22 ± 0.08	4.63 ± 0.1	$0.764^{+0.033}_{-0.025}$	$0.819^{+0.028}_{-0.030}$	10.680	
211606790	5445.0 ± 50.0	0.07 ± 0.08	4.05 ± 0.1	$1.48^{+0.22}_{-0.17}$	$0.947^{+0.073}_{-0.032}$	12.673	
211611158	5722.0 ± 50.0	-0.05 ± 0.08	4.58 ± 0.1	$0.914^{+0.044}_{-0.033}$	0.976 ± 0.028	12.414	
211682544	5410.0 ± 50.0	-0.04 ± 0.08	4.58 ± 0.1	$0.837^{+0.040}_{-0.027}$	$0.898^{+0.027}_{-0.031}$	11.407	
211733267	5319.0 ± 50.0	-0.05 ± 0.08	4.55 ± 0.1	$0.819^{+0.040}_{-0.028}$	$0.872^{+0.027}_{-0.029}$	12.150	
211736671	5414.0 ± 53.0	0.48 ± 0.08	3.75 ± 0.1	$2.31^{+0.38}_{-0.35}$	1.29 ± 0.11	12.160	
211743874	5985.0 ± 50.0	0.08 ± 0.08	4.14 ± 0.1	$1.41^{+0.18}_{-0.19}$	$1.128^{+0.056}_{-0.040}$	12.486	
211763214	5277.0 ± 50.0	-0.2 ± 0.08	4.54 ± 0.1	$0.782^{+0.043}_{-0.028}$	$0.826^{+0.030}_{-0.031}$	12.529	
211770696	5656.0 ± 52.0	-0.28 ± 0.08	4.23 ± 0.1	$1.06^{+0.12}_{-0.11}$	$0.872^{+0.037}_{-0.035}$	12.253	
211800191	5851.0 ± 70.0	-0.35 ± 0.08	4.43 ± 0.12	$0.906^{+0.091}_{-0.053}$	$0.917^{+0.036}_{-0.040}$	12.443	a
211818569	4695.0 ± 50.0	-0.14 ± 0.08	4.68 ± 0.1	$0.686^{+0.020}_{-0.021}$	$0.727^{+0.025}_{-0.024}$	12.935	
211886472	6398.0 ± 61.0	0.17 ± 0.08	4.03 ± 0.112	$1.74^{+0.32}_{-0.27}$	$1.39^{+0.11}_{-0.08}$	11.126	
211906650	5784.0 ± 50.0	0.06 ± 0.08	4.45 ± 0.1	$0.981^{+0.075}_{-0.041}$	$1.019^{+0.023}_{-0.027}$	12.193	
211913977	4942.0 ± 53.0	0.14 ± 0.08	4.66 ± 0.1	$0.770^{+0.022}_{-0.015}$	$0.833^{+0.020}_{-0.024}$	12.619	
211941472	5739.0 ± 50.0	0.02 ± 0.08	4.11 ± 0.1	$1.38^{+0.19}_{-0.16}$	$1.020^{+0.043}_{-0.033}$	11.788	

Table 5 — *Continued*

EPIC	$T_{\rm eff}$	$[m/{\rm H}]$	$\log g$	R_* ($R_\odot$)	M_* ($M_\odot$)	$K_{\rm p}$	Notes
211945201	6046.0 ± 50.0	0.05 ± 0.08	4.14 ± 0.1	$1.41^{+0.21}_{-0.18}$	$1.143^{+0.059}_{-0.040}$	10.115	
211978988	5759.0 ± 50.0	-0.03 ± 0.08	4.31 ± 0.1	$1.04^{+0.13}_{-0.09}$	$0.988^{+0.028}_{-0.030}$	12.588	
211993818	5265.0 ± 50.0	-0.04 ± 0.08	3.2 ± 0.1	$4.26^{+0.68}_{-0.52}$	$1.11^{+0.13}_{-0.06}$	7.218	b
212006318	5838.0 ± 50.0	0.03 ± 0.08	4.32 ± 0.1	$1.07^{+0.14}_{-0.09}$	$1.030^{+0.027}_{-0.028}$	12.909	
212008766	5098.0 ± 50.0	-0.15 ± 0.08	4.7 ± 0.1	$0.748^{+0.026}_{-0.021}$	$0.805^{+0.026}_{-0.027}$	12.802	
212012119	4822.0 ± 50.0	-0.08 ± 0.08	4.44 ± 0.1	$0.727^{+0.023}_{-0.021}$	$0.760^{+0.028}_{-0.025}$	11.753	
212110888	5990.0 ± 50.0	-0.01 ± 0.08	4.11 ± 0.1	$1.45^{+0.21}_{-0.20}$	$1.120^{+0.053}_{-0.044}$	11.441	
212132195	4789.0 ± 50.0	-0.18 ± 0.08	4.71 ± 0.1	$0.692^{+0.021}_{-0.020}$	$0.737^{+0.025}_{-0.024}$	11.670	
212138198	5182.0 ± 50.0	0.29 ± 0.08	4.55 ± 0.1	$0.839^{+0.038}_{-0.028}$	$0.898^{+0.027}_{-0.029}$	12.902	
212157262	5477.0 ± 50.0	0.26 ± 0.08	4.62 ± 0.1	$0.895^{+0.041}_{-0.026}$	$0.967^{+0.025}_{-0.024}$	12.864	
212164470	5982.0 ± 50.0	0.16 ± 0.08	4.36 ± 0.1	$1.11^{+0.11}_{-0.06}$	$1.107^{+0.031}_{-0.025}$	12.704	
212303338	5338.0 ± 50.0	0.19 ± 0.08	4.51 ± 0.1	$0.863^{+0.053}_{-0.030}$	$0.915^{+0.025}_{-0.029}$	9.957	
212357477	5733.0 ± 50.0	0.04 ± 0.08	4.51 ± 0.1	$0.947^{+0.058}_{-0.033}$	$1.000^{+0.024}_{-0.028}$	10.215	
212394689	5503.0 ± 50.0	-0.01 ± 0.08	4.61 ± 0.1	$0.862^{+0.038}_{-0.027}$	$0.928^{+0.024}_{-0.027}$	12.206	
212460519	4396.0 ± 50.0	-0.44 ± 0.08	4.73 ± 0.1	$0.589^{+0.016}_{-0.014}$	$0.610^{+0.019}_{-0.018}$	12.445	
212480208	5631.0 ± 50.0	-0.19 ± 0.08	4.38 ± 0.1	$0.912^{+0.096}_{-0.058}$	$0.905^{+0.033}_{-0.036}$	10.892	
212496592	5176.0 ± 50.0	0.31 ± 0.08	4.57 ± 0.1	$0.840^{+0.036}_{-0.026}$	$0.901^{+0.026}_{-0.028}$	12.966	
212521166	4877.0 ± 50.0	-0.3 ± 0.08	4.51 ± 0.1	$0.692^{+0.024}_{-0.023}$	$0.724^{+0.025}_{-0.024}$	11.590	
212534729	5378.0 ± 50.0	-0.06 ± 0.08	4.47 ± 0.1	$0.843^{+0.064}_{-0.034}$	$0.879^{+0.029}_{-0.032}$	13.066	
212555594	5252.0 ± 50.0	0.05 ± 0.08	4.49 ± 0.1	$0.828^{+0.042}_{-0.027}$	$0.873^{+0.024}_{-0.031}$	12.482	
212562715	5570.0 ± 50.0	0.04 ± 0.08	4.59 ± 0.1	$0.888^{+0.038}_{-0.027}$	$0.955^{+0.022}_{-0.026}$	13.046	
212577658	5343.0 ± 50.0	0.33 ± 0.08	4.51 ± 0.1	$0.890^{+0.052}_{-0.033}$	$0.945^{+0.027}_{-0.031}$	11.541	
212580872	5623.0 ± 50.0	0.21 ± 0.08	4.46 ± 0.1	$0.957^{+0.074}_{-0.045}$	$0.994^{+0.029}_{-0.027}$	13.047	
212586030	5084.0 ± 50.0	0.36 ± 0.08	3.95 ± 0.1	$1.82^{+0.22}_{-0.15}$	$1.007^{+0.077}_{-0.043}$	11.689	
212587672	5928.0 ± 50.0	-0.21 ± 0.08	4.49 ± 0.1	$0.953^{+0.057}_{-0.043}$	$0.987^{+0.034}_{-0.033}$	12.188	
212639319	5465.0 ± 50.0	0.29 ± 0.08	3.98 ± 0.1	$1.64^{+0.26}_{-0.23}$	$1.051^{+0.097}_{-0.073}$	12.471	
212645891	5759.0 ± 50.0	0.18 ± 0.08	4.46 ± 0.1	$0.990^{+0.072}_{-0.040}$	1.033 ± 0.026	12.641	
212672300	5979.0 ± 52.0	0.1 ± 0.08	4.21 ± 0.1	$1.28^{+0.18}_{-0.17}$	$1.110^{+0.046}_{-0.035}$	12.846	
212686205	4621.0 ± 50.0	-0.26 ± 0.08	4.7 ± 0.1	$0.651^{+0.021}_{-0.017}$	$0.687^{+0.023}_{-0.022}$	12.256	
212689874	5712.0 ± 50.0	-0.09 ± 0.08	4.55 ± 0.1	$0.906^{+0.047}_{-0.033}$	$0.963^{+0.028}_{-0.032}$	12.330	
212691422	6045.0 ± 50.0	0.01 ± 0.08	4.08 ± 0.1	$1.54^{+0.23}_{-0.19}$	$1.162^{+0.075}_{-0.045}$	11.923	
212697709	5773.0 ± 50.0	0.31 ± 0.08	4.43 ± 0.1	$1.040^{+0.087}_{-0.054}$	$1.068^{+0.035}_{-0.032}$	12.193	
212703473	5758.0 ± 50.0	0.11 ± 0.08	4.46 ± 0.1	$0.978^{+0.068}_{-0.039}$	$1.020^{+0.025}_{-0.027}$	10.729	
212735333	5675.0 ± 50.0	-0.01 ± 0.08	4.58 ± 0.1	$0.910^{+0.042}_{-0.031}$	$0.975^{+0.025}_{-0.029}$	11.977	
212768333	5262.0 ± 50.0	-0.16 ± 0.08	4.63 ± 0.1	$0.778^{+0.031}_{-0.024}$	0.836 ± 0.029	11.022	
212772313	5675.0 ± 50.0	0.03 ± 0.08	4.25 ± 0.1	$1.12^{+0.16}_{-0.13}$	0.972 ± 0.026	10.471	
212779596	4681.0 ± 50.0	-0.23 ± 0.08	4.69 ± 0.1	$0.667^{+0.020}_{-0.019}$	$0.706^{+0.024}_{-0.023}$	11.930	
212803289	6033.0 ± 50.0	0.15 ± 0.08	3.78 ± 0.1	$2.28^{+0.32}_{-0.26}$	$1.42^{+0.10}_{-0.11}$	11.014	
212828909	5233.0 ± 50.0	-0.04 ± 0.08	4.71 ± 0.1	$0.792^{+0.024}_{-0.022}$	$0.860^{+0.023}_{-0.027}$	12.244	
213546283	5631.0 ± 50.0	-0.15 ± 0.08	4.29 ± 0.1	$0.99^{+0.12}_{-0.10}$	0.911 ± 0.035	12.031	
213817056	4863.0 ± 50.0	0.27 ± 0.08	4.38 ± 0.1	$0.781^{+0.030}_{-0.022}$	$0.817^{+0.027}_{-0.026}$	12.964	
214234110	5608.0 ± 50.0	0.37 ± 0.08	4.46 ± 0.1	$0.985^{+0.077}_{-0.042}$	$1.032^{+0.028}_{-0.031}$	11.624	
214254518	4455.0 ± 50.0	-0.28 ± 0.08	4.68 ± 0.1	$0.624^{+0.019}_{-0.018}$	$0.653^{+0.022}_{-0.021}$	11.874	
215171927	4972.0 ± 50.0	0.02 ± 0.08	4.52 ± 0.1	$0.764^{+0.025}_{-0.018}$	$0.811^{+0.024}_{-0.026}$	12.692	
215502661	5694.0 ± 50.0	-0.0 ± 0.08	4.22 ± 0.1	$1.16^{+0.17}_{-0.14}$	$0.978^{+0.029}_{-0.027}$	12.032	
215854715	5310.0 ± 50.0	0.01 ± 0.08	4.63 ± 0.1	$0.821^{+0.029}_{-0.023}$	$0.885^{+0.023}_{-0.028}$	12.611	
216008129	5507.0 ± 50.0	0.13 ± 0.08	4.68 ± 0.1	$0.878^{+0.029}_{-0.021}$	$0.956^{+0.020}_{-0.021}$	11.966	
216050437	6391.0 ± 101.0	0.45 ± 0.095	4.18 ± 0.166	$1.52^{+0.28}_{-0.16}$	$1.381^{+0.094}_{-0.070}$	12.326	a
216114172	5742.0 ± 56.0	0.19 ± 0.08	4.5 ± 0.1	$0.977^{+0.061}_{-0.039}$	$1.029^{+0.028}_{-0.027}$	12.603	
216166748	5679.0 ± 50.0	0.35 ± 0.08	4.49 ± 0.1	$1.002^{+0.061}_{-0.046}$	$1.050^{+0.030}_{-0.034}$	11.884	
216387101	5529.0 ± 50.0	-0.22 ± 0.08	3.91 ± 0.1	$1.77^{+0.23}_{-0.21}$	$0.990^{+0.041}_{-0.038}$	12.897	
216405287	5491.0 ± 58.0	0.27 ± 0.08	4.55 ± 0.102	$0.911^{+0.051}_{-0.034}$	$0.971^{+0.030}_{-0.028}$	12.997	
216468514	6178.0 ± 50.0	0.35 ± 0.08	4.24 ± 0.1	$1.33^{+0.18}_{-0.10}$	$1.258^{+0.051}_{-0.046}$	12.749	
216494238	5767.0 ± 50.0	0.44 ± 0.08	4.47 ± 0.1	$1.064^{+0.069}_{-0.047}$	$1.101^{+0.025}_{-0.028}$	12.302	
217192839	4661.0 ± 50.0	-0.33 ± 0.08	4.66 ± 0.1	$0.646^{+0.021}_{-0.019}$	$0.678^{+0.023}_{-0.022}$	12.601	
217855533	6244.0 ± 50.0	-0.06 ± 0.08	4.11 ± 0.1	$1.47^{+0.23}_{-0.18}$	$1.203^{+0.089}_{-0.062}$	10.043	
217941732	4528.0 ± 50.0	-0.24 ± 0.08	4.62 ± 0.1	$0.644^{+0.020}_{-0.018}$	0.675 ± 0.021	12.283	
217977895	5570.0 ± 50.0	0.0 ± 0.08	4.61 ± 0.1	$0.882^{+0.038}_{-0.028}$	$0.948^{+0.025}_{-0.028}$	12.745	

Table 5 — *Continued*

EPIC	$T_{\rm eff}$	$[m/{\rm H}]$	$\log g$	R_* ($R_\odot$)	M_* ($M_\odot$)	$K_{\rm p}$	Notes
218131080	6235.0 ± 82.0	0.14 ± 0.08	4.22 ± 0.137	$1.29^{+0.24}_{-0.12}$	$1.214^{+0.064}_{-0.049}$	12.700	a
218170789	5250.0 ± 50.0	0.07 ± 0.08	4.31 ± 0.1	$0.874^{+0.051}_{-0.049}$	$0.858^{+0.028}_{-0.024}$	12.890	
218304292	5779.0 ± 51.0	-0.29 ± 0.08	4.13 ± 0.1	$1.23^{+0.17}_{-0.14}$	$0.918^{+0.057}_{-0.043}$	12.511	
218668602	5231.0 ± 50.0	0.21 ± 0.08	4.68 ± 0.1	$0.825^{+0.027}_{-0.019}$	$0.899^{+0.021}_{-0.023}$	12.411	
218916923	5425.0 ± 50.0	0.23 ± 0.08	4.66 ± 0.1	$0.872^{+0.034}_{-0.023}$	$0.949^{+0.024}_{-0.022}$	11.470	
219388192	5689.0 ± 50.0	0.16 ± 0.08	4.43 ± 0.1	$0.970^{+0.088}_{-0.045}$	$1.004^{+0.026}_{-0.025}$	12.336	
220170303	5000.0 ± 50.0	-0.07 ± 0.08	4.43 ± 0.1	$0.763^{+0.030}_{-0.024}$	$0.794^{+0.033}_{-0.028}$	12.114	
220186645	5755.0 ± 50.0	0.07 ± 0.08	4.23 ± 0.1	$1.18^{+0.16}_{-0.14}$	$1.009^{+0.031}_{-0.027}$	12.961	
220192485	5220.0 ± 50.0	-0.1 ± 0.08	4.54 ± 0.1	$0.793^{+0.040}_{-0.028}$	$0.840^{+0.027}_{-0.031}$	11.758	
220207765	5318.0 ± 50.0	0.26 ± 0.08	4.68 ± 0.1	$0.852^{+0.033}_{-0.023}$	$0.927^{+0.025}_{-0.023}$	12.170	
220211923	5890.0 ± 50.0	-0.26 ± 0.08	4.25 ± 0.1	$1.08^{+0.13}_{-0.11}$	$0.951^{+0.038}_{-0.036}$	12.250	
220216730	5043.0 ± 50.0	-0.14 ± 0.08	4.46 ± 0.1	$0.758^{+0.032}_{-0.027}$	$0.789^{+0.030}_{-0.028}$	12.826	
220218012	5522.0 ± 50.0	0.11 ± 0.08	4.41 ± 0.1	$0.928^{+0.092}_{-0.051}$	0.942 ± 0.028	12.971	
220225178	5582.0 ± 50.0	-0.11 ± 0.08	4.62 ± 0.1	$0.862^{+0.034}_{-0.030}$	0.925 ± 0.030	12.302	
220241529	4720.0 ± 50.0	-0.06 ± 0.08	4.46 ± 0.1	0.712 ± 0.020	$0.745^{+0.026}_{-0.024}$	10.717	
220245303	5121.0 ± 50.0	-0.03 ± 0.08	4.69 ± 0.1	$0.775^{+0.023}_{-0.021}$	$0.837^{+0.024}_{-0.028}$	11.821	
220250254	5396.0 ± 50.0	0.05 ± 0.08	4.55 ± 0.1	$0.852^{+0.042}_{-0.025}$	$0.912^{+0.023}_{-0.028}$	11.507	
220256496	5221.0 ± 50.0	0.11 ± 0.08	4.6 ± 0.1	$0.816^{+0.033}_{-0.019}$	$0.882^{+0.019}_{-0.027}$	12.872	
220292715	4895.0 ± 50.0	-0.15 ± 0.08	4.52 ± 0.1	$0.724^{+0.025}_{-0.022}$	$0.762^{+0.026}_{-0.025}$	12.213	
220294712	6057.0 ± 58.0	0.1 ± 0.08	4.38 ± 0.103	$1.115^{+0.098}_{-0.058}$	$1.120^{+0.031}_{-0.030}$	12.264	
220317172	5374.0 ± 50.0	0.09 ± 0.08	4.59 ± 0.1	$0.847^{+0.036}_{-0.023}$	$0.913^{+0.021}_{-0.026}$	12.107	
220321605	4349.0 ± 50.0	-0.33 ± 0.08	4.72 ± 0.1	$0.598^{+0.017}_{-0.014}$	$0.622^{+0.020}_{-0.018}$	12.588	
220341183	5794.0 ± 50.0	0.25 ± 0.08	4.25 ± 0.1	$1.20^{+0.17}_{-0.13}$	$1.070^{+0.055}_{-0.038}$	12.043	
220376054	5768.0 ± 50.0	0.12 ± 0.08	4.27 ± 0.1	$1.12^{+0.15}_{-0.12}$	$1.022^{+0.031}_{-0.028}$	11.597	
220383386	5366.0 ± 50.0	-0.01 ± 0.08	4.54 ± 0.1	$0.837^{+0.048}_{-0.027}$	$0.890^{+0.026}_{-0.029}$	8.945	
220397060	5333.0 ± 51.0	0.05 ± 0.08	4.2 ± 0.101	$0.99^{+0.24}_{-0.09}$	$0.869^{+0.025}_{-0.020}$	12.835	
220410754	5758.0 ± 50.0	-0.05 ± 0.08	4.22 ± 0.1	$1.16^{+0.18}_{-0.13}$	$0.993^{+0.032}_{-0.033}$	12.843	
220471666	5704.0 ± 50.0	0.11 ± 0.08	4.41 ± 0.1	$0.974^{+0.095}_{-0.049}$	$1.000^{+0.026}_{-0.027}$	12.798	
220481411	4591.0 ± 50.0	-0.18 ± 0.08	4.59 ± 0.1	$0.666^{+0.022}_{-0.019}$	0.699 ± 0.023	12.100	
220487418	5967.0 ± 50.0	0.04 ± 0.08	4.17 ± 0.1	$1.33^{+0.20}_{-0.17}$	$1.103^{+0.046}_{-0.037}$	12.062	
220503236	5757.0 ± 50.0	0.25 ± 0.08	4.45 ± 0.1	$1.008^{+0.080}_{-0.046}$	$1.047^{+0.031}_{-0.028}$	12.713	
220555384	4360.0 ± 50.0	-0.2 ± 0.08	4.69 ± 0.1	$0.622^{+0.020}_{-0.017}$	$0.650^{+0.021}_{-0.020}$	12.395	
220592745	5753.0 ± 50.0	0.13 ± 0.08	4.23 ± 0.1	$1.19^{+0.16}_{-0.14}$	$1.022^{+0.034}_{-0.030}$	11.923	
220621788	5599.0 ± 50.0	0.06 ± 0.08	4.43 ± 0.1	$0.930^{+0.089}_{-0.044}$	$0.960^{+0.026}_{-0.029}$	11.752	
220643470	4621.0 ± 50.0	-0.78 ± 0.08	2.17 ± 0.1	$13.7^{+2.3}_{-1.6}$	$0.97^{+0.22}_{-0.13}$	10.839	
220648214	5785.0 ± 50.0	0.01 ± 0.08	4.21 ± 0.1	$1.20^{+0.17}_{-0.15}$	$1.012^{+0.033}_{-0.027}$	12.390	
220650439	5716.0 ± 50.0	0.13 ± 0.08	4.57 ± 0.1	$0.948^{+0.045}_{-0.029}$	$1.011^{+0.024}_{-0.025}$	12.232	
220674823	5590.0 ± 50.0	0.08 ± 0.08	4.54 ± 0.1	$0.906^{+0.051}_{-0.029}$	$0.967^{+0.023}_{-0.028}$	11.958	
220679255	5966.0 ± 50.0	0.01 ± 0.08	4.33 ± 0.1	$1.08^{+0.13}_{-0.07}$	$1.071^{+0.027}_{-0.032}$	11.975	
220709978	5934.0 ± 50.0	-0.3 ± 0.08	4.29 ± 0.1	$1.04^{+0.13}_{-0.10}$	$0.950^{+0.040}_{-0.036}$	9.443	
228721452	5859.0 ± 50.0	0.19 ± 0.08	4.54 ± 0.1	$1.013^{+0.055}_{-0.035}$	1.067 ± 0.026	11.325	
228725972	5614.0 ± 50.0	-0.22 ± 0.08	4.63 ± 0.1	$0.840^{+0.038}_{-0.030}$	$0.902^{+0.028}_{-0.029}$	12.482	
228729473	4939.0 ± 50.0	-0.04 ± 0.08	3.54 ± 0.1	$2.88^{+0.38}_{-0.33}$	$1.00^{+0.11}_{-0.08}$	11.524	
228732031	5113.0 ± 50.0	-0.15 ± 0.08	4.5 ± 0.1	$0.765^{+0.033}_{-0.026}$	$0.803^{+0.028}_{-0.030}$	11.937	
228734889	5792.0 ± 50.0	0.0 ± 0.08	4.52 ± 0.1	$0.956^{+0.054}_{-0.037}$	$1.008^{+0.027}_{-0.029}$	12.59	
228734900	5733.0 ± 50.0	0.47 ± 0.08	4.26 ± 0.1	$1.21^{+0.20}_{-0.13}$	$1.115^{+0.054}_{-0.035}$	11.535	
228735255	5637.0 ± 50.0	0.29 ± 0.08	4.33 ± 0.1	$1.05^{+0.14}_{-0.08}$	$1.017^{+0.036}_{-0.034}$	12.483	
228736155	5397.0 ± 50.0	-0.08 ± 0.08	4.62 ± 0.1	$0.824^{+0.034}_{-0.027}$	$0.886^{+0.028}_{-0.030}$	12.042	
228737155	4382.0 ± 50.0	-0.72 ± 0.08	2.07 ± 0.1	$16.0^{+2.0}_{-1.4}$	$0.874^{+0.090}_{-0.046}$	11.081	
228754001	5035.0 ± 50.0	0.07 ± 0.08	3.8 ± 0.1	$2.16^{+0.26}_{-0.20}$	$0.984^{+0.072}_{-0.039}$	11.651	
228760097	5673.0 ± 50.0	-0.1 ± 0.08	4.58 ± 0.1	$0.891^{+0.041}_{-0.031}$	$0.951^{+0.028}_{-0.030}$	11.512	
228798746	4764.0 ± 50.0	-0.13 ± 0.08	4.67 ± 0.1	$0.699^{+0.022}_{-0.020}$	$0.742^{+0.025}_{-0.023}$	12.66	
228801451	5231.0 ± 50.0	-0.03 ± 0.08	4.59 ± 0.1	$0.802^{+0.034}_{-0.023}$	$0.858^{+0.025}_{-0.029}$	10.955	
228804845	6002.0 ± 50.0	0.21 ± 0.08	4.29 ± 0.1	$1.18^{+0.14}_{-0.09}$	$1.131^{+0.041}_{-0.029}$	12.551	
228809391	5611.0 ± 50.0	0.06 ± 0.08	4.55 ± 0.1	$0.907^{+0.046}_{-0.028}$	$0.970^{+0.022}_{-0.026}$	12.595	
228952747	4315.0 ± 50.0	-0.33 ± 0.08	4.73 ± 0.1	$0.593^{+0.017}_{-0.015}$	$0.615^{+0.019}_{-0.018}$	12.224	
229004835	5870.0 ± 50.0	-0.15 ± 0.08	4.4 ± 0.1	$0.975^{+0.088}_{-0.053}$	$0.990^{+0.034}_{-0.035}$	10.151	
229039390	5833.0 ± 50.0	-0.04 ± 0.08	4.41 ± 0.1	$0.987^{+0.088}_{-0.048}$	$1.013^{+0.029}_{-0.031}$	12.735	

Table 5 — *Continued*

EPIC	$T_{\rm eff}$	$[m/{\rm H}]$	$\log g$	R_* ($R_\odot$)	M_* ($M_\odot$)	$K_{\rm p}$	Notes
229131722	5928.0 ± 50.0	0.23 ± 0.08	4.42 ± 0.1	$1.078^{+0.092}_{-0.053}$	$1.100^{+0.034}_{-0.028}$	12.515	
229133720	4933.0 ± 50.0	-0.12 ± 0.08	4.65 ± 0.1	$0.728^{+0.022}_{-0.021}$	$0.778^{+0.026}_{-0.027}$	11.477	

[a] Stellar parameters for this star are derived from a single spectrum with a cross correlation function peak height < 0.9 (but > 0.8). We have decided the resulting stellar parameters are trustworthy for this analysis, but provide a note for the reader's discretion.
[b] S_{HK} values have been determined for this star and can be found in Table 3.

Table 6
Detailed FPP Table

New K2 Name	EPIC	Secondary Eclipse Threshold (ppm)	Aperture Radius (arcsec)	AO/ Speckle	P(Eclipsing Binary)	P(Eclipsing Binary) (x2 Per.)	P(Background Eclipsing Binary)	P(Background Eclipsing Binary) (x2 Per.)	P(Hierarchical Eclipsing Binary)	P(Hierarchical Eclipsing Binary) (x2 Per.)	RV Mass Limit	VESPA FPP	Multiplicity Boost	Adopted FPP	Disposition
K2-156 b	201110617.01	28	14.7	Y	$0.00e+00$	$0.00e+00$	$<1e-04$	$<1e-04$	$<1e-04$	$<1e-04$	Y	$2.18e-08$	-	$<1e-04$	Planet
	201111557.01	47	14.4	Y	$<1e-04$	$1.16e-03$	$<1e-04$	$<1e-04$	$<1e-04$	$<1e-04$	N	$1.22e-03$	-	$1.22e-03$	Candidate
	201127519.01	813	17.9	Y	-	-	-	-	-	-	Y	-	-	-	Candidate
K2-157 b	201130233.01	5	12.4	Y	$<1e-04$	$<1e-04$	$<1e-04$	$<1e-04$	$<1e-04$	$<1e-04$	N	$2.81e-08$	-	$<1e-04$	Planet
K2-158 b	201132684.01	95	19.2	Y	$<1e-04$	$<1e-04$	$<1e-04$	$<1e-04$	$<1e-04$	$<1e-04$	N	$3.62e-06$	-	$<1e-04$	Planet
	201166680.01	64	17.9	Y	$1.70e-03$	$<1e-04$	$<1e-04$	$<1e-04$	$<1e-04$	$<1e-04$	N	$1.73e-03$	-	$1.73e-03$	Candidate
	201211526.01	40	17.3	Y	$<1e-04$	$2.03e-03$	$<1e-04$	$<1e-04$	$<1e-04$	$<1e-04$	N	$2.10e-03$	-	$2.10e-03$	Candidate
K2-159 b	201225286.01	85	19.9	Y	$<1e-04$	$3.43e-04$	$<1e-04$	$<1e-04$	$<1e-04$	$<1e-04$	N	$3.53e-04$	-	$3.53e-04$	Planet
K2-160 b	201227197.01	53	14.7	Y	$6.72e-04$	$<1e-04$	$<1e-04$	$<1e-04$	$<1e-04$	$<1e-04$	N	$7.54e-04$	-	$7.54e-04$	Planet
K2-161 b	201231064.01	88	16.3	Y	$<1e-04$	$7.93e-04$	$<1e-04$	$<1e-04$	$<1e-04$	$<1e-04$	N	$7.97e-04$	-	$7.97e-04$	Planet
	201295312.01	27	14.4	Y	$<1e-04$	$<1e-04$	$<1e-04$	$<1e-04$	$<1e-04$	$<1e-04$	N	$1.29e-09$	-	$<1e-04$	Planet
	201299088.01	77	19.4	Y	$<1e-04$	$<1e-04$	$<1e-04$	$<1e-04$	$<1e-04$	$<1e-04$	N	$6.10e-05$	-	-	Candidate
	201352100.01	95	15.0	Y	-	-	-	-	-	-	N	-	-	-	Candidate
	201384232.01	95	20.5	Y	$<1e-04$	$<1e-04$	$<1e-04$	$<1e-04$	$<1e-04$	$<1e-04$	N	$2.50e-05$	-	$<1e-04$	Planet
K2-162 b	201390048.01	105	17.1	Y	$<1e-04$	$<1e-04$	$<1e-04$	$<1e-04$	$<1e-04$	$<1e-04$	N	$3.46e-06$	-	$<1e-04$	Planet
	201403446.01	47	16.3	Y	$0.00e+00$	$0.00e+00$	$<1e-04$	$<1e-04$	$<1e-04$	$<1e-04$	Y	$2.38e-06$	-	$<1e-04$	Planet
K2-163 b	201427874.01	92	17.7	Y	$<1e-04$	$<1e-04$	$<1e-04$	$<1e-04$	$<1e-04$	$<1e-04$	N	$3.52e-09$	-	$<1e-04$	Planet
	201437844.01	421	22.3	Y	$0.00e+00$	$0.00e+00$	$<1e-04$	$<1e-04$	$<1e-04$	$<1e-04$	Y	$-1.32e-04$	25	$<1e-04$	Planet
	201437844.02	846	22.3	Y	$0.00e+00$	$0.00e+00$	$<1e-04$	$<1e-04$	$<1e-04$	$<1e-04$	Y	$-2.76e-04$	25	$<1e-04$	Planet
	201441872.01	21	18.8	N	-	-	-	-	-	-	N	-	-	-	Candidate
K2-164 b	201460826.01	40	17.3	N	$<1e-04$	$<1e-04$	$<1e-04$	$<1e-04$	$<1e-04$	$<1e-04$	N	$1.76e-06$	-	$<1e-04$	Planet
	201505350.01	83	16.6	Y	$<1e-04$	$1.14e-04$	$<1e-04$	$<1e-04$	$<1e-04$	$<1e-04$	N	$1.17e-04$	50	$<1e-04$	Planet
	201505350.02	63	16.6	Y	$<1e-04$	$<1e-04$	$<1e-04$	$<1e-04$	$<1e-04$	$<1e-04$	N	$2.54e-07$	50	$<1e-04$	Planet
	201505350.03	36	16.6	Y	$<1e-04$	$<1e-04$	$<1e-04$	$<1e-04$	$<1e-04$	$<1e-04$	N	$1.11e-16$	50	$<1e-04$	Planet
K2-165 b	201528828.01	48	19.4	Y	$<1e-04$	$<1e-04$	$<1e-04$	$<1e-04$	$<1e-04$	$<1e-04$	N	$9.57e-06$	50	$<1e-04$	Planet
K2-165 c	201528828.02	67	19.4	Y	$<1e-04$	$<1e-04$	$<1e-04$	$<1e-04$	$<1e-04$	$<1e-04$	N	$2.09e-07$	50	$<1e-04$	Planet
K2-165 d	201528828.03	146	19.4	Y	$<1e-04$	$<1e-04$	$<1e-04$	$<1e-04$	$<1e-04$	$<1e-04$	N	$3.78e-05$	50	$<1e-04$	Planet
	201546283.01	37	15.8	Y	-	-	-	-	-	-	N	-	-	-	Candidate
	201577035.01	63	16.3	Y	$<1e-04$	$<1e-04$	$<1e-04$	$<1e-04$	$<1e-04$	$<1e-04$	N	$9.62e-05$	-	$<1e-04$	Planet
	201595106.01	26	21.6	Y	$2.94e-04$	$1.19e-03$	$<1e-04$	$<1e-04$	$<1e-04$	$<1e-04$	N	$1.55e-03$	-	$1.55e-03$	Candidate
	201613023.01	42	19.0	Y	$<1e-04$	$<1e-04$	$<1e-04$	$<1e-04$	$<1e-04$	$<1e-04$	N	$4.54e-08$	-	$<1e-04$	Planet
K2-166 b	201615463.01	35	20.1	Y	$<1e-04$	$<1e-04$	$<1e-04$	$<1e-04$	$<1e-04$	$<1e-04$	N	$1.92e-07$	-	$<1e-04$	Planet
	201713348.01	129	17.1	Y	$1.55e-01$	$1.21e-02$	$<1e-04$	$<1e-04$	$7.32e-03$	$1.05e-03$	N	$1.75e-01$	25	$7.00e-03$	Candidate
	201713348.02	28	17.1	Y	$<1e-04$	$<1e-04$	$<1e-04$	$<1e-04$	$<1e-04$	$<1e-04$	N	$9.58e-05$	25	$<1e-04$	Planet
	201828749.01	83	18.2	Y	-	-	-	-	-	-	N	-	-	-	Candidate
	201855371.01	160	22.3	Y	$<1e-04$	$<1e-04$	$<1e-04$	$<1e-04$	$<1e-04$	$<1e-04$	N	$1.28e-06$	-	$<1e-04$	Planet
	201920032.01	200	17.9	Y	$7.78e-03$	$1.66e-03$	$<1e-04$	$2.77e-04$	$<1e-04$	$<1e-04$	N	$9.73e-03$	-	$9.73e-03$	Candidate
	202089657.01	81	19.0	Y	-	-	-	-	-	-	Y	-	-	-	Candidate
	202091388.01	179	16.3	Y	-	-	-	-	-	-	N	-	-	-	Candidate
	202675839.01	291	18.2	Y	$5.82e-01$	$1.83e-01$	$<1e-04$	$<1e-04$	$2.76e-02$	$1.15e-02$	N	$8.03e-01$	-	-	Candidate
	202821899.01	184	21.1	N	-	-	-	-	-	-	Y	-	-	-	Candidate
	202900527.01	251	18.2	Y	-	-	-	-	-	-	N	-	-	-	Candidate
	203771098.01	109	16.8	Y	$<1e-04$	$<1e-04$	$<1e-04$	$<1e-04$	$<1e-04$	$<1e-04$	N	$1.23e-07$	25	$<1e-04$	Planet
	203771098.02	62	16.8	Y	$<1e-04$	$<1e-04$	$<1e-04$	$<1e-04$	$<1e-04$	$<1e-04$	N	$2.18e-05$	25	$<1e-04$	Planet
	203826436.01	72	15.8	Y	$<1e-04$	$<1e-04$	$<1e-04$	$<1e-04$	$<1e-04$	$<1e-04$	N	$4.73e-07$	50	$<1e-04$	Planet
	203826436.02	110	15.8	Y	$<1e-04$	$<1e-04$	$<1e-04$	$<1e-04$	$<1e-04$	$<1e-04$	N	$4.44e-05$	50	$<1e-04$	Planet
	203826436.03	64	15.8	Y	$<1e-04$	$<1e-04$	$<1e-04$	$<1e-04$	$<1e-04$	$<1e-04$	N	$1.28e-08$	50	$<1e-04$	Planet
	204750116.01	82	19.9	N	-	-	-	-	-	-	N	-	-	-	Candidate
	205029914.01	30	16.8	Y	-	-	-	-	-	-	N	-	-	-	Candidate
	205071984.01	107	21.1	Y	$<1e-04$	$<1e-04$	$<1e-04$	$<1e-04$	$<1e-04$	$<1e-04$	N	$2.22e-16$	50	$<1e-04$	Planet
	205071984.02	186	21.1	Y	$<1e-04$	$<1e-04$	$<1e-04$	$<1e-04$	$<1e-04$	$<1e-04$	N	$2.24e-09$	50	$<1e-04$	Planet
	205071984.03	153	21.1	Y	$<1e-04$	$<1e-04$	$<1e-04$	$<1e-04$	$<1e-04$	$<1e-04$	N	$2.04e-09$	50	$<1e-04$	Planet
K2-167 b	205904628.01	24	22.6	Y	$0.00e+00$	$0.00e+00$	$9.72e-04$	$<1e-04$	$<1e-04$	$<1e-04$	Y	$8.64e-04$	-	$8.64e-04$	Planet
	205944181.01	42	18.2	Y	$8.01e-01$	$1.33e-01$	$<1e-04$	$<1e-04$	$1.16e-02$	$3.39e-03$	N	$9.49e-01$	-	$9.49e-01$	Candidate
K2-168 b	205950854.01	78	18.2	N	$<1e-04$	$<1e-04$	$7.06e-04$	$<1e-04$	$<1e-04$	$<1e-04$	N	$7.10e-04$	-	$7.10e-04$	Planet
	205957328.01	94	16.3	N	$<1e-04$	$<1e-04$	$3.05e-03$	$8.46e-04$	$<1e-04$	$<1e-04$	N	$3.97e-03$	-	$3.97e-03$	Candidate
K2-169 b	206007892.01	30	15.3	N	$<1e-04$	$<1e-04$	$<1e-04$	$<1e-04$	$<1e-04$	$<1e-04$	N	$9.95e-05$	-	$<1e-04$	Planet
K2-170 c	206008091.01	52	13.8	N	$<1e-04$	$<1e-04$	$3.26e-04$	$<1e-04$	$<1e-04$	$<1e-04$	N	$3.36e-04$	25	$<1e-04$	Planet
K2-170 b	206008091.02	45	13.8	N	$<1e-04$	$<1e-04$	$1.01e-03$	$3.32e-04$	$<1e-04$	$<1e-04$	N	$1.35e-03$	25	$<1e-04$	Planet
	206011496.01	21	19.7	Y	-	-	-	-	-	-	N	-	-	-	Candidate
	206026904.01	48	15.3	Y	$1.08e-03$	$<1e-04$	$<1e-04$	$<1e-04$	$<1e-04$	$<1e-04$	N	$1.09e-03$	50	$<1e-04$	Planet
	206026904.02	25	15.3	Y	$<1e-04$	$<1e-04$	$<1e-04$	$<1e-04$	$<1e-04$	$<1e-04$	N	$3.43e-07$	50	$<1e-04$	Planet
	206026904.03	121	15.3	Y	$<1e-04$	$<1e-04$	$<1e-04$	$<1e-04$	$<1e-04$	$<1e-04$	N	$3.46e-05$	50	$<1e-04$	Planet
	206044803.01	28	13.8	N	$<1e-04$	$<1e-04$	$1.64e-04$	$<1e-04$	$<1e-04$	$<1e-04$	N	$2.16e-04$	-	$2.16e-04$	Planet
K2-171 b	206049764.01	33	16.1	N	$<1e-04$	$<1e-04$	$<1e-04$	$<1e-04$	$<1e-04$	$<1e-04$	N	$5.39e-10$	-	$<1e-04$	Planet
K2-172 c	206082454.01	87	13.8	N	$<1e-04$	$<1e-04$	$<1e-04$	$<1e-04$	$<1e-04$	$<1e-04$	N	$4.88e-05$	25	$<1e-04$	Planet
K2-172 b	206082454.02	58	13.8	N	$<1e-04$	$<1e-04$	$1.40e-03$	$1.23e-04$	$<1e-04$	$<1e-04$	N	$1.52e-03$	25	$<1e-04$	Planet
	206096602.01	41	16.6	Y	$<1e-04$	$<1e-04$	$<1e-04$	$<1e-04$	$<1e-04$	$<1e-04$	N	$1.77e-05$	25	$<1e-04$	Planet
	206096602.02	83	16.6	Y	$5.42e-04$	$<1e-04$	$<1e-04$	$<1e-04$	$<1e-04$	$<1e-04$	N	$6.41e-04$	25	$<1e-04$	Planet
	206114630.01	65	21.3	N	$4.11e-01$	$4.34e-02$	$2.31e-01$	$1.96e-01$	$1.03e-01$	$7.71e-03$	N	$9.91e-01$	-	$9.91e-01$	Candidate
	206119924.01	29	18.8	N	-	-	-	-	-	-	N	-	-	-	Candidate
	206144956.01	28	18.4	Y	$<1e-04$	$<1e-04$	$<1e-04$	$<1e-04$	$<1e-04$	$<1e-04$	N	$2.24e-06$	-	$<1e-04$	Planet
	206146957.01	37	21.3	N	$<1e-04$	$<1e-04$	$4.84e-03$	$3.71e-04$	$<1e-04$	$<1e-04$	N	$5.22e-03$	-	$5.22e-03$	Candidate

Table 6 — *Continued*

New K2 Name	EPIC	Secondary Eclipse Threshold (ppm)	Aperture Radius (arcsec)	AO/ Speckle	P(Eclipsing Binary)	P(Eclipsing Binary) (x2 Per.)	P(Background Eclipsing Binary)	P(Background Eclipsing Binary) (x2 Per.)	P(Hierarchical Eclipsing Binary)	P(Hierarchical Eclipsing Binary) (x2 Per.)	RV Mass Limit	VESPA FPP	Multiplicity Boost	Adopted FPP	Disposition
	206159027.01	49	14.1	Y	$< 1e-04$	$< 1e-04$	$< 1e-04$	$< 1e-04$	$< 1e-04$	$< 1e-04$	N	$4.81e-09$	-	$< 1e-04$	Planet
	206169375.01	8	21.1	N	$0.00e+00$	$0.00e+00$	$1.39e-04$	$9.24e-01$	$< 1e-04$	$1.04e-03$	Y	$9.25e-01$	-	$9.25e-01$	Candidate
	206181769.01	57	14.1	Y	$< 1e-04$	$< 1e-04$	$< 1e-04$	$< 1e-04$	$< 1e-04$	$< 1e-04$	N	$3.66e-05$	-	$< 1e-04$	Planet
	206192335.01	47	16.3	Y	-	-	-	-	-	-	N	-	-	-	Candidate
	206245553.01	26	15.8	Y	$< 1e-04$	$< 1e-04$	$< 1e-04$	$< 1e-04$	$< 1e-04$	$< 1e-04$	N	$3.58e-06$	-	$< 1e-04$	Planet
	206268299.01	49	16.3	Y	$4.04e-04$	$1.13e-04$	$< 1e-04$	$< 1e-04$	$< 1e-04$	$< 1e-04$	N	$5.17e-04$	-	$5.17e-04$	Planet
	206348688.01	49	16.8	Y	$< 1e-04$	$< 1e-04$	$< 1e-04$	$< 1e-04$	$< 1e-04$	$< 1e-04$	N	$4.06e-10$	25	$< 1e-04$	Planet
	206348688.02	65	16.8	Y	$< 1e-04$	$< 1e-04$	$< 1e-04$	$< 1e-04$	$< 1e-04$	$< 1e-04$	N	$1.30e-04$	25	$< 1e-04$	Planet
	206439513.01	11	18.2	Y	$< 1e-04$	$1.37e-03$	$< 1e-04$	$9.99e-01$	$< 1e-04$	$< 1e-04$	N	$1.00e+00$	-	-	Candidate
	206535016.01	118	21.1	N	$1.06e-01$	$6.79e-03$	$4.84e-02$	$2.73e-02$	$3.18e-03$	$4.64e-04$	N	$1.92e-01$	-	$1.92e-01$	Candidate
	210363145.01	77	20.3	Y	$< 1e-04$	$< 1e-04$	$< 1e-04$	$< 1e-04$	$< 1e-04$	$< 1e-04$	N	$6.29e-10$	-	$< 1e-04$	Planet
	210365511.01	56	18.2	N	$< 1e-04$	$< 1e-04$	$< 1e-04$	$1.00e+00$	$< 1e-04$	$< 1e-04$	N	$1.00e+00$	-	-	Candidate
	210402237.01	52	18.2	Y	$< 1e-04$	$< 1e-04$	$< 1e-04$	$< 1e-04$	$< 1e-04$	$< 1e-04$	N	$7.83e-13$	-	$< 1e-04$	Planet
	210403955.01	73	18.2	Y	$< 1e-04$	$< 1e-04$	$< 1e-04$	$< 1e-04$	$< 1e-04$	$< 1e-04$	N	$8.22e-07$	50	$< 1e-04$	Planet
	210403955.02	39	18.2	Y	$< 1e-04$	$< 1e-04$	$< 1e-04$	$< 1e-04$	$< 1e-04$	$< 1e-04$	N	$6.09e-07$	50	$< 1e-04$	Planet
K2-80 d	210403955.03	90	18.2	Y	$< 1e-04$	$< 1e-04$	$< 1e-04$	$< 1e-04$	$< 1e-04$	$< 1e-04$	N	$2.63e-05$	50	$< 1e-04$	Planet
	210423938.01	184	16.6	N	$0.00e+00$	$0.00e+00$	$7.43e-02$	$1.05e-02$	$< 1e-04$	$< 1e-04$	Y	$8.45e-02$	-	$8.45e-02$	Candidate
K2-173 b	210512842.01	48	13.1	Y	$< 1e-04$	$< 1e-04$	$6.56e-04$	$< 1e-04$	$< 1e-04$	$< 1e-04$	N	$7.20e-04$	-	$7.20e-04$	Planet
K2-174 b	210558622.01	42	17.1	Y	$< 1e-04$	$< 1e-04$	$< 1e-04$	$< 1e-04$	$< 1e-04$	$< 1e-04$	N	$2.11e-15$	-	$< 1e-04$	Planet
	210609658.01	85	13.8	Y	$< 1e-04$	$< 1e-04$	$< 1e-04$	$< 1e-04$	$< 1e-04$	$< 1e-04$	N	$4.35e-07$	-	-	Candidate
	210629082.01	41	12.8	Y	$2.36e-04$	$1.86e-04$	$1.51e-03$	$1.58e-04$	$< 1e-04$	$< 1e-04$	N	$2.09e-03$	-	$2.09e-03$	Candidate
K2-175 b	210643811.01	21	18.2	Y	$< 1e-04$	$< 1e-04$	$4.46e-04$	$< 1e-04$	$< 1e-04$	$< 1e-04$	N	$5.26e-04$	-	$5.26e-04$	Planet
K2-176 b	210667381.01	31	12.8	Y	$< 1e-04$	$< 1e-04$	$4.76e-04$	$< 1e-04$	$< 1e-04$	$< 1e-04$	N	$5.38e-04$	-	$5.38e-04$	Planet
	210707130.01	18	14.4	Y	$< 1e-04$	$< 1e-04$	$< 1e-04$	$< 1e-04$	$< 1e-04$	$< 1e-04$	N	$3.40e-06$	-	$< 1e-04$	Planet
	210718708.01	111	16.3	Y	$< 1e-04$	$< 1e-04$	$< 1e-04$	$< 1e-04$	$< 1e-04$	$< 1e-04$	N	$2.26e-06$	-	$< 1e-04$	Planet
	210775710.01	72	16.3	Y	$0.00e+00$	$0.00e+00$	$1.65e-03$	$< 1e-04$	$< 1e-04$	$< 1e-04$	Y	$1.55e-03$	-	$1.55e-03$	Candidate
	210848071.01	45	17.7	Y	$6.56e-04$	$< 1e-04$	$9.07e-04$	$< 1e-04$	$< 1e-04$	$< 1e-04$	N	$1.62e-03$	-	$1.62e-03$	Candidate
K2-177 b	210857328.01	35	14.1	Y	$< 1e-04$	$< 1e-04$	$< 1e-04$	$< 1e-04$	$< 1e-04$	$< 1e-04$	N	$1.19e-04$	-	$1.19e-04$	Planet
	210894022.01	27	13.5	Y	$< 1e-04$	$< 1e-04$	$< 1e-04$	$< 1e-04$	$< 1e-04$	$< 1e-04$	N	$4.62e-08$	-	$< 1e-04$	Planet
	210957318.01	132	15.6	Y	$< 1e-04$	$< 1e-04$	$< 1e-04$	$< 1e-04$	$< 1e-04$	$< 1e-04$	N	$9.00e-05$	-	-	Candidate
K2-178 b	210965800.01	117	18.2	Y	$0.00e+00$	$0.00e+00$	$6.54e-04$	$< 1e-04$	$< 1e-04$	$< 1e-04$	Y	$3.47e-04$	-	$3.47e-04$	Planet
K2-179 b	211048999.01	66	16.3	Y	$< 1e-04$	$< 1e-04$	$3.42e-04$	$1.54e-04$	$< 1e-04$	$< 1e-04$	N	$4.97e-04$	-	$4.97e-04$	Planet
	211089792.01	60	18.2	Y	-	-	-	-	-	-	Y	-	-	-	Candidate
	211106187.01	479	16.3	N	-	-	-	-	-	-	N	-	-	-	Candidate
	211147528.01	351	21.1	Y	-	-	-	-	-	-	N	-	-	-	Candidate
K2-180 b	211319617.01	71	24.9	Y	$< 1e-04$	$< 1e-04$	$< 1e-04$	$< 1e-04$	$< 1e-04$	$< 1e-04$	N	$2.62e-10$	-	$< 1e-04$	Planet
	211351816.01	112	21.1	Y	$1.53e-01$	$6.36e-04$	$< 1e-04$	$< 1e-04$	$< 1e-04$	$< 1e-04$	N	$1.53e-01$	-	-	Candidate
K2-181 b	211355342.01	64	21.1	Y	$7.85e-04$	$1.93e-04$	$< 1e-04$	$< 1e-04$	$< 1e-04$	$< 1e-04$	N	$9.95e-04$	-	$9.95e-04$	Planet
K2-182 b	211359660.01	30	19.9	N	$< 1e-04$	$< 1e-04$	$5.96e-04$	$< 1e-04$	$< 1e-04$	$< 1e-04$	N	$5.97e-04$	-	$5.97e-04$	Planet
	211391664.01	41	22.3	Y	$1.66e-04$	$< 1e-04$	$< 1e-04$	$< 1e-04$	$< 1e-04$	$< 1e-04$	N	$2.65e-04$	-	$2.65e-04$	Planet
	211401787.01	28	31.6	Y	$3.63e-03$	$< 1e-04$	$< 1e-04$	$< 1e-04$	$< 1e-04$	$< 1e-04$	N	$3.65e-03$	-	$3.65e-03$	Candidate
	211418290.01	945	16.1	N	$1.30e-01$	$5.04e-01$	$< 1e-04$	$< 1e-04$	$< 1e-04$	$< 1e-04$	N	$6.35e-01$	-	-	Candidate
	211424769.01	286	22.3	N	-	-	-	-	-	-	N	-	-	-	Candidate
	211491383.01	22	15.0	N	$< 1e-04$	$< 1e-04$	$9.21e-04$	$1.47e-03$	$< 1e-04$	$< 1e-04$	N	$2.40e-03$	-	$2.40e-03$	Candidate
	211525389.01	53	18.2	Y	$< 1e-04$	$< 1e-04$	$< 1e-04$	$< 1e-04$	$< 1e-04$	$< 1e-04$	N	$1.33e-06$	-	$< 1e-04$	Planet
K2-183 c	211562654.01	156	16.3	Y	$< 1e-04$	$< 1e-04$	$< 1e-04$	$< 1e-04$	$< 1e-04$	$< 1e-04$	N	$3.65e-06$	50	$< 1e-04$	Planet
K2-183 d	211562654.02	174	16.3	Y	$4.47e-04$	$1.72e-04$	$< 1e-04$	$< 1e-04$	$< 1e-04$	$< 1e-04$	N	$6.31e-04$	50	$< 1e-04$	Planet
K2-183 b	211562654.03	13	16.3	Y	$< 1e-04$	$< 1e-04$	$< 1e-04$	$< 1e-04$	$< 1e-04$	$< 1e-04$	N	$5.40e-08$	50	$< 1e-04$	Planet
K2-184 b	211594205.01	35	20.1	Y	$< 1e-04$	$< 1e-04$	$< 1e-04$	$< 1e-04$	$< 1e-04$	$< 1e-04$	N	$2.38e-05$	-	$< 1e-04$	Planet
	211606790.01	106	21.1	N	-	-	-	-	-	-	N	-	-	-	Candidate
K2-185 b	211611158.01	48	16.8	N	$1.90e-04$	$< 1e-04$	$1.42e-02$	$3.62e-03$	$< 1e-04$	$< 1e-04$	N	$1.81e-02$	25	$7.24e-04$	Planet
	211611158.02	131	16.8	N	$2.07e-02$	$2.28e-03$	$7.93e-02$	$1.45e-03$	$2.89e-04$	$< 1e-04$	N	$1.04e-01$	25	$4.16e-03$	Candidate
	211682544.01	77	16.3	N	$2.62e-03$	$< 1e-04$	$2.65e-04$	$< 1e-04$	$< 1e-04$	$< 1e-04$	N	$2.92e-03$	-	$2.92e-03$	Candidate
	211733267.01	87	15.3	N	$0.00e+00$	$0.00e+00$	$5.64e-02$	$1.43e-03$	$3.75e-01$	$6.90e-03$	Y	$4.40e-01$	-	$4.40e-01$	Candidate
	211736671.01	34	18.2	Y	$8.43e-03$	$< 1e-04$	$< 1e-04$	$< 1e-04$	$< 1e-04$	$< 1e-04$	N	$8.45e-03$	-	$8.45e-03$	Candidate
	211743874.01	43	14.7	N	-	-	-	-	-	-	N	-	-	-	Candidate
	211763214.01	49	16.3	N	$< 1e-04$	$< 1e-04$	$4.23e-03$	$1.10e-03$	$< 1e-04$	$< 1e-04$	N	$5.33e-03$	-	$5.33e-03$	Candidate
	211770696.01	46	16.1	Y	-	-	-	-	-	-	N	-	-	-	Candidate
	211800191.01	68	14.1	Y	$4.91e-01$	$4.64e-01$	$< 1e-04$	$< 1e-04$	$2.76e-02$	$1.76e-02$	N	$1.00e+00$	-	-	Candidate
	211818569.01	51	15.0	Y	$0.00e+00$	$0.00e+00$	$< 1e-04$	$< 1e-04$	$< 1e-04$	$< 1e-04$	Y	$1.50e-05$	-	$< 1e-04$	Planet
	211886472.01	55	21.1	Y	-	-	-	-	-	-	N	-	-	-	Candidate
K2-186 b	211906650.01	55	18.2	N	$< 1e-04$	$< 1e-04$	$< 1e-04$	$< 1e-04$	$< 1e-04$	$< 1e-04$	N	$3.48e-05$	-	$< 1e-04$	Planet
	211913977.01	94	13.8	N	$0.00e+00$	$0.00e+00$	$4.12e-03$	$< 1e-04$	$< 1e-04$	$< 1e-04$	Y	$4.27e-03$	-	$4.27e-03$	Candidate
	211941472.01	19	15.8	N	-	-	-	-	-	-	N	-	-	-	Candidate
	211945201.01	37	24.1	Y	$1.62e-01$	$1.17e-03$	$< 1e-04$	$< 1e-04$	$< 1e-04$	$< 1e-04$	N	$1.64e-01$	-	$1.64e-01$	Candidate
	211978988.01	55	13.8	N	$< 1e-04$	$< 1e-04$	$2.40e-03$	$< 1e-04$	$< 1e-04$	$< 1e-04$	N	$2.57e-03$	-	$2.57e-03$	Candidate
	211993818.01	85	42.2	N	-	-	-	-	-	-	Y	-	-	-	Candidate
	212006318.01	53	14.1	N	$< 1e-04$	$< 1e-04$	$8.78e-04$	$2.55e-04$	$< 1e-04$	$< 1e-04$	N	$1.13e-03$	-	$1.13e-03$	Candidate
	212008766.01	70	15.3	Y	$< 1e-04$	$1.49e-03$	$< 1e-04$	$< 1e-04$	$< 1e-04$	$< 1e-04$	N	$1.50e-03$	-	$1.50e-03$	Candidate
	212012119.01	152	19.0	N	$< 1e-04$	$< 1e-04$	$2.20e-03$	$< 1e-04$	$< 1e-04$	$< 1e-04$	N	$2.26e-03$	-	$2.26e-03$	Candidate
	212110888.01	32	19.5	Y	$0.00e+00$	$0.00e+00$	$1.23e-03$	$< 1e-04$	$1.31e-04$	$< 1e-04$	Y	$9.17e-04$	-	$9.17e-04$	Planet
	212132195.01	85	21.5	N	$< 1e-04$	$< 1e-04$	$2.28e-03$	$< 1e-04$	$< 1e-04$	$< 1e-04$	N	$2.29e-03$	-	$2.29e-03$	Candidate
	212138198.01	73	17.9	Y	-	-	-	-	-	-	N	-	-	-	Candidate
K2-187 d	212157262.01	127	16.3	Y	$< 1e-04$	$5.15e-04$	$1.12e-04$	$< 1e-04$	$< 1e-04$	$< 1e-04$	N	$6.29e-04$	50	$< 1e-04$	Planet

Table 6 — *Continued*

New K2 Name	EPIC	Secondary Eclipse Threshold (ppm)	Aperture Radius (arcsec)	AO/ Speckle	P(Eclipsing Binary)	P(Eclipsing Binary) (x2 Per.)	P(Background Eclipsing Binary)	P(Background Eclipsing Binary) (x2 Per.)	P(Hierarchical Eclipsing Binary)	P(Hierarchical Eclipsing Binary) (x2 Per.)	RV Mass Limit	VESPA FPP	Multiplicity Boost	Adopted FPP	Disposition
K2-187 e	212157262.02	118	16.3	Y	$< 1e-04$	$1.78e-04$	$< 1e-04$	$< 1e-04$	$< 1e-04$	$< 1e-04$	N	$2.25e-04$	50	$< 1e-04$	Planet
K2-187 c	212157262.03	83	16.3	Y	$< 1e-04$	$< 1e-04$	$< 1e-04$	$< 1e-04$	$< 1e-04$	$< 1e-04$	N	$1.24e-09$	50	$< 1e-04$	Planet
K2-187 b	212157262.04	25	16.3	Y	$< 1e-04$	$< 1e-04$	$< 1e-04$	$< 1e-04$	$< 1e-04$	$< 1e-04$	N	$1.66e-07$	50	$< 1e-04$	Planet
K2-188 b	212164470.01	15	18.2	N	$< 1e-04$	$< 1e-04$	$1.38e-04$	$2.39e-04$	$< 1e-04$	$< 1e-04$	N	$3.77e-04$	25	$< 1e-04$	Planet
K2-188 c	212164470.02	44	18.2	N	$1.30e-04$	$< 1e-04$	$6.87e-04$	$< 1e-04$	$< 1e-04$	$< 1e-04$	N	$8.67e-04$	25	$< 1e-04$	Planet
	212303338.01	10	24.3	Y	-	-	-	-	-	-	N	-	-	-	Candidate
	212357477.01	27	29.1	Y	$2.99e-03$	$< 1e-04$	$< 1e-04$	$< 1e-04$	$< 1e-04$	$< 1e-04$	N	$3.04e-03$	-	$3.04e-03$	Candidate
K2-189 b	212394689.01	177	16.1	Y	$< 1e-04$	$< 1e-04$	$< 1e-04$	$< 1e-04$	$< 1e-04$	$< 1e-04$	N	$3.05e-06$	25	$< 1e-04$	Planet
K2-189 c	212394689.02	53	16.1	Y	$< 1e-04$	$< 1e-04$	$< 1e-04$	$< 1e-04$	$< 1e-04$	$< 1e-04$	N	$2.35e-06$	25	$< 1e-04$	Planet
	212460519.01	43	17.3	Y	$< 1e-04$	$< 1e-04$	$< 1e-04$	$< 1e-04$	$< 1e-04$	$< 1e-04$	N	$3.56e-10$	-	$< 1e-04$	Planet
K2-190 b	212480208.01	19	18.4	Y	$< 1e-04$	$< 1e-04$	$< 1e-04$	$< 1e-04$	$< 1e-04$	$< 1e-04$	N	$1.83e-10$	25	$< 1e-04$	Planet
K2-190 c	212480208.02	25	18.4	Y	$< 1e-04$	$< 1e-04$	$< 1e-04$	$< 1e-04$	$< 1e-04$	$< 1e-04$	N	$2.73e-07$	25	$< 1e-04$	Planet
K2-191 b	212496592.01	55	15.0	Y	$< 1e-04$	$< 1e-04$	$< 1e-04$	$< 1e-04$	$< 1e-04$	$< 1e-04$	N	$2.40e-07$	-	$< 1e-04$	Planet
	212521166.01	37	17.1	Y	$< 1e-04$	$< 1e-04$	$< 1e-04$	$< 1e-04$	$< 1e-04$	$< 1e-04$	N	$8.44e-07$	-	$< 1e-04$	Planet
	212534729.01	61	14.4	Y	-	-	-	-	-	-	N	-	-	-	Candidate
K2-192 b	212555594.01	55	13.8	Y	$< 1e-04$	$< 1e-04$	$< 1e-04$	$< 1e-04$	$< 1e-04$	$< 1e-04$	N	$1.71e-04$	-	$1.71e-04$	Planet
	212562715.01	78	16.1	Y	$4.01e-03$	$< 1e-04$	$< 1e-04$	$< 1e-04$	$< 1e-04$	$< 1e-04$	N	$4.03e-03$	-	$4.03e-03$	Candidate
	212577658.01	38	18.2	Y	-	-	-	-	-	-	N	-	-	-	Candidate
K2-193 b	212580872.01	62	13.1	Y	$< 1e-04$	$< 1e-04$	$< 1e-04$	$< 1e-04$	$< 1e-04$	$< 1e-04$	N	$1.97e-05$	-	$< 1e-04$	Planet
	212586030.01	79	16.6	Y	-	-	-	-	-	-	N	-	-	-	Candidate
	212587672.01	71	15.0	Y	$1.34e-02$	$1.95e-03$	$< 1e-04$	$< 1e-04$	$2.65e-04$	$< 1e-04$	N	$1.57e-02$	-	$1.57e-02$	Candidate
	212639319.01	84	17.5	Y	$8.66e-01$	$6.03e-02$	$< 1e-04$	$< 1e-04$	$6.11e-02$	$8.06e-03$	N	$9.96e-01$	-	$9.96e-01$	Candidate
	212645891.01	42	18.2	Y	$< 1e-04$	$9.88e-01$	$< 1e-04$	$< 1e-04$	$< 1e-04$	$1.22e-02$	N	$1.00e+00$	-	-	Candidate
K2-194 b	212672300.01	45	16.3	Y	$< 1e-04$	$< 1e-04$	$< 1e-04$	$< 1e-04$	$< 1e-04$	$< 1e-04$	N	$9.79e-05$	-	$< 1e-04$	Planet
	212686205.01	44	15.3	Y	$< 1e-04$	$< 1e-04$	$< 1e-04$	$< 1e-04$	$< 1e-04$	$< 1e-04$	N	$4.25e-05$	-	$< 1e-04$	Planet
K2-195 b	212689874.01	53	19.4	Y	$< 1e-04$	$< 1e-04$	$< 1e-04$	$< 1e-04$	$< 1e-04$	$< 1e-04$	N	$4.99e-10$	25	$< 1e-04$	Planet
K2-195 c	212689874.02	104	19.4	Y	$< 1e-04$	$< 1e-04$	$< 1e-04$	$< 1e-04$	$< 1e-04$	$< 1e-04$	N	$1.91e-05$	25	$< 1e-04$	Planet
K2-196 b	212691422.01	51	19.4	Y	$< 1e-04$	$< 1e-04$	$< 1e-04$	$< 1e-04$	$< 1e-04$	$< 1e-04$	N	$8.89e-05$	-	$< 1e-04$	Planet
	212697709.01	77	16.8	Y	$0.00e+00$	$0.00e+00$	$< 1e-04$	$< 1e-04$	$< 1e-04$	$< 1e-04$	Y	$3.49e-04$	-	$3.49e-04$	Planet
	212703473.01	18	18.8	Y	-	-	-	-	-	-	N	-	-	-	Candidate
	212703473.02	39	18.8	Y	-	-	-	-	-	-	N	-	-	-	Candidate
K2-197 b	212735333.01	82	17.3	Y	$< 1e-04$	$< 1e-04$	$< 1e-04$	$< 1e-04$	$< 1e-04$	$< 1e-04$	N	$2.06e-05$	-	$< 1e-04$	Planet
K2-198 b	212768333.01	273	24.7	Y	$2.33e-04$	$< 1e-04$	$< 1e-04$	$< 1e-04$	$< 1e-04$	$< 1e-04$	N	$2.74e-04$	-	$2.74e-04$	Planet
	212772313.01	227	21.1	Y	$2.26e-02$	$9.50e-03$	$< 1e-04$	$< 1e-04$	$< 1e-04$	$1.65e-04$	N	$3.23e-02$	-	$3.23e-02$	Candidate
K2-199 b	212779596.01	45	21.6	Y	$< 1e-04$	$< 1e-04$	$< 1e-04$	$< 1e-04$	$< 1e-04$	$< 1e-04$	N	$2.27e-09$	25	$< 1e-04$	Planet
K2-199 c	212779596.02	69	21.6	Y	$< 1e-04$	$< 1e-04$	$< 1e-04$	$< 1e-04$	$< 1e-04$	$< 1e-04$	N	$1.72e-10$	25	$< 1e-04$	Planet
	212803289.01	31	26.7	Y	$< 1e-04$	$< 1e-04$	$< 1e-04$	$< 1e-04$	$< 1e-04$	$< 1e-04$	N	$5.80e-14$	-	-	Candidate
K2-200 b	212828909.01	56	21.1	Y	$< 1e-04$	$< 1e-04$	$< 1e-04$	$< 1e-04$	$< 1e-04$	$< 1e-04$	N	$1.11e-04$	-	$1.11e-04$	Planet
	213546283.01	58	18.2	Y	-	-	-	-	-	-	N	-	-	-	Candidate
	213817056.01	492	18.6	N	$3.99e-03$	$9.03e-03$	$2.07e-01$	$1.40e-01$	$3.23e-04$	$2.64e-04$	N	$3.60e-01$	-	$3.60e-01$	Candidate
	214234110.01	39	15.6	Y	$1.95e-01$	$5.14e-02$	$< 1e-04$	$< 1e-04$	$< 1e-04$	$6.60e-04$	N	$2.47e-01$	-	$2.47e-01$	Candidate
	214254518.01	42	18.2	N	$< 1e-04$	$< 1e-04$	$8.84e-03$	$5.85e-03$	$< 1e-04$	$< 1e-04$	N	$1.47e-02$	-	$1.47e-02$	Candidate
	215171927.01	78	18.2	Y	-	-	-	-	-	-	N	-	-	-	Candidate
	215171927.02	104	18.2	Y	-	-	-	-	-	-	N	-	-	-	Candidate
	215502661.01	64	18.2	N	$5.86e-04$	$2.37e-02$	$2.19e-01$	$7.35e-01$	$< 1e-04$	$3.94e-04$	N	$9.78e-01$	-	$9.78e-01$	Candidate
	215854715.01	86	18.2	Y	-	-	-	-	-	-	N	-	-	-	Candidate
K2-201 b	216008129.01	32	20.3	Y	$< 1e-04$	$< 1e-04$	$< 1e-04$	$< 1e-04$	$< 1e-04$	$< 1e-04$	N	$1.68e-07$	25	$< 1e-04$	Planet
K2-201 c	216008129.02	120	20.3	Y	$3.88e-03$	$2.88e-03$	$< 1e-04$	$< 1e-04$	$< 1e-04$	$< 1e-04$	N	$6.77e-03$	25	$2.71e-04$	Planet
	216050437.01	95	21.1	Y	-	-	-	-	-	-	N	-	-	-	Candidate
	216114172.01	71	21.1	Y	-	-	-	-	-	-	N	-	-	-	Candidate
	216166748.01	54	16.3	Y	-	-	-	-	-	-	N	-	-	-	Candidate
	216387101.01	56	15.0	N	$9.75e-04$	$1.69e-03$	$8.22e-03$	$1.91e-02$	$< 1e-04$	$< 1e-04$	N	$3.00e-02$	-	$3.00e-02$	Candidate
K2-202 b	216405287.01	53	13.5	Y	$< 1e-04$	$< 1e-04$	$< 1e-04$	$< 1e-04$	$< 1e-04$	$< 1e-04$	N	$1.93e-06$	-	$< 1e-04$	Planet
	216468514.01	46	12.8	Y	-	-	-	-	-	-	N	-	-	-	Candidate
	216494238.01	39	15.3	Y	-	-	-	-	-	-	N	-	-	-	Candidate
	217192839.01	44	13.8	Y	-	-	-	-	-	-	Y	-	-	-	Candidate
	217192839.02	92	13.8	Y	-	-	-	-	-	-	Y	-	-	-	Candidate
	217192839.03	77	13.8	Y	-	-	-	-	-	-	Y	-	-	-	Candidate
	217855533.01	25	21.1	N	$0.00e+00$	$0.00e+00$	$8.42e-04$	$1.03e-04$	$< 1e-04$	$< 1e-04$	Y	$1.24e-03$	-	$1.24e-03$	Candidate
	217941732.01	23	15.6	Y	$< 1e-04$	$< 1e-04$	$< 1e-04$	$< 1e-04$	$< 1e-04$	$< 1e-04$	N	$5.36e-07$	-	$< 1e-04$	Planet
	217977895.01	101	13.8	Y	$1.75e-04$	$3.92e-02$	$< 1e-04$	$< 1e-04$	$< 1e-04$	$6.70e-04$	N	$4.00e-02$	-	$4.00e-02$	Candidate
	218131080.01	25	15.6	Y	-	-	-	-	-	-	N	-	-	-	Candidate
	218170789.01	54	16.3	N	$< 1e-04$	$< 1e-04$	$1.89e-02$	$9.81e-01$	$< 1e-04$	$< 1e-04$	N	$1.00e+00$	-	-	Candidate
	218304292.01	92	15.3	Y	$7.45e-01$	$3.15e-02$	$< 1e-04$	$< 1e-04$	$5.09e-02$	$3.99e-03$	N	$8.32e-01$	-	$8.32e-01$	Candidate
	218668602.01	66	15.8	N	$< 1e-04$	$< 1e-04$	$1.18e-03$	$3.86e-04$	$< 1e-04$	$< 1e-04$	N	$1.57e-03$	-	$1.57e-03$	Candidate
	218916923.01	83	21.1	Y	-	-	-	-	-	-	N	-	-	-	Candidate
	219388192.01	81	18.8	Y	$< 1e-04$	$< 1e-04$	$< 1e-04$	$< 1e-04$	$< 1e-04$	$< 1e-04$	N	$2.82e-08$	-	-	Candidate
K2-203 b	220170303.01	76	21.1	Y	$< 1e-04$	$< 1e-04$	$< 1e-04$	$< 1e-04$	$< 1e-04$	$< 1e-04$	N	$1.17e-06$	-	$< 1e-04$	Planet
K2-204 b	220186645.01	70	19.7	Y	$< 1e-04$	$< 1e-04$	$< 1e-04$	$< 1e-04$	$< 1e-04$	$< 1e-04$	N	$4.57e-05$	-	$< 1e-04$	Planet
	220192485.01	190	20.6	Y	-	-	-	-	-	-	Y	-	-	-	Candidate
	220207765.01	112	20.1	Y	$4.28e-04$	$4.51e-03$	$< 1e-04$	$< 1e-04$	$< 1e-04$	$2.90e-04$	N	$5.27e-03$	-	$5.27e-03$	Candidate
K2-205 b	220211923.01	51	18.2	Y	$< 1e-04$	$< 1e-04$	$< 1e-04$	$< 1e-04$	$< 1e-04$	$< 1e-04$	N	$9.85e-06$	-	$< 1e-04$	Planet
K2-206 b	220216730.01	164	18.2	Y	$< 1e-04$	$< 1e-04$	$< 1e-04$	$< 1e-04$	$< 1e-04$	$< 1e-04$	N	$5.22e-08$	-	$< 1e-04$	Planet
K2-207 b	220218012.01	113	16.3	Y	$< 1e-04$	$1.82e-04$	$< 1e-04$	$< 1e-04$	$< 1e-04$	$< 1e-04$	N	$1.86e-04$	-	$1.86e-04$	Planet

Table 6 — *Continued*

New K2 Name	EPIC	Secondary Eclipse Threshold (ppm)	Aperture Radius (arcsec)	AO/ Speckle	P(Eclipsing Binary)	P(Eclipsing Binary) (x2 Per.)	P(Background Eclipsing Binary)	P(Background Eclipsing Binary) (x2 Per.)	P(Hierarchical Eclipsing Binary)	P(Hierarchical Eclipsing Binary) (x2 Per.)	RV Mass Limit	VESPA FPP	Multiplicity Boost	Adopted FPP	Disposition
K2-208 b	220225178.01	53	18.2	Y	$< 1e-04$	$< 1e-04$	$< 1e-04$	$< 1e-04$	$< 1e-04$	$< 1e-04$	N	$8.30e-06$	-	$< 1e-04$	Planet
K2-209 b	220241529.01	14	19.2	Y	$< 1e-04$	$< 1e-04$	$< 1e-04$	$< 1e-04$	$< 1e-04$	$< 1e-04$	N	$2.21e-06$	-	$< 1e-04$	Planet
	220245303.01	37	18.2	Y	$< 1e-04$	$1.07e-03$	$< 1e-04$	$< 1e-04$	$< 1e-04$	$1.45e-04$	N	$1.22e-03$	-	$1.22e-03$	Candidate
K2-210 b	220250254.01	13	17.1	Y	$0.00e+00$	$0.00e+00$	$< 1e-04$	$< 1e-04$	$< 1e-04$	$< 1e-04$	Y	$2.31e-04$	-	$2.31e-04$	Planet
K2-211 b	220256496.01	36	18.4	Y	$< 1e-04$	$1.59e-04$	$< 1e-04$	$< 1e-04$	$< 1e-04$	$< 1e-04$	N	$2.16e-04$	-	$2.16e-04$	Planet
	220292715.01	136	15.8	Y	$1.08e-01$	$< 1e-04$	$< 1e-04$	$< 1e-04$	$3.13e-03$	$< 1e-04$	N	$1.11e-01$	-	$1.11e-01$	Candidate
	220294712.01	60	14.7	Y	-	-	-	-	-	-	N	-	-	-	Candidate
	220317172.01	50	16.3	Y	$4.05e-02$	$8.73e-03$	$< 1e-04$	$< 1e-04$	$3.79e-04$	$1.43e-03$	N	$5.11e-02$	-	$5.11e-02$	Candidate
K2-212 b	220321605.01	59	15.0	Y	$< 1e-04$	$< 1e-04$	$< 1e-04$	$< 1e-04$	$< 1e-04$	$< 1e-04$	N	$2.01e-08$	-	$< 1e-04$	Planet
K2-213 b	220341183.01	39	16.3	Y	$0.00e+00$	$0.00e+00$	$< 1e-04$	$< 1e-04$	$< 1e-04$	$< 1e-04$	Y	$2.10e-05$	-	$< 1e-04$	Planet
K2-214 b	220376054.01	34	16.3	Y	$3.62e-04$	$< 1e-04$	$< 1e-04$	$< 1e-04$	$< 1e-04$	$< 1e-04$	N	$3.73e-04$	-	$3.73e-04$	Planet
	220383386.01	13	25.5	N	$< 1e-04$	$< 1e-04$	$7.20e-03$	$< 1e-04$	$< 1e-04$	$< 1e-04$	N	$7.26e-03$	25	$2.90e-04$	Planet
	220383386.02	72	25.5	N	$< 1e-04$	$1.14e-04$	$1.68e-03$	$< 1e-04$	$< 1e-04$	$< 1e-04$	N	$1.80e-03$	25	$< 1e-04$	Planet
	220397060.01	56	18.2	Y	-	-	-	-	-	-	N	-	-	-	Candidate
	220410754.01	67	15.0	Y	$8.39e-04$	$2.23e-04$	$< 1e-04$	$< 1e-04$	$< 1e-04$	$< 1e-04$	N	$1.06e-03$	-	$1.06e-03$	Candidate
K2-215 b	220471666.01	64	13.8	Y	$0.00e+00$	$0.00e+00$	$< 1e-04$	$< 1e-04$	$< 1e-04$	$< 1e-04$	Y	$3.76e-04$	-	$3.76e-04$	Planet
K2-216 b	220481411.01	30	18.2	Y	$< 1e-04$	$< 1e-04$	$< 1e-04$	$< 1e-04$	$< 1e-04$	$< 1e-04$	N	$4.56e-09$	-	$< 1e-04$	Planet
K2-217 b	220487418.01	50	17.3	Y	$< 1e-04$	$3.21e-04$	$< 1e-04$	$< 1e-04$	$< 1e-04$	$< 1e-04$	N	$3.56e-04$	-	$3.56e-04$	Planet
K2-218 b	220503236.01	35	16.3	Y	$< 1e-04$	$< 1e-04$	$< 1e-04$	$< 1e-04$	$< 1e-04$	$< 1e-04$	N	$7.91e-07$	-	$< 1e-04$	Planet
	220555384.01	46	16.3	Y	-	-	-	-	-	-	N	-	-	-	Candidate
K2-219 b	220592745.01	26	18.2	Y	$< 1e-04$	$< 1e-04$	$< 1e-04$	$< 1e-04$	$< 1e-04$	$< 1e-04$	N	$8.82e-07$	50	$< 1e-04$	Planet
K2-219 c	220592745.02	25	18.2	Y	$< 1e-04$	$< 1e-04$	$< 1e-04$	$< 1e-04$	$< 1e-04$	$< 1e-04$	N	$3.18e-09$	50	$< 1e-04$	Planet
K2-219 d	220592745.03	29	18.2	Y	$< 1e-04$	$< 1e-04$	$< 1e-04$	$< 1e-04$	$< 1e-04$	$< 1e-04$	N	$1.86e-07$	50	$< 1e-04$	Planet
K2-220 b	220621788.01	39	17.5	Y	$3.77e-04$	$< 1e-04$	$< 1e-04$	$< 1e-04$	$< 1e-04$	$< 1e-04$	N	$3.78e-04$	-	$3.78e-04$	Planet
	220643470.01	182	22.4	Y	-	-	-	-	-	-	Y	-	-	-	Candidate
	220648214.01	66	17.3	Y	$6.32e-03$	$< 1e-04$	$< 1e-04$	$< 1e-04$	$< 1e-04$	$< 1e-04$	N	$6.32e-03$	-	$6.32e-03$	Candidate
K2-221 b	220650439.01	28	16.3	Y	$< 1e-04$	$< 1e-04$	$< 1e-04$	$< 1e-04$	$< 1e-04$	$< 1e-04$	N	$1.03e-09$	-	$< 1e-04$	Planet
	220674823.01	8	20.1	Y	$< 1e-04$	$< 1e-04$	$< 1e-04$	$< 1e-04$	$< 1e-04$	$< 1e-04$	N	$5.90e-10$	25	$< 1e-04$	Planet
	220674823.02	76	20.1	Y	$< 1e-04$	$1.32e-04$	$< 1e-04$	$< 1e-04$	$< 1e-04$	$< 1e-04$	N	$1.34e-04$	25	$< 1e-04$	Planet
	220679255.01	99	18.2	Y	$2.35e-02$	$1.49e-03$	$< 1e-04$	$< 1e-04$	$4.83e-04$	$< 1e-04$	N	$2.56e-02$	-	$2.56e-02$	Candidate
K2-222 b	220709978.01	31	23.3	Y	$0.00e+00$	$0.00e+00$	$< 1e-04$	$< 1e-04$	$< 1e-04$	$< 1e-04$	Y	$6.92e-05$	-	$< 1e-04$	Planet
K2-223 b	228721452.01	17	21.1	Y	$< 1e-04$	$< 1e-04$	$< 1e-04$	$< 1e-04$	$< 1e-04$	$< 1e-04$	N	$1.09e-04$	25	$< 1e-04$	Planet
K2-223 c	228721452.02	34	21.1	Y	$< 1e-04$	$< 1e-04$	$< 1e-04$	$< 1e-04$	$< 1e-04$	$< 1e-04$	N	$2.88e-08$	25	$< 1e-04$	Planet
K2-224 b	228725972.01	68	18.2	Y	$< 1e-04$	$< 1e-04$	$< 1e-04$	$< 1e-04$	$< 1e-04$	$< 1e-04$	N	$3.23e-06$	25	$< 1e-04$	Planet
	228725972.02	77	18.2	Y	-	-	-	-	-	-	N	-	-	-	Candidate
	228729473.01	53	18.2	Y	$< 1e-04$	$< 1e-04$	$< 1e-04$	$< 1e-04$	$< 1e-04$	$< 1e-04$	N	$7.43e-11$	-	-	Candidate
	228732031.01	19	21.1	Y	$< 1e-04$	$< 1e-04$	$< 1e-04$	$< 1e-04$	$< 1e-04$	$< 1e-04$	N	$1.63e-08$	-	$< 1e-04$	Planet
	228734889.01	534	19.9	Y	-	-	-	-	-	-	N	-	-	-	Candidate
K2-225 b	228734900.01	38	21.1	Y	$< 1e-04$	$< 1e-04$	$< 1e-04$	$< 1e-04$	$< 1e-04$	$< 1e-04$	N	$8.06e-07$	-	$< 1e-04$	Planet
	228735255.01	60	19.7	Y	-	-	-	-	-	-	N	-	-	-	Candidate
K2-226 b	228736155.01	36	24.7	Y	$< 1e-04$	$< 1e-04$	$< 1e-04$	$< 1e-04$	$< 1e-04$	$< 1e-04$	N	$2.21e-08$	-	$< 1e-04$	Planet
	228737155.01	51	24.7	N	-	-	-	-	-	-	Y	-	-	-	Candidate
	228754001.01	66	23.9	Y	-	-	-	-	-	-	N	-	-	-	Candidate
K2-227 b	228760097.01	59	21.1	Y	$< 1e-04$	$< 1e-04$	$< 1e-04$	$< 1e-04$	$< 1e-04$	$< 1e-04$	N	$2.15e-05$	-	$< 1e-04$	Planet
K2-228 b	228798746.01	35	15.0	Y	$< 1e-04$	$< 1e-04$	$< 1e-04$	$< 1e-04$	$< 1e-04$	$< 1e-04$	N	$2.64e-06$	-	$< 1e-04$	Planet
K2-229 b	228801451.01	16	18.4	Y	$< 1e-04$	$< 1e-04$	$< 1e-04$	$< 1e-04$	$< 1e-04$	$< 1e-04$	N	$1.07e-07$	25	$< 1e-04$	Planet
K2-229 c	228801451.02	128	18.4	Y	$2.58e-04$	$< 1e-04$	$< 1e-04$	$< 1e-04$	$< 1e-04$	$< 1e-04$	N	$3.67e-04$	25	$< 1e-04$	Planet
K2-230 b	228804845.01	60	18.2	Y	$< 1e-04$	$< 1e-04$	$< 1e-04$	$< 1e-04$	$< 1e-04$	$< 1e-04$	N	$2.20e-07$	-	$< 1e-04$	Planet
	228809391.01	125	15.8	Y	$0.00e+00$	$0.00e+00$	$< 1e-04$	$< 1e-04$	$1.57e-03$	$< 1e-04$	Y	$1.68e-03$	-	$1.68e-03$	Candidate
	228952747.01	224	15.3	Y	$2.69e-01$	$7.38e-02$	$< 1e-04$	$< 1e-04$	$6.60e-03$	$4.69e-03$	N	$3.54e-01$	-	$3.54e-01$	Candidate
	229004835.01	48	20.5	Y	$1.82e-02$	$< 1e-04$	$< 1e-04$	$< 1e-04$	$< 1e-04$	$< 1e-04$	N	$1.83e-02$	-	$1.83e-02$	Candidate
	229039390.01	24	15.3	Y	-	-	-	-	-	-	Y	-	-	-	Candidate
	229131722.01	63	20.5	Y	$6.84e-04$	$1.84e-03$	$< 1e-04$	$< 1e-04$	$< 1e-04$	$< 1e-04$	N	$2.52e-03$	-	$2.52e-03$	Candidate
	229133720.01	39	17.3	Y	-	-	-	-	-	-	N	-	-	-	Candidate

Table 7
High-resolution Imaging

EPIC	Filter	Instrument
201110617	562	NESSI
201110617	832	NESSI
201111557	562	NESSI
201111557	832	NESSI
201127519	562	NESSI
201127519	832	NESSI
201130233	562	NESSI
201130233	832	NESSI
201132684	562	NESSI
201132684	832	NESSI
201132684	562	NESSI
201132684	832	NESSI
201166680	562	NESSI
201166680	832	NESSI
201211526	562	NESSI
201211526	832	NESSI
201225286	562	NESSI
201225286	832	NESSI
201227197	562	NESSI
201227197	832	NESSI
201231064	562	NESSI
201231064	832	NESSI
201295312	K	PHARO
201295312	K	NIRC2
201299088	562	NESSI
201299088	832	NESSI
201352100	562	NESSI
201352100	832	NESSI
201384232	K	NIRC2
201390048	562	NESSI
201390048	832	NESSI
201403446	K	NIRC2
201427874	562	NESSI
201427874	832	NESSI
201437844	562	NESSI
201437844	832	NESSI
201505350	K	PHARO
201505350	K	NIRC2
201528828	562	NESSI
201528828	832	NESSI
201546283	K	NIRC2
201577035	K	PHARO
201577035	K	NIRC2
201595106	562	NESSI
201595106	832	NESSI
201613023	K	PHARO
201613023	K	NIRC2
201615463	562	NESSI
201615463	832	NESSI
201713348	K	PHARO
201713348	K	NIRC2
201828749	J	PHARO
201828749	K	PHARO
201828749	J	NIRC2
201828749	K	NIRC2
201855371	K	NIRC2
201920032	K	NIRC2
202089657	K	LMIRcam
202089657	K	PHARO
202089657	692	DSSI
202089657	880	DSSI
202091388	692	DSSI
202091388	880	DSSI
202675839	K	NIRC2
202900527	K	NIRC2
203771098	K	NIRC2
203826436	K	NIRC2
205029914	K	NIRC2
205071984	K	NIRC2
205904628	J	Unknown
205904628	692	DSSI
205904628	880	DSSI
205944181	K	NIRC2
205944181	692	DSSI
205944181	880	DSSI

Table 7 — *Continued*

EPIC	Filter	Instrument
206011496	J	NIRC2
206011496	K	NIRC2
206026904	K	NIRC2
206096602	K	NIRC2
206144956	K	NIRC2
206159027	K	NIRI
206159027	K	PHARO
206159027	K	NIRC2
206181769	K	NIRC2
206192335	K	NIRI
206192335	K	PHARO
206245553	K	NIRC2
206268299	K	NIRC2
206348688	K	NIRC2
206439513	K	NIRC2
210363145	K	NIRI
210363145	692	DSSI
210363145	880	DSSI
210363145	692	DSSI
210363145	880	DSSI
210363145	692	DSSI
210363145	880	DSSI
210402237	K	NIRI
210402237	692	DSSI
210402237	880	DSSI
210403955	K	NIRI
210512842	692	DSSI
210512842	880	DSSI
210558622	K	NIRC2
210558622	K	NIRC2
210558622	692	DSSI
210558622	880	DSSI
210558622	692	DSSI
210558622	880	DSSI
210609658	K	NIRI
210609658	692	DSSI
210609658	880	DSSI
210629082	692	DSSI
210629082	880	DSSI
210643811	692	DSSI
210643811	880	DSSI
210667381	692	DSSI
210667381	880	DSSI
210707130	K	NIRC2
210707130	K	NIRC2
210707130	692	DSSI
210707130	880	DSSI
210718708	K	NIRI
210718708	692	DSSI
210718708	880	DSSI
210775710	692	DSSI
210775710	880	DSSI
210848071	692	DSSI
210848071	880	DSSI
210857328	692	DSSI
210857328	880	DSSI
210894022	K	NIRI
210957318	K	NIRI
210965800	692	DSSI
210965800	880	DSSI
211048999	692	DSSI
211048999	880	DSSI
211089792	K	NIRI
211147528	K	NIRC2
211147528	692	DSSI
211147528	880	DSSI
211147528	692	DSSI
211147528	880	DSSI
211319617	K	NIRC2
211319617	692	DSSI
211319617	880	DSSI
211351816	K	NIRC2
211351816	K	PHARO
211355342	K	NIRC2
211391664	K	NIRC2
211401787	K	PHARO
211525389	J	NIRC2

Table 7 — *Continued*

EPIC	Filter	Instrument
211525389	K	NIRC2
211525389	692	DSSI
211525389	880	DSSI
211562654	K	NIRC2
211594205	K	PHARO
211736671	K	NIRC2
211736671	692	DSSI
211736671	880	DSSI
211770696	K	PHARO
211800191	K	NIRC2
211818569	K	PHARO
211886472	J	NIRC2
211886472	K	NIRC2
211886472	692	DSSI
211886472	880	DSSI
211945201	K	NIRC2
211945201	692	DSSI
211945201	880	DSSI
212008766	K	NIRC2
212110888	692	DSSI
212110888	880	DSSI
212138198	J	NIRC2
212138198	K	NIRC2
212138198	692	DSSI
212138198	880	DSSI
212157262	K	NIRC2
212303338	692	DSSI
212303338	880	DSSI
212357477	692	DSSI
212357477	880	DSSI
212394689	K	NIRC2
212394689	692	DSSI
212394689	880	DSSI
212460519	692	DSSI
212460519	880	DSSI
212480208	692	DSSI
212480208	880	DSSI
212496592	692	DSSI
212496592	880	DSSI
212521166	692	DSSI
212521166	880	DSSI
212534729	692	DSSI
212534729	880	DSSI
212555594	692	DSSI
212555594	880	DSSI
212562715	692	DSSI
212562715	880	DSSI
212577658	692	DSSI
212577658	880	DSSI
212580872	692	DSSI
212580872	880	DSSI
212580872	692	DSSI
212580872	880	DSSI
212586030	J	PHARO
212586030	K	PHARO
212586030	692	DSSI
212586030	880	DSSI
212587672	692	DSSI
212587672	880	DSSI
212639319	692	DSSI
212639319	880	DSSI
212645891	692	DSSI
212645891	880	DSSI
212672300	692	DSSI
212672300	880	DSSI
212686205	692	DSSI
212686205	880	DSSI
212689874	692	DSSI
212689874	880	DSSI
212689874	692	DSSI
212689874	880	DSSI
212691422	692	DSSI
212691422	880	DSSI
212697709	692	DSSI
212697709	880	DSSI
212697709	692	DSSI
212697709	880	DSSI

Table 7 — *Continued*

EPIC	Filter	Instrument
212703473	J	PHARO
212703473	K	PHARO
212703473	692	DSSI
212703473	880	DSSI
212735333	K	PHARO
212735333	692	DSSI
212735333	880	DSSI
212768333	692	DSSI
212768333	880	DSSI
212772313	692	DSSI
212772313	880	DSSI
212779596	692	DSSI
212779596	880	DSSI
212779596	692	DSSI
212779596	880	DSSI
212803289	692	DSSI
212803289	880	DSSI
212828909	692	DSSI
212828909	880	DSSI
213546283	K	NIRI
213546283	692	DSSI
213546283	880	DSSI
214234110	692	DSSI
214234110	880	DSSI
215171927	692	DSSI
215171927	880	DSSI
215854715	692	DSSI
215854715	880	DSSI
216008129	692	DSSI
216008129	880	DSSI
216050437	K	NIRI
216050437	692	DSSI
216050437	880	DSSI
216114172	692	DSSI
216114172	880	DSSI
216166748	692	DSSI
216166748	880	DSSI
216405287	692	DSSI
216405287	880	DSSI
216468514	K	NIRI
216468514	K	NIRI
216468514	692	DSSI
216468514	880	DSSI
216494238	K	NIRI
216494238	692	DSSI
216494238	880	DSSI
217192839	K	NIRI
217192839	692	DSSI
217192839	880	DSSI
217941732	692	DSSI
217941732	880	DSSI
217977895	692	DSSI
217977895	880	DSSI
218131080	K	NIRI
218131080	692	DSSI
218131080	880	DSSI
218304292	692	DSSI
218304292	880	DSSI
218916923	K	PHARO
218916923	692	DSSI
218916923	880	DSSI
219388192	K	NIRI
219388192	692	DSSI
219388192	880	DSSI
220170303	562	NESSI
220170303	832	NESSI
220170303	562	NESSI
220170303	832	NESSI
220186645	562	NESSI
220186645	832	NESSI
220186645	562	NESSI
220186645	832	NESSI
220192485	562	NESSI
220192485	832	NESSI
220192485	562	NESSI
220192485	832	NESSI
220207765	562	NESSI

Table 7 — *Continued*

EPIC	Filter	Instrument
220207765	832	NESSI
220211923	562	NESSI
220211923	832	NESSI
220216730	562	NESSI
220216730	832	NESSI
220218012	562	NESSI
220218012	832	NESSI
220225178	562	NESSI
220225178	832	NESSI
220241529	562	NESSI
220241529	832	NESSI
220245303	562	NESSI
220245303	832	NESSI
220250254	562	NESSI
220250254	832	NESSI
220256496	562	NESSI
220256496	832	NESSI
220292715	562	NESSI
220292715	832	NESSI
220292715	562	NESSI
220292715	832	NESSI
220292715	562	NESSI
220292715	832	NESSI
220294712	562	NESSI
220294712	832	NESSI
220294712	K	PHARO
220317172	562	NESSI
220317172	832	NESSI
220321605	562	NESSI
220321605	832	NESSI
220321605	K	PHARO
220341183	562	NESSI
220341183	832	NESSI
220376054	562	NESSI
220376054	832	NESSI
220397060	562	NESSI
220397060	832	NESSI
220397060	J	PHARO
220397060	K	PHARO
220410754	562	NESSI
220410754	832	NESSI
220471666	562	NESSI
220471666	832	NESSI
220481411	562	NESSI
220481411	832	NESSI
220481411	562	NESSI
220481411	832	NESSI
220481411	562	NESSI
220481411	832	NESSI
220481411	K	PHARO
220487418	562	NESSI
220487418	832	NESSI
220487418	K	PHARO
220503236	562	NESSI
220503236	832	NESSI
220555384	562	NESSI
220555384	832	NESSI
220555384	J	PHARO
220555384	K	PHARO
220555384	K	NIRI
220592745	562	NESSI
220592745	832	NESSI
220621788	562	NESSI
220621788	832	NESSI
220643470	562	NESSI
220643470	832	NESSI
220643470	J	PHARO
220643470	K	PHARO
220648214	562	NESSI
220648214	832	NESSI
220650439	562	NESSI
220650439	832	NESSI
220650439	K	PHARO
220674823	562	NESSI
220674823	832	NESSI
220679255	562	NESSI
220679255	832	NESSI

Table 7 — *Continued*

EPIC	Filter	Instrument
220709978	562	NESSI
220709978	832	NESSI
220709978	K	PHARO
228721452	562	NESSI
228721452	832	NESSI
228725972	562	NESSI
228725972	832	NESSI
228729473	562	NESSI
228729473	832	NESSI
228729473	562	NESSI
228729473	832	NESSI
228732031	562	NESSI
228732031	832	NESSI
228734889	562	NESSI
228734889	832	NESSI
228734900	562	NESSI
228734900	832	NESSI
228735255	562	NESSI
228735255	832	NESSI
228736155	562	NESSI
228736155	832	NESSI
228754001	562	NESSI
228754001	832	NESSI
228760097	562	NESSI
228760097	832	NESSI
228798746	562	NESSI
228798746	832	NESSI
228801451	562	NESSI
228801451	832	NESSI
228804845	562	NESSI
228804845	832	NESSI
228809391	562	NESSI
228809391	832	NESSI
228952747	562	NESSI
228952747	832	NESSI
229004835	562	NESSI
229004835	832	NESSI
229039390	562	NESSI
229039390	832	NESSI
229131722	562	NESSI
229131722	832	NESSI
229131722	562	NESSI
229131722	832	NESSI
229133720	562	NESSI
229133720	832	NESSI